NOTE TO USERS

Controlled Oxidative Precipitation of Manganese from an Industrial Zinc Sulphate Solution using a Sulphur Dioxide and Oxygen Gas Mixture

Vincent Ménard

Department of Mining, Metals and Materials Engineering

McGill University

Montreal, Canada

December, 2004

A Thesis submitted to McGill University in partial fulfillment of the requirements of the degree of Master of Engineering

Your file Votre référence
ISBN: 0-494-12632-9
Our file Notre référence
ISBN: 0-494-12632-9

Abstract

Manganese is an impurity in many hydrometallurgical processes that needs to be removed from solution prior to metal recovery. The simplest method of removal is precipitation as hydroxide, i.e. $Mn(OH)_2$, by pH adjustment. However, this method is not selective as most of the other elements present in the solution precipitate as well. An alternative method of manganese removal is by oxidative precipitation. This method consists in oxidizing Mn^{2+} to Mn^{3+}/Mn^{4+} which precipitate readily as hydrous manganese oxide.

The purpose of the present work was to remove selectively manganese from a neutral leach zinc-rich solution at 80°C using the gas mixture of sulphur dioxide (SO_2) and oxygen (O_2) as oxidizing agent. In order to determine the optimum conditions for manganese removal using SO_2/O_2, several semi-batch experiments were performed, where the effects of pH, ORP, SO_2/O_2 ratio, mixing intensity, etc. were investigated. Results of these tests showed that SO_2/O_2 was a fast and effective oxidant for removing manganese down to ppm level provided that the appropriate reactor design, agitation and SO_2/O_2 ratio were employed. In an attempt to improve the precipitate's characteristics, e.g. crystallinity and solid/liquid separation, a new technique called Step-Wise Oxidative Precipitation (S.W.O.P) was investigated using a two-reactor continuous circuit employing pH and ORP control and precipitate recycling. These tests revealed that a birnessite-like phase with general formula $(Na_{0.7}Ca_{0.3})Mn_7O_{14}\bullet 2.8H_2O$ was produced with co-precipitation of a significant amount of zinc apparently via substitution. The applied technique (S.W.O.P combined with recycling) proved effective in producing dense particles but not on lowering zinc losses. The biggest advantage of this novel oxidation technique was the total elimination of scaling.

Résumé

Le manganèse est une impureté dans de nombreux procédés hydrométallurgiques qui doit être éliminée de la solution avant la récupération du métal. La méthode d'élimination la plus simple est par précipitation sous forme d'hydroxydes, i.e. $Mn(OH)_2$, par ajustement du pH. Cependant, cette méthode n'est pas sélective puisque la plupart des autres éléments présents en solution précipitent aussi. Une méthode alternative d'élimination du manganèse est par précipitation oxydante. Cette méthode consiste à oxyder Mn^{2+} en Mn^{3+}/Mn^{4+} qui précipite instantanément sous forme d'oxyde de manganèse hydraté.

L'objet de cette étude était d'éliminer sélectivement le manganèse d'une solution de lixiviat neutralisée riche en zinc à 80°C utilisant le mélange gazeux de dioxyde de soufre (SO_2) et d'oxygène (O_2). Afin de déterminer les conditions optimales d'élimination du manganèse utilisant du SO_2/O_2, plusieurs expériences en semi batch furent effectuées ou les effets du pH, de l'ORP, du ratio SO_2/O_2, de l'intensité d'agitation, etc. furent étudiés. Les résultats de ces tests ont montré que le SO_2/O_2 était un oxydant rapide et efficace pour l'élimination du manganèse jusqu'à des concentrations de l'ordre du ppm des lors que le design du réacteur, de l'agitation et du ratio SO_2/O_2 soit adequatement employés.

Afin d'améliorer les caractéristiques des précipités, e.g. cristallinité et séparation solide/liquide, une nouvelle technique appelée Précipitation Oxydante par Pas Avisés (P.O.P.A) fut étudiée grâce à un circuit de deux réacteurs en continue utilisant un control de pH et d'ORP et de re-circulation des précipités. Ces tests ont révélé qu'une phase de type birnessite ayant une formule générale $(Na_{0.7}Ca_{0.3})Mn_7O_{14}\bullet 2.8H_2O$ fut apparemment produite avec co-précipitation d'une part significative de zinc apparemment via substitution. La technique employée (P.O.P.A combinée avec la recirculation) s'est montrée effective à produire des particules denses mais non à réduire les pertes de zinc. Le plus gros avantage de cette nouvelle technique d'oxydation fut l'élimination totale de l'encroûtement.

Acknowledgments

First and foremost I would like to express my deepest consideration and respect for my supervisor Dr. George P. Demopoulos whose guidance and persistent "all around" help made this thesis come true. Thanks to his legendary "flexibility", he gave me a great and much appreciated freedom to investigate new ideas and have new experiences. I look forward to work on a Ph.D. under his supervision in the upcoming years.

I would also like to thank everyone at the Inco Technology Center, including Dr. Gord Bacon, Dr. Derek Kerfoot and especially Dr. Eberhard Krause for accepting and welcoming me on work terms at ITSL. A special thank you to Dr. Yoshi Okita, Justin Raskauskas, Lesley Joy, and other INCO research personnel.

I am also thankful to Jean-Paul Duterque from GORO Nickel for his help and Dr. Elyse Benguerel of CEZinc for providing me the impure neutral leach solution.

Thank you to the McGill staff especially to Monique Riendeau, Barbara Hanley, Carole Rousseau and Norma Procyshyn.

I thank all the members of the hydrometallurgy research group (Georgiana, Marie-Claude, Amani, Cinziana, Seref, Felipe, Jean-Francois, Terry, Yongfeng, Yuanbing, Zhibao) for their help and friendship. Special thanks to Felipe and Seref for the fun and for introducing me to Pisco and Rakï, to Jeff for our soccer talks and his help with microscopes and to Terry for his help in the lab.

I thank also all my friends in Montreal, in France and in New Caledonia.

A very special thanks to Sophie for the great time we had.

Finally, I am very grateful to my parents and sister for their love and for giving me the opportunity to travel around the globe and to become a better person.

Table of Contents

Abstract **2**
Résumé **3**
Acknowledgments **4**
Table of Contents **5**
List of Figures **8**
List of Tables **11**
Chapter 1 Introduction **12**
1.1 The Issue 12
1.2 The Aim 12
1.3 The CEZinc Operation 13
1.4 The Plan 14
Chapter 2 Literature Review **15**
2.1 Manganese Removal 15
2.1.1 Introduction 15
2.1.2 Oxidation by SO_2/O_2 17
2.2 Fundamentals of Crystallization 20
2.2.1 Introduction 20
2.2.2 Supersaturation 21
2.2.3 The Metastable Zone 22
2.2.4 Nucleation 23
2.2.5 Growth 27
2.3 Continuous-Mode Precipitation Processes 29
2.3.1 Introduction 29
2.3.2 Step-Wise Precipitation 31
2.3.3 Step-Wise Oxidative Precipitation (S.W.O.P) 32
Chapter 3 Experimental **34**
3.1 Reagents 34
3.2 Reactor Set-up 35

3.3 Operating Problems 37
3.4 Procedures 38
3.4.1 Semi-batch Tests 38
3.4.2 Continuous-mode Tests 39
3.4.3 Sampling 40
3.4.4 Settling Test 40
3.4.5 Mass Balance 41
3.5 Analysis and Characterization 41
Chapter 4 Results and Discussion 42
4.1 Introduction 42
4.2 Semi-batch Tests 42
4.2.1 Zinc Hydrolysis 42
4.2.2 Effect of Agitation 43
4.2.3 Effect of SO_2/O_2 Ratio 47
4.2.4 Effect of the SO_2 Flowrate 48
4.2.5 Effect of Closed vs. Open Reactor 53
4.2.6 Effect of Seed 55
4.2.7 Summary 56
4.3 Continuous-mode Tests 57
4.3.1 Non-Staged, Non-Seeded Operation at 715 mV 57
4.3.1.1 Mass Balance 57
4.3.1.2 Manganese Removal 58
4.3.1.3 Reagent Over-Stoichiometry 60
4.3.1.4 Precipitate Characterization 61
4.3.2 Non-Staged Seeded Operation at 715 mV 70
4.3.2.1 Mass Balance 70
4.3.2.2 Manganese Removal 71
4.3.2.3 Reagent Over-Stoichiometry 72
4.3.2.4 Precipitate Characterization 73
4.3.3 Staged and Seeded Operation at 665 mV and 715mV 80
4.3.3.1 Mass Balance 80

4.3.3.2 Manganese Removal 81
4.3.3.3 Reagent Over-Stoichiometry 82
4.3.3.4 Precipitate Characterization 82
4.3.4 Summary 90
Chapter 5 Conclusion 92
References 94

List of Figures

Figure 1: The CEZinc flowsheet. 13
Figure 2: Manganese Eh-pH diagram. 16
Figure 3: The metastable zone. 22
Figure 4: Nucleation mechanisms 23
Figure 5: The metastable zone width (M.Z.W) vs. pH. 24
Figure 6: The Metastable zone width vs. temperature. 24
Figure 7: Nucleation free energy vs. size of nucleus. 25
Figure 8: Nucleation rate vs. saturation ratio. 26
Figure 9: Simplified illustration of uniform deposition and aggregation growth mechanisms. 27
Figure 10: Crystal growth mechanism. 28
Figure 11: Standard continuous hydrolytic precipitation circuit configuration. 30
Figure 12: Standard hydrolytic precipitation. 30
Figure 13: Step-wise continuous hydrolytic precipitation circuit configuration. 31
Figure 14: The step-wise precipitation method. 32
Figure 15: The step-wise oxidative precipitation method 32
Figure 16: Step-wise continuous oxidative precipitation circuit configuration. 33
Figure 17: Experimental set-up 35
Figure 18: Hydrolytic precipitation of zinc at 80°C. 43
Figure 19: Effect of impeller configuration on manganese removal. 45
Figure 20: Variation of manganese concentration with time during a typical oxidative precipitation test (Conditions: SO_2/O_2=200/500 sccm; 2000 RPM). 46
Figure 21: The effect of SO_2/O_2 ratio on manganese removal at fixed SO_2 flowrate equal to 40 sccm. 47
Figure 22: The effect of SO_2 flowrate on manganese removal kinetics at fixed O_2 flowrate equal to 500 sccm 48
Figure 23: Residual manganese concentration and ORP level as a function of SO_2/O_2 ratio. 49

Figure 24: Correlation of final manganese concentration with ORP at various SO_2/O_2 ratios..... 50
Figure 25: Variation of the SO_2 over-stoichiometry factor with time at various SO_2 flowrates..... 51
Figure 26: Variation of $Mg(OH)_2$ over-stoichiometry factor with time for various SO_2 flowrates..... 52
Figure 27: The relationships between final manganese concentration and $Mg(OH)_2$ and SO_2 consumption (expressed as over-stoichiometric factors) for the case of SO_2/O_2=100/500 sccm. 53
Figure 28: The effect of closed vs. open reactor configuration on manganese removal kinetics at various SO_2 flowrates. 54
Figure 29: The effect of seed addition on manganese removal kinetics..... 55
Figure 30: Mass balance of the 715/715/NR test..... 58
Figure 31: ORP and residual manganese during the 715/715/NR test. 59
Figure 32: Manganese removal during the 715/715/NR test. 60
Figure 33: Reagent over-stoichiometry factors for the 715/715/NR test..... 61
Figure 34: Zinc losses during the 715/715/NR test. 62
Figure 35: Precipitate's particle size distribution by volume (715/715/NR). 62
Figure 36: Precipitate mean diameter from the 715/715/NR test. 63
Figure 37: XRD patterns of the 715/715/NR product..... 65
Figure 38: SEM images of the 715/715/NR product. 66
Figure 39: Precipitate's cross-section imaging (715/715/NR)..... 66
Figure 40: Mapping of precipitate's cross-section (715/715/NR). 67
Figure 41: Settling behaviour of the 715/715/NR product. 68
Figure 42: Settling rate of the 715/715/NR product. 68
Figure 43: Solids flux (715/715/NR) 69
Figure 44: Mass balance of the 715/715/R test..... 70
Figure 45: ORP and residual manganese during the 715/715/R test. 71
Figure 46: Manganese removal during the 715/715/R test. 72
Figure 47: Reagent over-stoichiometry factors for the 715/715/R test..... 72
Figure 48: Zinc losses incurred during the 715/715/R test. 73

Figure 49: Particle size distribution by volume of the 715/715/R product. 74
Figure 50: Mean diameter of the 715/715/R product 74
Figure 51: XRD patterns of the 715/715/R product 75
Figure 52: SEM image of the 715/715/R product 76
Figure 53: Cross-section imaging of the 715/715/R product. 77
Figure 54: Mapping of precipitate's cross-section (715/715/R). 77
Figure 55: Precipitate's settling behaviour (715/715/R) 78
Figure 56: Precipitate's settling rate (715/715/R) 78
Figure 57: Solids flux of the 715/715/R product. 79
Figure 58: Mass balance of the 665/715/R test 80
Figure 59: ORP and residual manganese (665/715/R). 81
Figure 60: Manganese removal during the 665/715/R test. 81
Figure 61: Reagent over-stoichiometry factors for the 665/715/R test 82
Figure 62: Zinc losses incurred during the 665/715/R test. 83
Figure 63: Precipitate's particle size distribution by volume (665/715/R). 84
Figure 64: Precipitate's mean diameter (665/715/R). 84
Figure 65: XRD patterns of the 665/715/R product 85
Figure 66: SEM images of the 665/715/R product. 86
Figure 67: Precipitate's cross-section imaging (665/715/R). 86
Figure 68: Mapping of precipitate's cross-section (665/715/R). 87
Figure 69: Precipitate's settling behaviour (665/715/R) 88
Figure 70: Precipitate's settling rate (665/715/R) 88
Figure 71: Solids flux (665/715/R) 89

List of Tables

Table 1: Impure neutral leach solution composition..... 34
Table 2: Description of set-up items..... 36
Table 3: Different impeller configurations..... 44
Table 4: Composition of the precipitates obtained from the 715/715/NR test..... 61
Table 5: Composition of precipitates obtained from the 715/715/R test..... 73
Table 6: Composition of precipitates obtained from the 665/715/R test..... 82

Chapter 1 Introduction

1.1 The Issue

The bulk of zinc is produced from zinc sulphide concentrates via hydrometallurgical processing involving flotation, roasting, leaching, purification and electrolysis steps. The manganese present in the ore as well as that added as manganese-based oxidant dissolves and build-ups in solution. Depending on the concentration, some manganese can be advantageous for leaching and electrolysis. About 1-5 g/L Mn^{2+} in the electrolyte minimizes lead anode corrosion by deposition of a protective MnO_2 coating on the anodes. However, if the concentration of Mn^{2+} is too high (> 5 g/L), a decrease in current efficiency may occur because of the reduction of the higher valence manganese species at the cathode. It can also create an anode sludge disposal problem hence requiring a higher frequency of anode cleaning [1]. In order to regulate the manganese level in solution, bleeding off of electrolyte is often used. However, a chemical method is necessary when the manganese concentration is elevated. This is expected to become a true necessity, especially when concentrates rich in manganese start been processed.

1.2 The Aim

In order to prevent complications during zinc electrowinning due to high manganese level, it is desirable to develop a process which permits a partial or complete removal of manganese prior to zinc electrowinning. Manganese removal in the form of manganese hydroxide by rising the pH near to neutrality is not suitable in this case as zinc hydroxide would precipitate first. On the other hand, manganese removal at lower pH by oxidative precipitation pH is promising.

Hence, it is the aim of the present work to investigate the removal of manganese from an industrial zinc neutral leach solution by oxidative precipitation using the gas mixture of sulphur dioxide and oxygen [2].

1.3 The CEZinc Operation

The feed solution that was mainly used throughout this investigation was provided by a zinc producing facility, namely CEZinc (Valleyfield, Quebec, Canada). Figure 1 shows the simplified flowsheet for the unit operations of the CEZinc processing facility. The manganese removal step is envisaged to be implemented between the leaching and the purification steps.

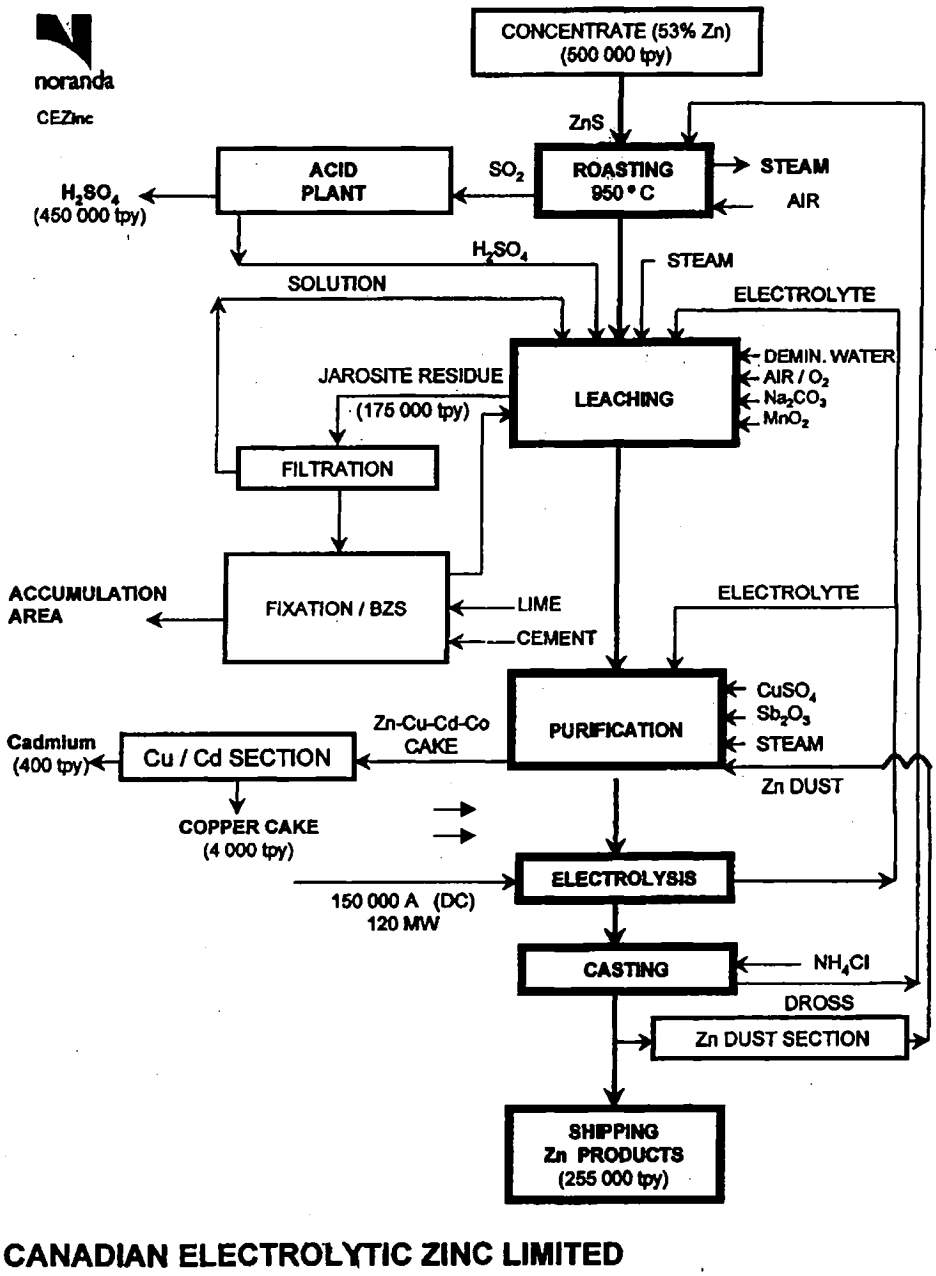

Figure 1: The CEZinc flowsheet [3].

Although the manganese concentration of the CEZinc's zinc electrolyte is regularly over 7 g/L, the solution provided to the author was averaging 4 g/L of manganese. It was decided to maintain the solution manganese level as such, i.e. 4 g/L, and to study the manganese oxidative precipitation by SO_2/O_2 in the 4 to near 0 g/L Mn range.

1.4 The Plan

This work is divided in four chapters:

- Chapter 1 is an introduction.
- Chapter 2 is a literature review of the manganese removal chemistry where various techniques for manganese removal are briefly presented; a larger part being devoted to the oxidative precipitation technique using SO_2/O_2. This is followed by an introduction to the fundamentals of crystallization which play a crucial role in manganese oxidative precipitation. Subsequently, it is explained how these crystallization fundamentals can be applied in practice for manganese removal and the Step-Wise Oxidative Precipitation (S.W.O.P) concept is introduced.
- Chapter 3 presents the equipment and the experimental procedures that were used.
- Chapter 4 presents and discusses the experimental results. This chapter is separated in two main parts: the batch/semi-batch tests and the continuous-mode tests. The role of the bacth/semi-batch tests being to determine the optimum conditions, e.g. pH, mixing, SO_2/O_2 ratio, etc., for the continuous-mode tests. Characterization of the precipitates involving SEM, XRD, EDS, ICP, etc., is also included in this chapter.
- Chapter 5 is dedicated to conclusions.

Chapter 2 Literature Review

2.1 Manganese Removal

2.1.1 Introduction

Many processes exist to remove manganese from solution, each having their own advantages and disadvantages. The most commonly used processes are:

- **Ion Exchange [4, 5]:** Glauconite, also known as manganese greensand, is an example of medium used to remove ppm levels of manganese from water. Reduced manganese present in the process solution adsorbs on the manganese dioxide coating of the filter media, giving a final solution free of manganese. Filter media can be regenerated by oxidizing adsorbed manganous ions to manganese dioxide using chlorine or permanganate. This sequence of reactions can be represented as:

$$Mn^{2+} + MnO_{2(s)} \rightarrow MnO_{2(s)}\text{-}Mn^{2+}{}_{(ads)}$$

$$MnO_{2(s)}\text{-}Mn^{2+}{}_{(ads)} + HOCl + H_2O \rightarrow 2MnO_{2(s)} + Cl^- + 3H^+$$

This method is very efficient at ppm level of manganese for water softening. However, this method is not economically applicable in the context of this investigation as the concentration of manganese is much too high, i.e. 4g/L.

- **Sulphide Precipitation [6, 7]:** Manganese can be precipitated as MnS using H_2S gas:

$$Mn^{2+} + H_2S_{(g)} \leftrightarrow MnS_{(s)} + 2H^+$$

This method is not suitable in the context investigated in this thesis because of the lack of selectivity against zinc [8].

- **Hydroxide/Carbonate Precipitation [9, 10, 11, 12]:** Manganese can be precipitated as hydroxide or carbonate using alkaline agents like $Mg(OH)_2$ or Na_2CO_3:

$$Mn^{2+} + 2OH^- \rightarrow Mn(OH)_2$$

$$Mn^{2+} + CO_3^{2-} \rightarrow MnCO_3$$

This is a common method for heavy metal removal in effluent treatment applications but it is not suitable in the present context because of the lack of selectivity against zinc, cf. chapter 4.2.

- **Electro-Oxidation of Manganese [13, 14, 15, 16]:** Electrolytic Manganese Dioxide (EMD) of high purity (>99.9%) can be produced via electrolysis:

$$Mn^{2+} + 2H_2O \rightarrow MnO_2 + 4H^+ + 2e^-$$

This method is the common method of production of alkaline battery-grade manganese dioxide. However, this method is not applicable presently as a solution containing at least 30 g/L of manganese is required to be economically viable.

- **Solvent Extraction Separation [17, 18, 19]:** Manganese can also be separated from other metals by solvent extraction using extractants like Cyanex 272, Cyanex 301, LIX 84-I. However, zinc is usually extracted at lower pH than manganese and is therefore not suitable in the present case.

- **Oxidative Precipitation:** This method is appropriate to remove multivalent metal impurities which upon oxidation to a higher valence state undergo hydrolysis and precipitate *in situ* at low pH. Manganese is well suited for this type of precipitation. This process can be explained with the aid of the E_h-pH diagram of Figure 2 which was constructed by the author using FactSage® 5.0 for a Mn(0.1m)-H_2O system at 80°C.

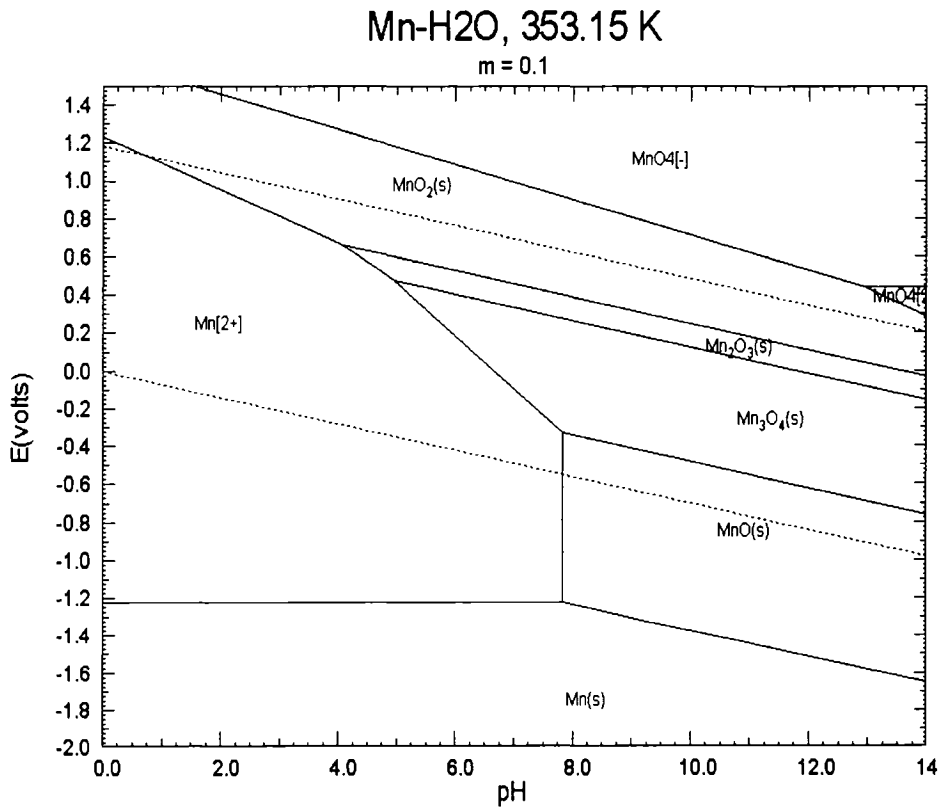

Figure 2: Manganese Eh-pH diagram.

One can notice that it is possible to oxidize Mn^{2+} to Mn^{3+} (Mn_2O_3), Mn^{4+} (MnO_2) and/or $Mn^{2.66+}$ (Mn_3O_4) at pH>5 depending on the oxidation potential. With a very strong oxidizing agent, it is even possible to oxidize manganese to the seventh oxidation state as soluble MnO_4^-. Various oxidants of different oxidizing power can be used to oxidize manganese. Some of them are the object of patents covering in particular the removal of manganese from zinc sulphate solutions, the case investigated in this thesis:

- **Potassium Persulphate [10, 20, 21]:**

$$MnSO_4 + K_2S_2O_8 + 2H_2O \rightarrow MnO_2 + K_2SO_4 + 2H_2SO_4$$

- **Potassium Permanganate [11, 12]:**

Manganese dioxide can be produced by oxidation of manganous salt with potassium permanganate.

$$2KMnO_4 + 3MnSO_4 + 2H_2O \rightarrow 5MnO_{2(s)} + K_2SO_4 + 2H_2SO_4$$

This method is expensive and is used only for the synthesis of high purity battery-grade manganese dioxide.

- **Ozone [22, 23, 24]:**

$$MnSO_4 + O_{3(g)} + H_2O \rightarrow MnO_{2(s)} + H_2SO_4 + O_{2(g)}$$

Ozone is a very strong oxidant having a redox potential of 2.07 V (vs. SHE) that is capable of oxidizing manganese even at sulphuric acid concentration of 5.0 mol/L [25].

- **Caro's acid [26]:**

$$MnSO_4 + H_2SO_5 + H_2O \rightarrow MnO_{2(s)} + 2H_2SO_4$$

and SO_2/O_2 are some of them.

2.1.2 Oxidation by SO_2/O_2

It is well known that sulphur dioxide, which is a strong reducing agent when used alone, gives rise to a very powerful oxidizing agent when mixed with oxygen in the presence of

suitable catalysts. The oxidizing power of SO_2/O_2 mixtures was discovered in the 1920s by United States Bureau of Mines (USBM) during an investigation involving the $Fe^{2+}/Fe^{3+}/H_2SO_4$ system [27]. Since then, SO_2/O_2 has been used for the oxidation of many elements including iron [28, 29, 30], nickel [31], cyanide [31] and arsenic [32, 33, 34]:

Iron Oxidation:

$$2Fe^{2+} + SO_{2(g)} + O_{2(g)} \rightarrow 2Fe^{3+} + SO_4^{2-}$$

Nickel Oxidation:

$$2Ni^{2+} + SO_{2(g)} + O_{2(g)} \rightarrow 2Ni^{3+} + SO_4^{2-}$$

Cyanide Oxidation:

$$CN^- + SO_{2(g)} + O_{2(g)} + H_2O \rightarrow CNO^- + H_2SO_4$$

Arsenic Oxidation:

$$As^{3+} + SO_{2(g)} + O_{2(g)} \rightarrow As^{5+} + SO_4^{2-}$$

Several mechanisms have been proposed to explain the oxidizing power of SO_2/O_2. However, the formation of intermediate peroxy species and $SO_5^{\bullet-}/HSO_5^-$ and HSO_5^-/SO_4^{2-} redox couples are considered by many [31, 35, 36, 37] as responsible for the high redox potential of SO_2/O_2 that is placed between 1.5 V and 1.81V versus the standard hydrogen electrode.

Numerous papers have been published on the subject of manganese removal with a mixture of sulphur dioxide gas and an oxygen-containing gas, e.g. air and/or pure oxygen [2, 38, 39, 40, 41,42]. The overall reactions for Mn(II) oxidation with SO_2/O_2 may be expressed as:

Manganese Oxidative Precipitation with SO_2/O_2:

$$3Mn^{2+} + SO_{2(g)} + O_{2(g)} + 4H_2O \rightarrow Mn_3O_{4(s)} + SO_4^{2-} + 8H^+$$

$$2Mn^{2+} + SO_{2(g)} + O_{2(g)} + 3H_2O \rightarrow Mn_2O_{3(s)} + SO_4^{2-} + 6H^+$$

$$Mn^{2+} + SO_{2(g)} + O_{2(g)} + 2H_2O \rightarrow MnO_{2(s)} + SO_4^{2-} + 4H^+$$

From these equations, it becomes evident that acid is generated from the oxidation of Mn(II). Therefore a base has to be added to the solution if pH control is required, as higher pH improves manganese oxidation rate [2].

Neutralization of Acid with $Mg(OH)_2$:

$$2H^+ + Mg(OH)_2 \rightarrow Mg^{2+} + 2H_2O$$

Catalysts like iron can be very effective for Mn(II) oxidation. In their experiments, Khoe and Zaw [40] showed that the addition of few ppm of Fe(III) increased the oxidation rate of manganese by about ten fold.

On the other hand, the solubility of SO_2 in aqueous solution is many times higher than the solubility of O_2 so dissolution of the latter becomes rate limiting [31]:

$$SO_{2(g)} \rightarrow SO_{2(aq)}$$

$$O_{2(g)} \rightarrow O_{2(aq)}$$

As a result of the differences in solubility characteristics between the two gases, the concentration ratio $[SO_2]/[O_2]$ in the solution is usually superior to one, i.e. SO_2 is in excess, so the following undesirable reactions may occur:

$MnO_2/Mn_2O_3/Mn_3O_4$ Dissolution with Excess SO_2:

$$MnO_{2(s)} + SO_{2(aq)} \rightarrow Mn^{2+} + SO_4^{2-}$$

$$Mn_2O_{3(s)} + SO_{2(aq)} + 2H^+ \rightarrow 2Mn^{2+} + SO_4^{2-} + H_2O$$

$$Mn_3O_{4(s)} + SO_{2(aq)} + 4H^+ \rightarrow 3Mn^{2+} + SO_4^{2-} + 2H_2O$$

An additional undesirable side reaction is the following:

Acid Generation with Excess SO_2:

$$SO_{2(aq)} + \tfrac{1}{2}\, O_{2(aq)} + H_2O \leftrightarrow H_2SO_4$$

These reactions reduce the average oxidation rate of Mn(II) and increase the SO_2 and base consumption. Therefore, to prevent these side reactions, O_2 should be supplied in excess with regards to SO_2 but this is costly because of the low utilization of O_2. For example, the optimum oxidation rate for MnO_2 precipitation obtained by Zhang et al. [35] at 80°C was with a SO_2/O_2 volumetric ratio of 5.7 % while Ferron and Turner [39] used a ratio between 2 % and 3 %. Demopoulos et al. [2] on the other hand were able to obtain very high rates (and high efficiencies) with a surprising SO_2/O_2 volumetric ratio slightly over the stoichiometric one, i.e. one or 50 %. The latter authors have used very high agitation speeds and sparging of gases under the impeller.

A need exists to look closer to the issue of how the utilization of SO_2/O_2 can be improved by considering the mass transfer aspects of the process. This is one of the objectives of the work described in this thesis. It is natural to expect to increase the oxidation rate by increasing the dissolution rate of O_2 in the solution with appropriate mixing. The problem is that configurations that are great for gas dissolution, like the use of a porous sparger ring right under a high-speed Rushton turbine, are usually inappropriate for crystallization. This creates a zone of high local specific power inputs at the outlet of the impeller which promotes very short micromixing times and leads to high supersaturated region with high nucleation rate that yield fines and amorphous particles [43]. Poor macromixing and high attrition rate are other detrimental effects of a Rushton turbine. Therefore, a compromise has to be found between oxidation efficiency and precipitates growth and crystallinity.

2.2 Fundamentals of Crystallization

2.2.1 Introduction

In order to use the manganese oxidation process industrially, a special attention should be accorded to the precipitate characteristics, i.e. particle size, crystallinity, density, morphology, etc. Actually, it was reported elsewhere [44] that manganese dioxide can be difficult to settle and filter and can even be used for trace metals removal because of its high adsorption capacity. Therefore, it is of interest that the precipitate exhibits a certain level of growth and crystallinity as these properties improve:

- The settling rate so results in reduction of the size of the thickener required to separate the solids from solution.
- The filtration rate so results in reduction of the size and cost of the filtration unit.
- The percentage of solids in thickener underflow so results in reduction of the volume of slurry sent to a filter unit and/or to a sludge pond.
- The selectivity of the process as co-precipitation and adsorption of other metal species is minimized. Hence the value of the manganese dioxide precipitate can potentially increase while metal losses (in this case zinc) are controlled.

2.2.2 Supersaturation

Crystallization may be defined as a phase change in which a crystalline product is obtained from a solution [45]. At a given temperature and a given pH there is a maximum amount of solute that can dissolve in a given amount of solvent. When this maximum is reached the solution is said to be saturated. The amount of solute required to make a saturated solution at a given condition is called the solubility.

Crystallization from solution can be considered as a two-step process. The first step is a phase separation, called nucleation, and the second step is the subsequent growth of nuclei to crystals. The prerequisite for crystallization to occur is a supersaturated solution. A supersaturated solution is a solution in which the solute concentration exceeds the equilibrium (saturation) solute concentration at a given pH and a given temperature.

Supersaturation, which is the fundamental driving force for crystallization, can be expressed in dimensionless form [45]:

$$\frac{\mu - \mu^*}{RT} = \ln\frac{a}{a^*} = \ln\frac{\gamma c}{\gamma^* c^*}$$

where μ is the chemical potential, c is the concentration, a is the activity, γ is the activity coefficient, and * represents the property at saturation.

Supersaturation is also often expressed as saturation ratio:

$$S=\frac{c}{c^*}$$

or as absolute supersaturation:

$$\Delta c=c-c^*$$

In most situations, the activity coefficients are not known and the dimensionless chemical potential difference is approximated by a dimensionless concentration difference:

$$\sigma=\frac{\Delta c}{c^*}=\frac{c}{c^*}-1$$

Supersaturated solutions are not at equilibrium and since every system strives to reach equilibrium, supersaturated solutions finally crystallize. Upon crystallizing the solutions move towards equilibrium and supersaturation is relieved by a combination of nucleation and crystal growth. However, in uncontrolled crystallization processes

nucleation starts stochastically and as a result, product characteristics vary greatly. The relation of the degree of nucleation to crystal growth determines important product properties, such as product crystal size and size distribution. Furthermore, the purity of crystalline products strongly depends on the growth rate, since fast growth may lead to liquid inclusions.

2.2.3 The Metastable Zone

Supersaturated solutions exhibit a metastable zone where spontaneous nucleation is not likely to occur. Spontaneous nucleation would occur only by further increase of the supersaturation to the "metastable limit" (refer to Figure 3). This metastable limit is in contrast to the saturation limit, not thermodynamically founded but relates to the kinetics of the system. It depends on a number of parameters such as temperature level, rate of generating the supersaturation, solution history, impurities, fluid dynamics, etc. A control of the actual supersaturation is mandatory to exert the desired influence on nucleation and growth processes.

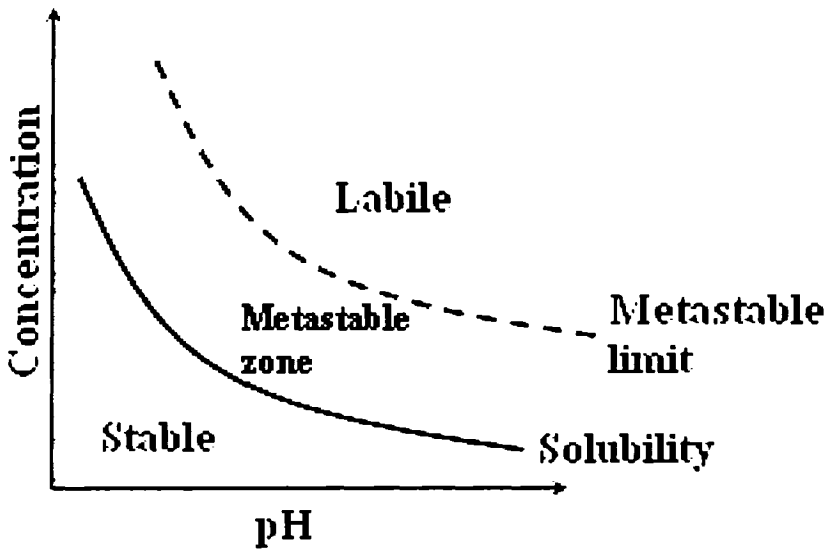

Figure 3: The metastable zone.

2.2.4 Nucleation

Nucleation mechanisms are classified between primary and secondary nucleation (refer to Figure 4). Primary nucleation takes place without the presence of any crystalline solute particles. It can be subdivided into homogeneous nucleation (spontaneous) and heterogeneous nucleation (induced by foreign particles, surface roughness). Secondary nucleation requires the presence of crystals interacting with the environment, e.g. crystallizer walls or impellers. Secondary nuclei originate either from the seed crystal or from the boundary layer of the growing crystal.

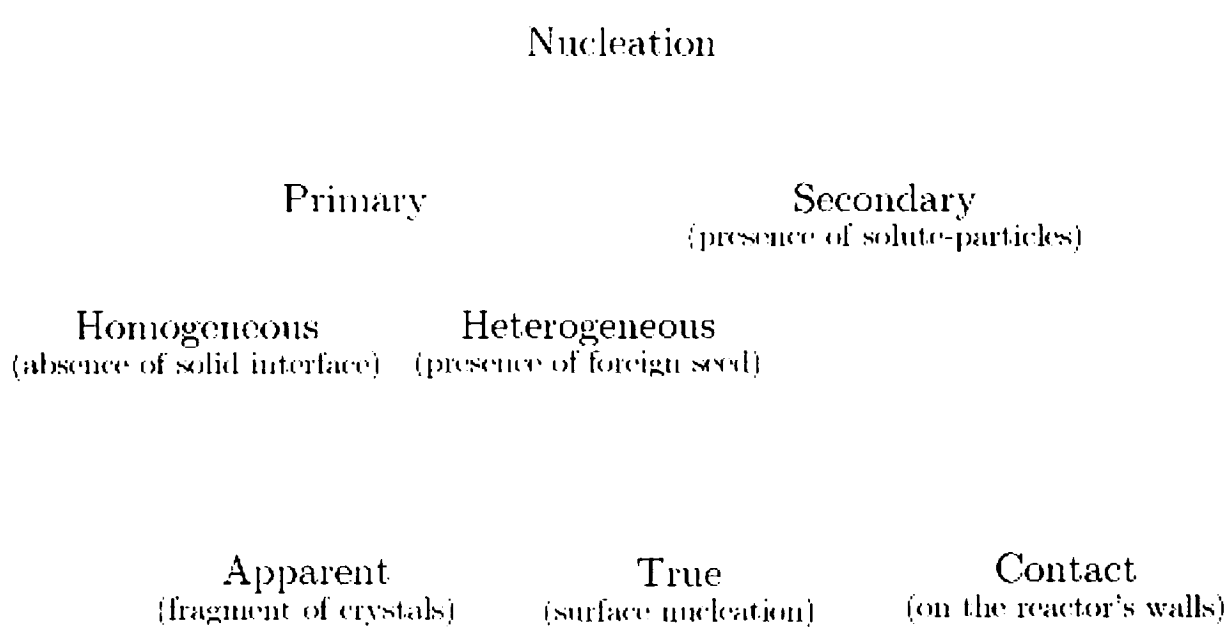

Figure 4: Nucleation mechanisms [46].

Figure 5 and Figure 6 show the variation of the metastable zone width to depend on the type of nucleation. These profiles can change depending on the elements under concern. Thus, the primary homogeneous nucleation line is not always parallel to the solubility line that is itself not always diminishing with pH or rising with temperature.

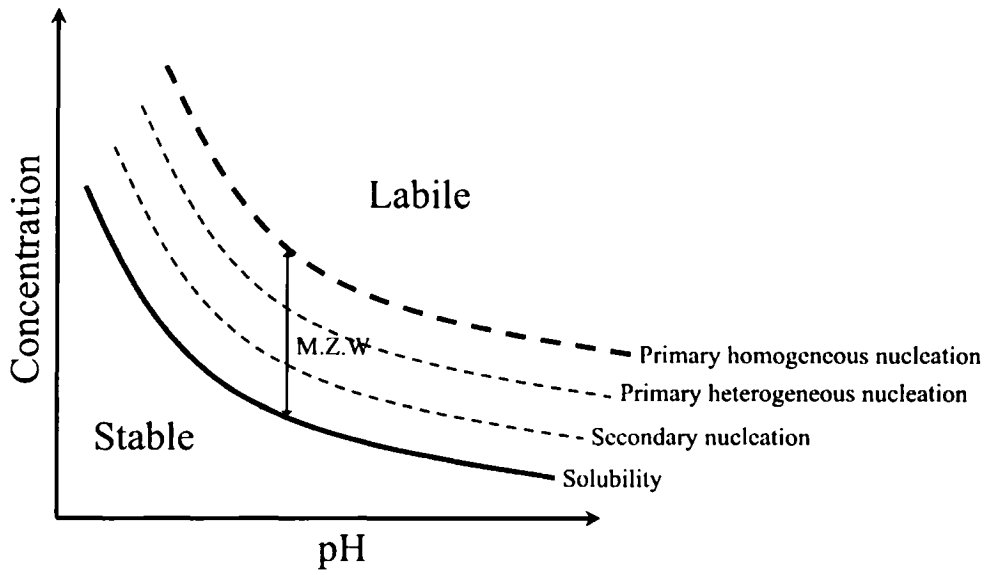

Figure 5: The metastable zone width (M.Z.W) vs. pH (adapted from [47]).

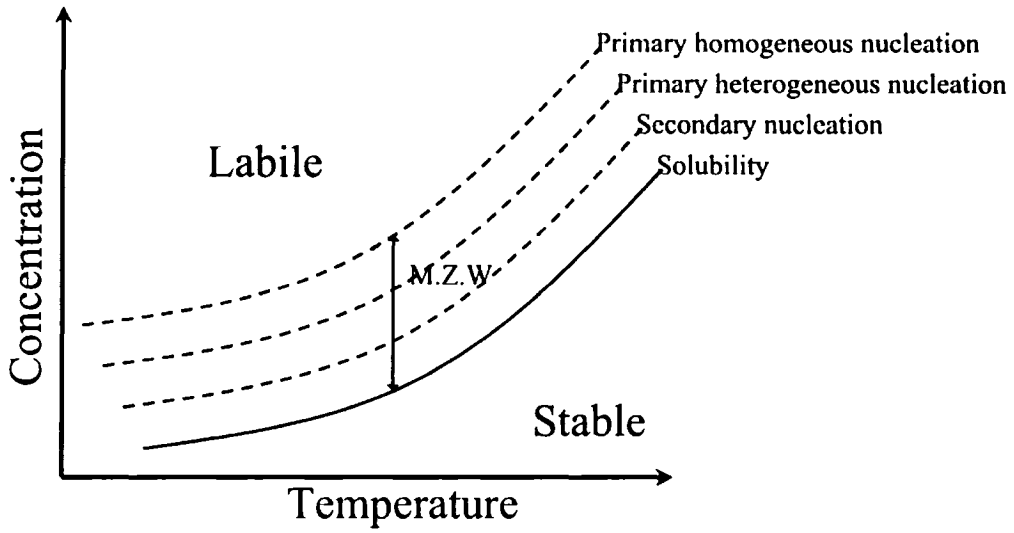

Figure 6: The metastable zone width vs. temperature [47].

- **Primary Homogeneous Nucleation:** Primary homogeneous nucleation occurs in the absence of a solid surface. A supersaturated solution that contains no solid foreign particles or solution-own precipitates will produce a large number of monosized nuclei through primary homogeneous nucleation. A critical supersaturation is required for clusters of the solids to precipitate from solution, to stabilize and to develop. The

behaviour of a newly created crystalline lattice structure in a supersaturated solution depends on its size; it can either grow or redissolve, but the process that it undergoes should result in the decrease in the free energy of the particle. On Figure 7, the critical size r_c represents the minimum size of a stable nucleus. Particles smaller than r_c will dissolve because only in this way can the particle achieve a reduction in its free energy. Similarly, particles larger than r_c will continue to grow.

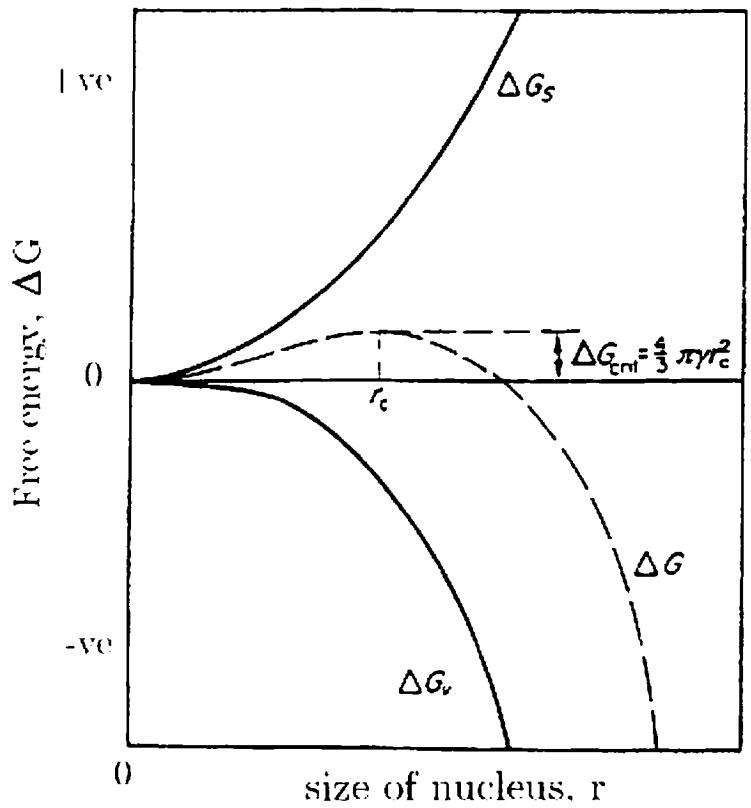

Figure 7: Nucleation free energy vs. size of nucleus [48].

(*ΔG, ΔG$_s$ and ΔG$_v$* are the overall, the surface and the volume excess free energy respectively. ΔG_{crit}, γ and r_c are the critical free energy for nucleation, the interfacial tension and the critical particle radius)

The homogeneous nucleation rate of solid particles is following an exponential relation with supersaturation, cf. Figure 8. The particles produced in this homogeneous nucleation regime are often amorphous and very small, ~1 μm in diameter and have lower solids density values.

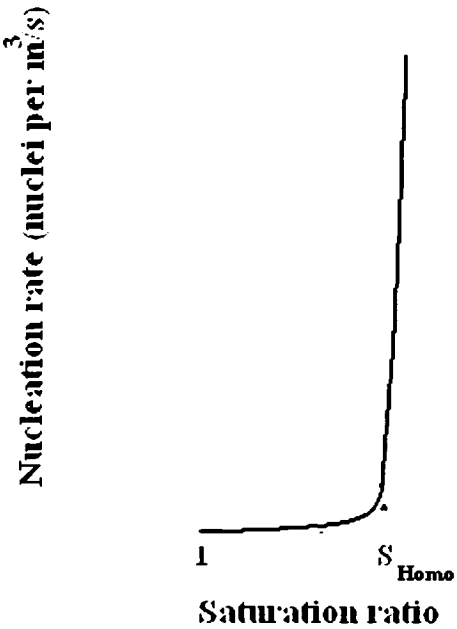

Figure 8: Nucleation rate vs. saturation ratio [48].

(S_{Homo} is the saturation ratio at which homogeneous nucleation occurs)

- **Primary Heterogeneous Nucleation:** Primary heterogeneous nucleation is induced by surfaces of a different material, e.g. dust, insoluble particles, bubbles, wall, stirring equipment, than the one that is precipitated. The degree of critical supersaturation required for this mechanism is lower than the degree of critical supersaturation required for primary homogeneous nucleation.

- **Secondary Nucleation:** Secondary nucleation occurs in the presence of crystal surfaces with the same composition as the materials that precipitate (solution-own). These particles have to be present in solution and can be added as seed. As could be seen on Figure 5 and Figure 6, the critical supersaturation required for this mode of nucleation is lower than that required for either primary homogeneous or primary heterogeneous nucleation, i.e. $S_{cr,surface} < S_{cr,het} < S_{cr,hom}$. This mode of nucleation (involving seed of the same kind of material with the one that precipitates) is termed true or surface secondary nucleation. Also, it tends to proceed at a slower rate than primary homogeneous nucleation. Another type of secondary nucleation is contact secondary nucleation that

occurs when a growing particle collapses on the walls of the reactor due to the hydrodynamic stirring force, thus leaving behind residual solute particles. This mechanism in combination with heterogeneous nucleation is responsible for scaling problems in conventional crystallizations systems that are not carefully controlled.

2.2.5 Growth

After the nuclei are formed, the particles grow according to two main mechanisms: growth by uniform deposition and/or growth by aggregation. Figure 9 shows the characteristic differences between the two growth mechanisms. During growth by uniform deposition a new layer is continuously deposited onto an individual particle, hereby increasing the diameter of the particle. During growth by aggregation two or more individual particles are clustered together and the freshly deposited material cements the particles and causes the particle to develop irregular morphology. These two mechanisms often occur simultaneously, where at lower S values growth by deposition dominates and at higher S values growth by aggregation becomes the dominant mechanism.

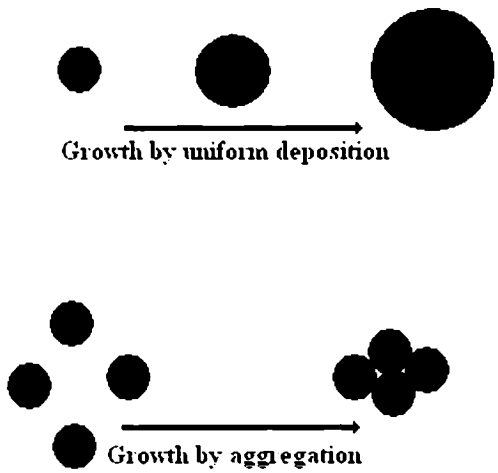

Figure 9: Simplified illustration of uniform deposition and aggregation growth mechanisms.

It is important to note that the fast nucleation process depends on the local supersaturation. On the contrary, the process of crystal growth takes minutes instead of

the milliseconds only that are necessary for primary nucleation. Therefore, the mean supersaturation is decisive for growth.

The process of crystal growth occurs in a sequence of stages [49] depicted in the Figure 10:

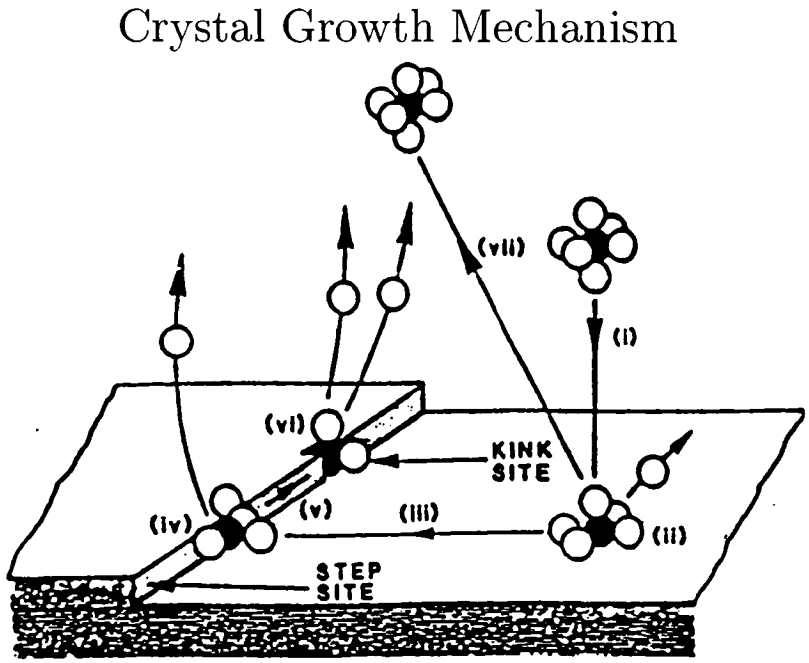

Figure 10: Crystal growth mechanism [50].

i. Transport of solute from the bulk to the crystal surface.
ii. Adsorption on the crystal surface.
iii. Diffusion over the surface.
iv. Attachment to a step.
v. Diffusion along a step.
vi. Integration into the crystal at a kink site.
vii. Diffusion of coordination shell of the solvent molecule away from the crystal surface.

If crystal growth can occur at lower supersaturation level than for nucleation, the release of supersaturation is slower. Therefore depending on the residence time allowed in the reactor, on the final solute concentration required and on the precipitate's characteristics, a mix of nucleation and growth processes may be desired.

2.3 Continuous-Mode Precipitation Processes

2.3.1 Introduction

In industry, although crystallization often occurs in batch or semi-batch mode, precipitation, i.e. reactive crystallization, usually occurs in continuous operation mode. Batch and semi-batch mode offers the advantage of a better control of precipitate characteristics, e.g. size distribution, purity, crystallinity, but is more labour intensive, offers a lower production rate and is finally more expensive than the continuous mode of operation. Therefore batch or semi-batch mode is usually used for the production of small quantity of high value saleable material, e.g. medicine, fine chemicals, etc.; while continuous mode of operation is popular for raw material processing, e.g. impurity removal, waste water treatment and raw chemicals production.

It is a common practice that laboratory experiments are done in batch mode while industrial processes are done in continuous mode. Because the results can be drastically different between the two types of operation, it is imperative that bench scale continuous tests be performed [51].

Figure 11 represents the standard industrial hydrolytic precipitation practice involving continuous mode of operation. A feed solution having an initial pH named pH_i is neutralized to a final pH named pH_f in the first reactor while the second offers just additional residence time. The solid/liquid separation is achieved using a combination of thickener and filter.

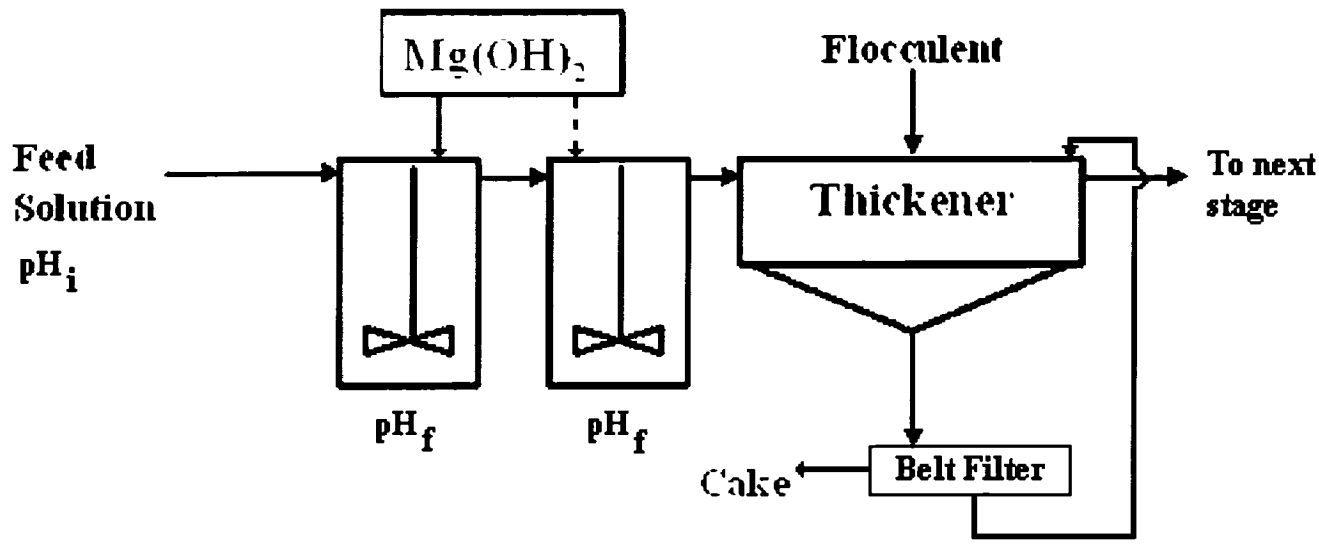

Figure 11: Standard continuous hydrolytic precipitation circuit configuration.

As graphically illustrated in Figure 12, such practice results in high supersaturation so the process is dominated by primary homogeneous nucleation which produces small amorphous particles having poor characteristics, i.e. difficult solid/liquid separation, low purity, etc.

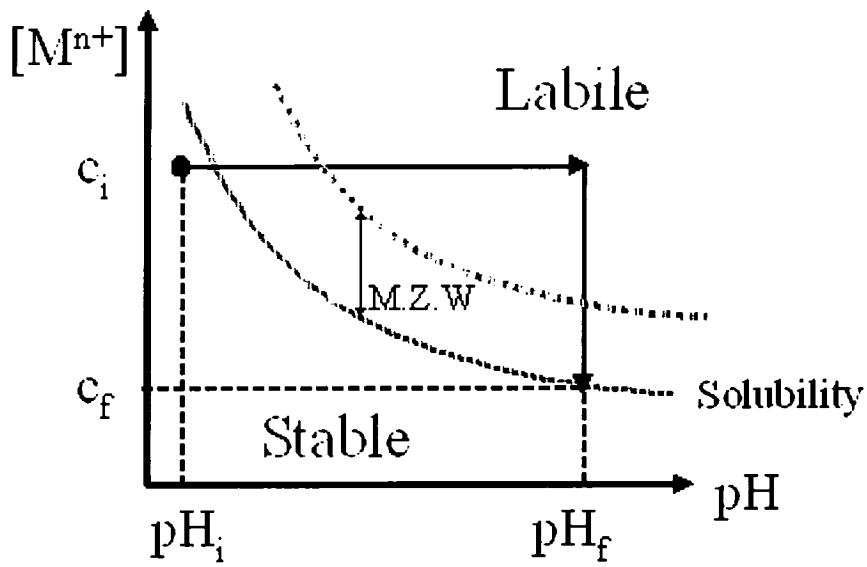

Figure 12: Standard hydrolytic precipitation.

2.3.2 Step-Wise Precipitation

The purpose of the present work is to remove manganese selectively from a neutral leach zinc solution to an acceptable level. The purity of the manganese product is not much of an issue but the manganese removal process must be inexpensive and selective versus zinc, i.e. solid/liquid separation must be smooth and zinc losses must remain to an acceptable level. In order to meet these requirements, one of the patented precipitation processes may be employed. The High Density Sludge (HDS) process [52, 53, 54] is one of them. Another one is the step-wise precipitation process [55, 56, 57, 58] which results in controlling supersaturation upon neutralization hence favoring surface nucleation on seed, cf. Figure 13.

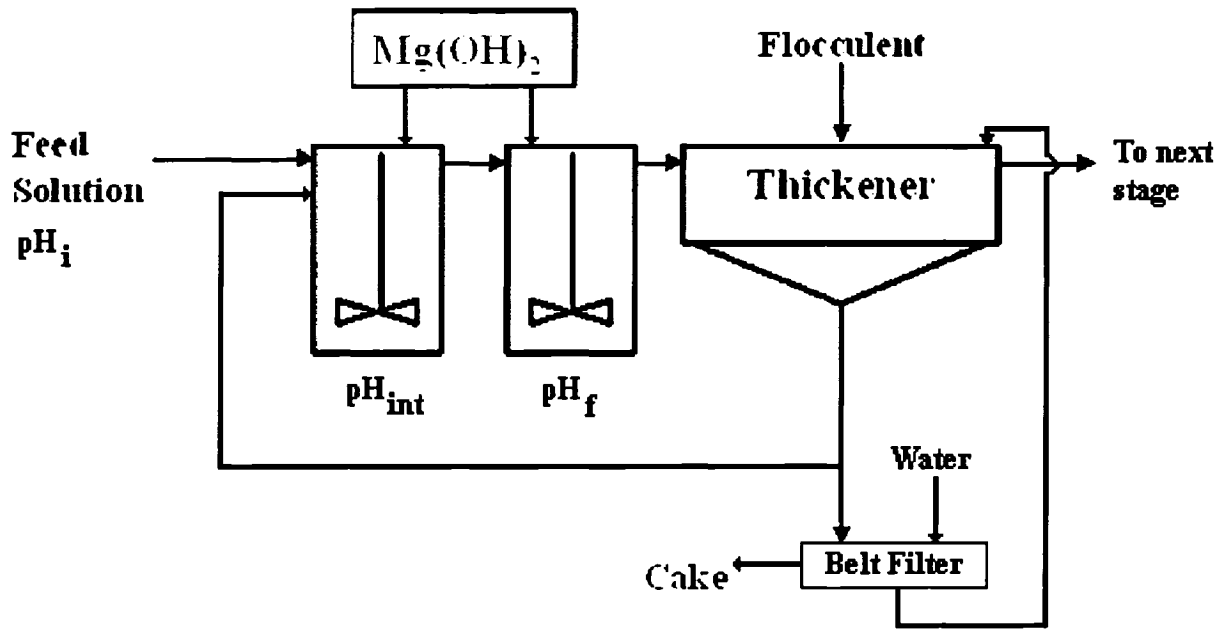

Figure 13: Step-wise continuous hydrolytic precipitation circuit configuration.

During the step-wise precipitation process, the pH of the solution is raised to the final pH in several steps while a part of the thickener underflow is recycled back to the first precipitation reactor for seeding purposes. Therefore supersaturation is controlled within the metastable zone, cf. Figure 14 , which favours surface nucleation resulting in the formation of larger and more crystalline particles having advantageous characteristics, i.e. easier solid/liquid separation, higher purity, etc.

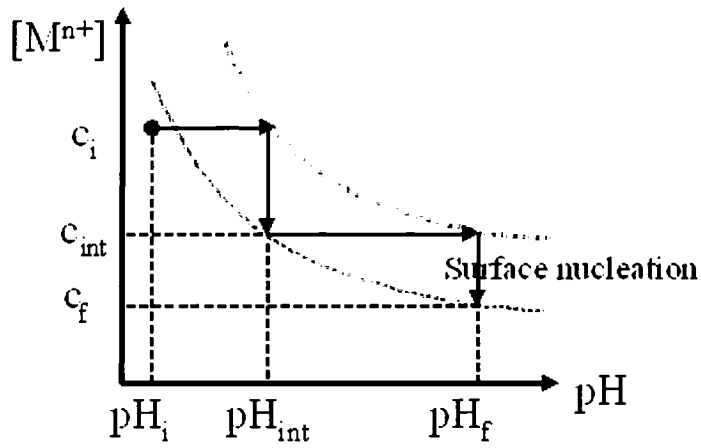

Figure 14: The step-wise precipitation method.

2.3.3 Step-Wise Oxidative Precipitation (S.W.O.P)

It is the aim of the present work to apply the step-wise precipitation concept to the oxidative precipitation of manganese. This new concept is called "Step-Wise Oxidative Precipitation" or S.W.O.P.

Unlike the standard step-wise precipitation concept in which supersaturation is controlled by pH adjustment, the step-wise oxidative precipitation involves supersaturation control by adjusting the redox potential of the solution. The S.W.O.P concept consists of removing manganese by increasing the ORP in two steps (or more if necessary) is illustrated in Figure 15.

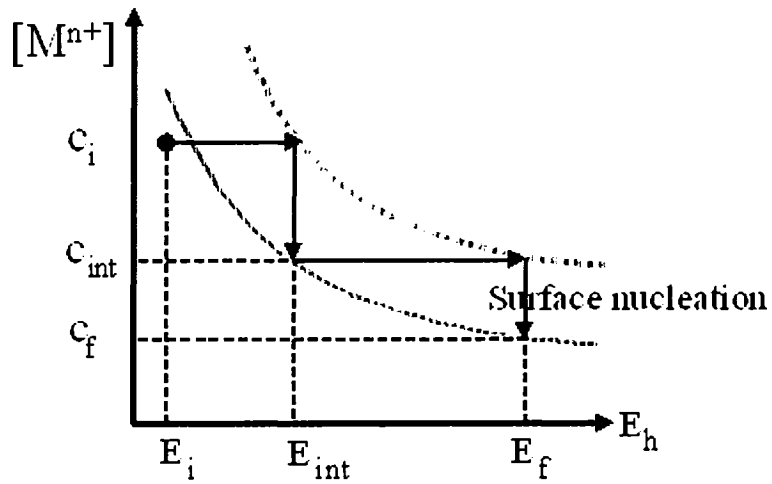

Figure 15: The step-wise oxidative precipitation method.

Each step is achieved in a reactor where SO_2/O_2 is introduced along an alkaline agent, here $Mg(OH)_2$, to control the pH, cf. Figure 16. The resultant slurry is decanted in a thickener whose overflow with reduced manganese content is sent downstream, e.g. to purification and electrolysis. The thickener underflow which contains the manganese oxide precipitate and entrained zinc-rich solution is split into two streams: the first one is returned to the precipitation circuit for seeding purposes while the other stream is sent to a filter unit where the manganese precipitate is washed and then discarded or recovered for selling purposes if so desired.

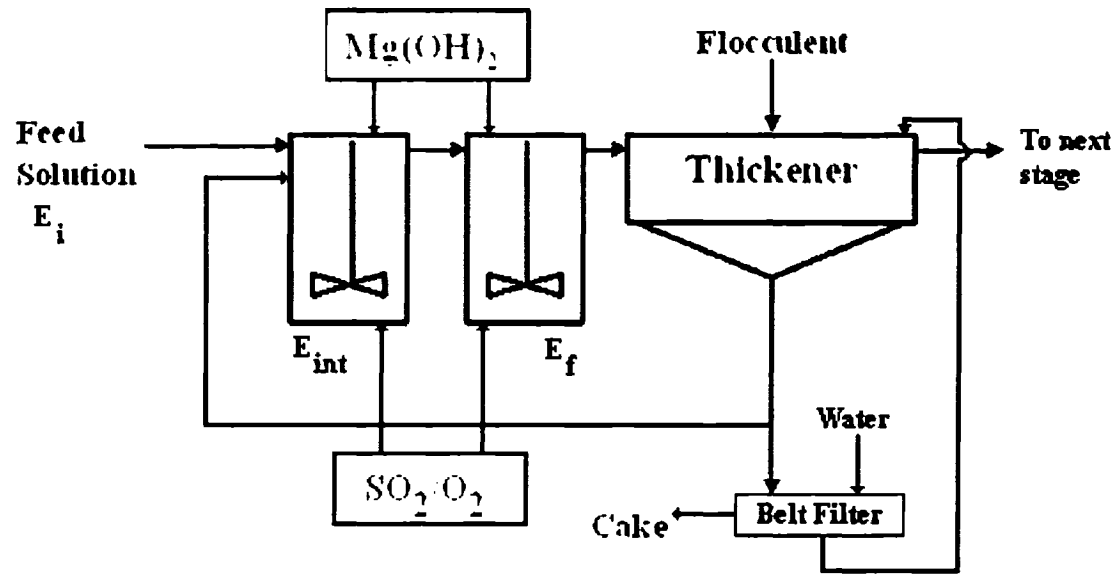

Figure 16: Step-wise continuous oxidative precipitation circuit configuration.

Chapter 3 Experimental

3.1 Reagents

A list of the main gaseous, aqueous and solid reagents that were used throughout this work is presented below:

- **Water:** tap water was distilled then de-ionized (18 MΩ/cm) before use.
- **Impure Neutral Leach Solution (feed solution):** most of the experiments were done using the impure neutral leach solution provided by CEZinc that had a pH of about 3.8 at 80°C, cf. Table 1.

Table 1: Impure neutral leach solution composition.

Element	Concentration (g/L)
Zinc	150
Manganese	4
Magnesium	6
Sodium	3
Copper	1.0
Calcium	0.5
Cobalt	0.01
Iron	0.01

- **Magnesium Hydroxide ($Mg(OH)_2$):** reagent grade powder.
- **Manganous sulphate monohydrate ($MnSO_4.H_2O$):** reagent grade (98.3% purity).
- **Sulphuric Acid (H_2SO_4):** concentrated analytical grade (95-98% purity).
- **Hydrochloric acid (HCl):** concentrated reagent grade (37.5% purity).
- **Sodium hydroxide (NaOH):** 5N certified.
- **Sodium Meta-Bisulphite ($Na_2S_2O_5$):** analytical grade (99.4 % purity).

- **Flocculant:** Percol 351(nonionic polyacrylamide, 20 million molecular weight).
- **Oxygen gas (O_2):** compressed, extra-dry (99.6% purity min).
- **Sulphur dioxide gas (SO_2):** compressed, liquid phase, anhydrous (99.98% purity min).

3.2 Reactor Set-up

Figure 17 and Table 2 presents the reactor set-up that was put together to carry out both semi-batch and continuous-mode tests. Minor modifications were necessary to switch from semi-batch to continuous mode providing great flexibility. As this set-up has two reactors, reactor 1 (R1) and reactor 2 (R2), it was possible to conduct two experiments at a time in semi-batch mode.

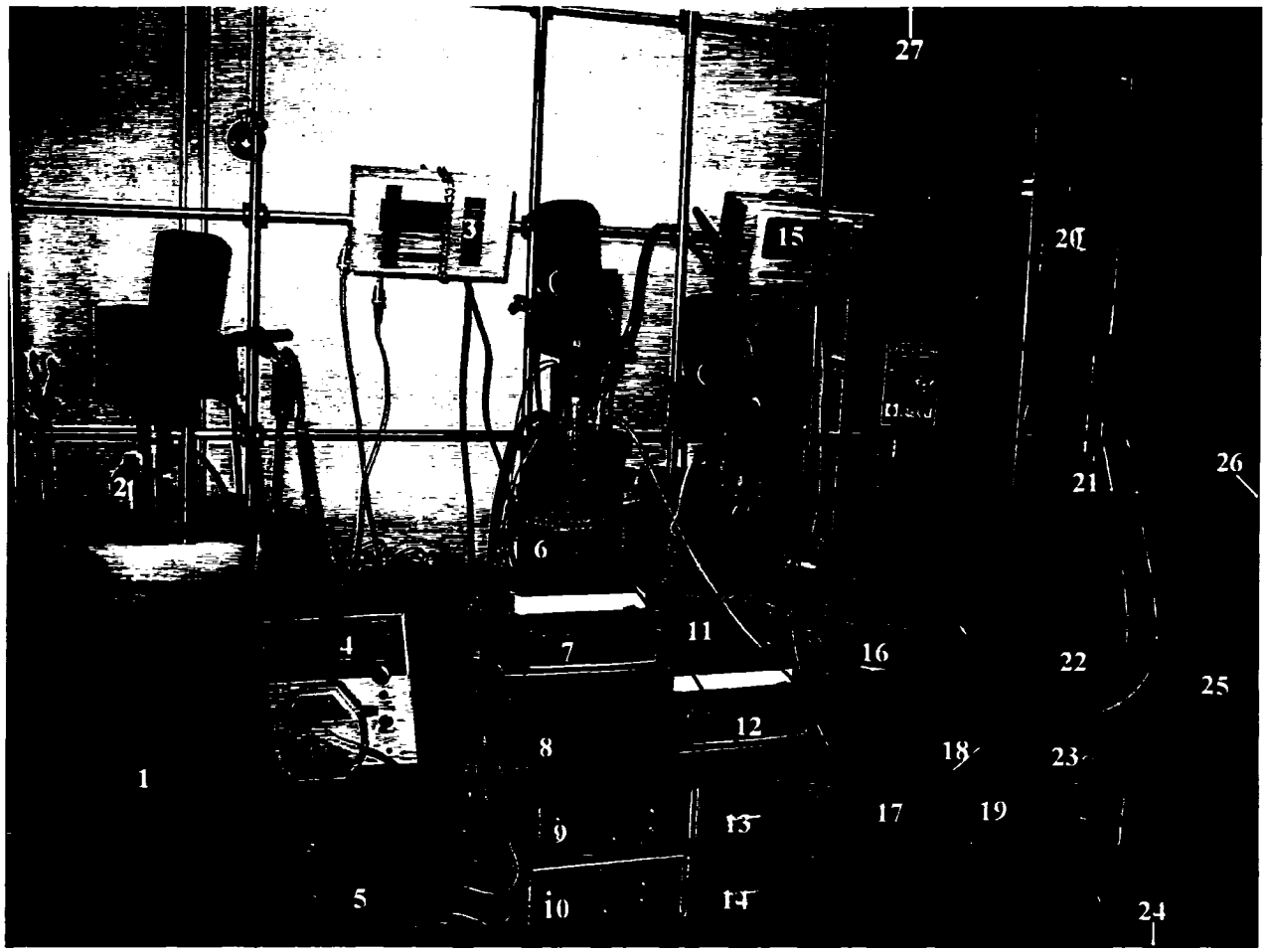

Figure 17: Experimental set-up.

Table 2: Description of set-up items.

1	Feed Tank	**15**	pH/ORP Controller (R2)
2	Feed Tank Heater	**16**	Thickener
3	pH/ORP Controller (R1)	**17**	Thickener Underflow Recycle Pump (R1)
4	Feed Pump (R1)	**18**	Flocculant Tank
5	Temperature Controller (Feed Tank, R1, R2)	**19**	Flocculant Pump (Thickener)
6	Reactor 1 (R1)	**20**	SO_2 and O_2 Mass Flow Transducers (R1, R2)
7	Hot Plate (R1)	**21**	$Mg(OH)_2$ Slurry Tank
8	pH/ORPmeter (back-up)	**22**	$Mg(OH)_2$ Pump (R1)
9	O_2 Mass Flow Controller (R1)	**23**	$Mg(OH)_2$ Pump (R2)
10	SO_2 Mass Flow Controller (R1)	**24**	Thickener Overflow Container
11	Reactor 2 (R2)	**25**	O_2 Cylinder
12	Hot Plate (R2)	**26**	SO_2 Cylinder
13	O_2 Mass Flow Controller (R2)	**27**	Fume Extractor
14	SO_2 Mass Flow Controller (R2)		

Equipments Details:

- **Feed Tank:** 40 litres polypropylene tank.
- **Feed Tank Heater:** 1100W electrical coil heater.
- **$Mg(OH)_2$ Tank:** 2 litres glass beaker with CPVC baffles (baffles width is $1/12^{th}$ of reactor diameter) and cover with O-ring.
- **Reactors (R1, R2):** 2 litres glass beaker with custom made glass overflow, CPVC baffles (baffles width is $1/12^{th}$ of reactor diameter) and cover with O-ring.
- **Reactor Mixers:** 1/10 HP dual-range mixers (240-2400 RPM) with 316 stainless steel 6 blades impellers of various design (upward/downward pitched blades, flat blades).
- **Thickener:** 2 litres custom-made deep cone glass thickener (covered by insulating foam) with cover, underflow opening, CPVC feed well with flocculant addition port.
- **Thickener Mixer:** 1/40 HP dual-shaft mixer (1-4000 RPM) with custom-made polypropylene rake and flocculant mixing paddle.
- **pH/ORP Controllers:** CONSORT® dual-input process controller with on/off or proportional control.
- **pH Probes:** Accumet® Accu•pHast® flushable plastic double junction probes with large annular junction. Calibrated with OAKTON® pH 4 and pH 3 buffers.
- **ORP Probes:** Cole-Parmer® double junction probes with large annular junction and large platinum band. Calibrated with ORION® ORP standard.

- **Pumps:** Peristaltic pumps with Teflon tubing.
- **Gas Spargers:** 316 stainless steel hollow tubes with outlet located under the impeller.
- **SO_2 and O_2 Mass Flow Controllers:** MATHESON® thermal digital gas controllers.
- **O_2 Mass Flow Transducers:** MATHESON® thermal transducers with maximum flowrate of 200 and 500 sccm.
- **SO_2 Mass Flow Transducers:** MATHESON® thermal transducers with maximum flowrate of 50 and 200 sccm.

3.3 Operating Problems

Although the set-up in general performed satisfactorily, some problems were experienced at the beginning:

- ORP control was difficult with the ORP controllers switching on and off. Smoother control was achieved by introducing continuously gasses at a fixed flowrate while pH was controlled on and off by the pH controller. Gas flowrates just required to be readjusted manually now and then in order to maintain the ORP set-point
- A glass-frit porous gas sparger with 30μm holes located under the impeller was used at the beginning but was getting plugged fairly rapidly in continuous-mode. It was replaced by a hollow tube located under the impeller which provided good oxidative precipitation characteristics without plugging.
- Without flocculant, the thickener overflow was too dirty as fine precipitates were not settling well enough, i.e. percent solids of the thickener overflow was around 0.3%. Therefore flocculent was added in the thickener feedwell which improved thickening and reduced the percent solids of the thickener overflow down to about 0.05%.
- pH and ORP probes necessitated frequent cleaning when no seed was used, i.e every 2 hours. The use of a back-up pH/ORP meter for double-checking was necessary.
- Due to heat losses, the temperature dropped in the thickener from 80°C to 40°C. The thickener was then covered using insulating foam so the temperature dropped only from 80°C to 60°C.

- Control of the thickener bed level was originally not easy as there was no clear liquid/solid interface but that was slightly improved with the use of flocculant.

However, once the set-up was tuned, it did provide very satisfactory performance and it was possible to operate without problems for the whole duration of a test, i.e. 12 hours. Almost no intervention from the author-operator was necessary except for probes cleaning and sampling every 4 hours.

3.4 Procedures

Wang and Demopoulos [59] already conducted several semi-batch experiments on the impure neutral leach solution provided by CEZinc, in which they determined the effect of various experimental parameters like pH, neutralizing agent, etc. In their experiments, they have shown that magnesium hydroxide was the neutralizing agent providing one of the fastest manganese oxidative precipitation rates. Therefore magnesium hydroxide was used for neutralization in the present work in the form of a 15 w/w % solid slurry that provides good pH control without tubing plugging problems. All the experiments were conducted at 80°C as this is the usual impure neutral leach solution temperature at CEZinc. Moreover, the reactors were always "closed", i.e. gas escape to the outside of the reactors was minimized using seals and Teflon tape, except when the effect of "open" reactor was investigated when some cover stoppers were removed. Typical procedures for semi-batch, continuous-mode and settling tests are presented hereafter.

3.4.1 Semi-batch Tests

Typical semi-batch test procedure:

1. Reactor was filled with 800 mL of feed solution.
2. Agitator was switched on to desired speed (usually 2000 RPM).
3. Solution was heated up to 80°C.
4. pH was adjusted to the set-point (usually pH 4.0) with diluted sulphuric acid or slaked magnesium hydroxide if necessary.

5. At initial time t_0, gasses were introduced in the reactor at specified flowrates while pH was automatically controlled.

6. Samples were taken periodically; pH, ORP and the volume of the $Mg(OH)_2$ slurry were recorded.

7. When the test was completed, O_2 flowrate was turned down and pH control was turned off.

8. Slurry was filtered for precipitate analysis if necessary and/or reactors were cleaned up by sparging pure SO_2 to dissolve scaling. Remaining solution was then discarded.

3.4.2 Continuous-mode Tests

Typical continuous-mode test procedure:

1. A continuous mode test started like a semi-batch test conducted in reactor 1, cf. step 1 to 5 of the semi-batch test procedure.

2. When the slurry level in reactor 1 reached about 900 mL (operating time t≈1h), the stopper that plugs the reactor 1 overflow was replaced by a plastic tube that was connected to the reactor 2 top feed entry.

3. The feed pump delivering the feed solution from the feed tank to reactor 1 was switched on and set to the appropriate flowrate.

4. As reactor 1 overflowed in reactor 2, slurry level increased in reactor 2. When this level reached about 300 mL and the impeller was submerged, temperature and pH controls of reactor 2 were switched on.

5. When the temperature and pH in reactor 2 were correct, SO_2/O_2 was introduced in R2 at appropriate flowrate.

6. When the slurry level in reactor 2 attained about 900 mL (t≈2h), the stopper that plugs the reactor 2 overflow was replaced by a plastic tube that was connected to the thickener feedwell.

7. As reactor 2 overflowed in the thickener, flocculant addition started and the thickener rake was turned on at very low speed, i.e. 1 RPM.

8. When the slurry level in the thickener reached one litre (t≈3h), the thickener underflow was either discarded or returned to reactor 1 for seeding purposes at a flowrate that allowed to maintain an appropriate bed level in the thickener.

9. When the thickener was full (t≈4h), it overflowed to a graduated container.

10. For tests involving recirculation of the thickener underflow, it was necessary to increase the flowrate of the thickener underflow and of the flocculant in order to maintain a constant bed level.

11. When the test was considered over, O_2 flowrate was turned down and pH control was turned off.

12. Reactors were finally cleaned up by sparging pure SO_2 to dissolve scaling. Remaining solution was then discarded.

3.4.3 Sampling

Many samples were taken during experimentation for aqueous and/or solid phase analysis. For aqueous phase analysis, samples were taken using a syringe fitted with a 0.2 μm pore size syringe filter. To prevent post-precipitation, the filtered solution was appropriately diluted with distilled/de-ionized water which ORP and pH were lowered down to approximately 200 mV (SHE) and pH 2.0 using sodium meta-bisulphite and sulphuric acid. Diluted samples were then kept in sealed sample tubes.

For solid phase analysis, slurry samples were filtered under vacuum through a 0.2 μm pore size membrane. Precipitates were then washed thoroughly with hot (80°C) distilled/de-ionized water. Precipitates were then placed in an oven at 60°C for 24 hours. Dry solids were then kept in sealed plastic bottles.

3.4.4 Settling Test

In order to assess the solid/liquid separation characteristics of the manganese precipitates during continuous mode tests, settling tests were carried out on the reactor 2 overflow (no flocculant was used for these settling tests). Settling tests were performed by redirecting momentarily the reactor 2 overflow from the thickener feedwell to a hot 100 mL graduate cylinder (the graduate cylinder was originally placed in an oven at 80°C). The slurry-filled graduated cylinder was sealed with a stopper, gently turned upside down five times and placed in an oven at 80°C for "at temperature" settling test. The solid/liquid interface

was periodically noted down by briefly opening the oven without significant temperature change.

3.4.5 Mass Balance

Mass balances of the continuous-mode tests were performed in order to have a better understanding of the process. Among other things, it allowed to determine the retention time of each reactor, the zinc losses, the seed to feed ratio, etc. For this duty, the consumption of feed solution, slaked magnesium hydroxide, flocculant, SO_2 and O_2 were recorded. In addition, catch-tests of feed solution, reactor 2 overflow, thickener underflow and overflow were performed to determine their flowrates.

3.5 Analysis and Characterization

Several methods of analysis and characterization were used to determine the composition and the physical-chemical characteristics of the aqueous solution and precipitates.

- **Inductive Coupled Plasma Spectroscopy (ICP):** A Thermo Jarrell Ash ICP-MS was used for aqueous and solids composition determination. Solids samples were first digested in pure hydrochloric acid then placed in an oven at 90°C for 5 hours. The resulting solution was then further diluted in 0.1M nitric acid and kept in sealed sample tubes. Diluted aqueous samples were processed directly.
- **X-ray Powder Diffraction Analysis (XRD):** A Phillips PW1710 with a 1.5405Å CuKα radiation source was used for phase determination.
- **Variable Pressure Scanning Electron Microscope (VP-SEM):** A Hitachi S-3000N VP-SEM was used for particles imaging. It was used either in conventional SEM mode (high vacuum) with carbon coated samples or in VP-SEM (low vacuum) with epoxy-resin mounted samples for cross-section imaging and mapping.
- **Particle Size Analyzer (PSA):** A Horiba LA-920 using laser scattering technology was used for particle size distribution determination. Precipitates were processed in distilled/de-ionized water.

Chapter 4 Results and Discussion

4.1 Introduction

The main goal of this work was to optimize a recently developed process [2] for manganese removal from industrial zinc electrolyte solution using SO_2/O_2. As this process is aimed to be employed in industry, it was of utmost importance to test it in continuous-mode so to better approximate industrial operation. However, prior to performing any continuous-mode experimentation, it was necessary to conduct some preliminary semi-batch tests in order to determine the optimum operating conditions of manganese removal by SO_2/O_2.

In this work, the optimum conditions of manganese removal were those that would allow to investigate the manganese step-wise oxidative precipitation process (S.W.O.P) within the duration of a test, i.e. 12 hours. As the S.W.O.P process requires the recirculation of the precipitate several times, it was therefore important to enhance as much as possible the manganese oxidative precipitation rate in order to shorten the time of a pass so to allow more precipitate recycling and growth within 12 hours. Special attention was also accorded to maximize the reagent's efficiency so to minimize their consumption.

4.2 Semi-batch Tests

4.2.1 Zinc Hydrolysis

As the feed solution was a zinc electrolyte solution, it was critical to prevent as much as possible the losses of zinc by hydrolysis during manganese removal, cf. Equation 4.1.

$$Zn^{2+} + Mg(OH)_2 \rightarrow Zn(OH)_{2\,(s)} + Mg^{2+} \qquad (4.1)$$

Therefore, the apparent solubility of zinc was assessed at 80°C, using slaked magnesium hydroxide at 15% solids and 1000 RPM, cf. Figure 18.

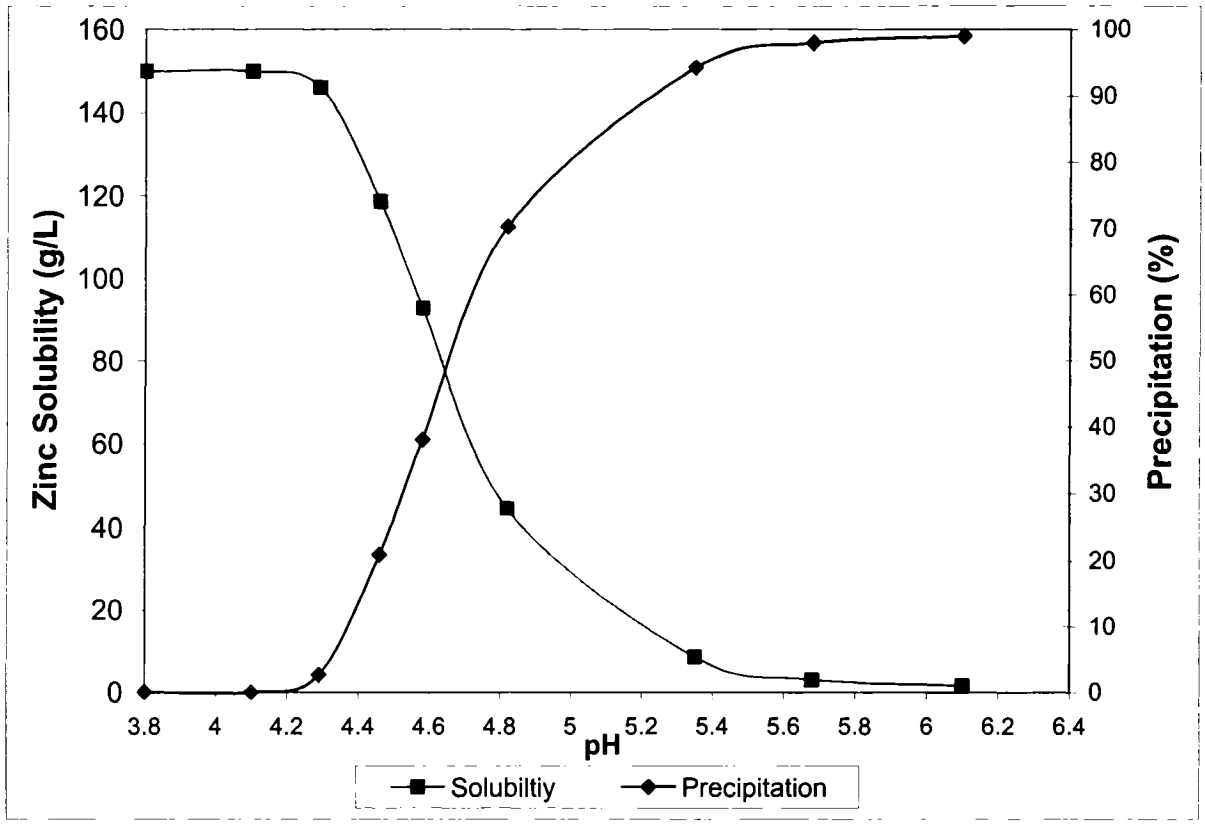

Figure 18: Hydrolytic precipitation of zinc at 80°C.

From Figure 18, it can be seen that zinc at 150 g/L was getting hydrolyzed around pH 4.3 and that 98% of it was precipitated around pH 5.7. It was therefore necessary to conduct manganese removal below pH 4.3 to minimize zinc losses. On the other hand, as it was demonstrated by Wang and Demopoulos [59], manganese oxidative precipitation with SO_2/O_2 is faster as pH increases. Consequently, it was decided to conduct all the experiments at pH 4.0 as it provides the fastest manganese oxidative precipitation rate while giving enough room for pH control before zinc starts precipitating.

4.2.2 Effect of Agitation

As it was explained in chapter 2, a good agitation is critical to attain high redox potential and reduce the formation of sulphuric acid when using SO_2/O_2. In order to determine the most efficient mixing configuration, several tests were performed at the maximum flowrate of SO_2/O_2 that could be delivered by the available equipment, i.e. 200 sccm SO_2 and 500 sccm O_2. For these tests, different kind and configuration of impellers were used.

Configurations with one or two flat blades (Rushton turbine) and/or 45° pitched blades (upward and/or downward) impellers were used. All the impellers were made of 316 stainless steel, had 6 blades and an overall diameter (D) of 5 cm (impeller diameter to tank diameter (T) ratio equal to 0.5). The bottom impeller was located at 2.5 cm (D/2) of the reactor bottom while the top impeller, when utilized, was located at 2.5 cm (D/2) under the liquid/vapour interface. SO_2/O_2 was sparged trough a hollow tube located under the impeller and 4 baffles having a width of 0.8 cm (≈T/12) were installed in the reactors.

Tests were done at 80°C, pH 4.0, slaked $Mg(OH)_2$ at 15% solids and 2000 RPM (except for the last test that was done at 1000 RPM). Table **3** presents the details of the impeller configurations, while Figure 19 summarizes the percentage of manganese removal after 1 hour of operation.

Table 3: Different impeller configurations.

Designation	Top Impeller	Bottom Impeller
FB		Flat Blade
PBD		Pitched Blade Downward
PBU		Pitched Blade Upward
FB+FB	Flat Blade	Flat Blade
PBD+PBD	Pitched Blade Downward	Pitched Blade Downward
PBU+PBU	Pitched Blade Upward	Pitched Blade Upward
PBD+PBU	Pitched Blade Downward	Pitched Blade Upward
PBU+PBD	Pitched Blade Upward	Pitched Blade Downward
FB+PBD	Flat Blade	Pitched Blade Downward
FB+PBU	Flat Blade	Pitched Blade Upward
FB+PBU (1000RPM)	Flat Blade	Pitched Blade Upward

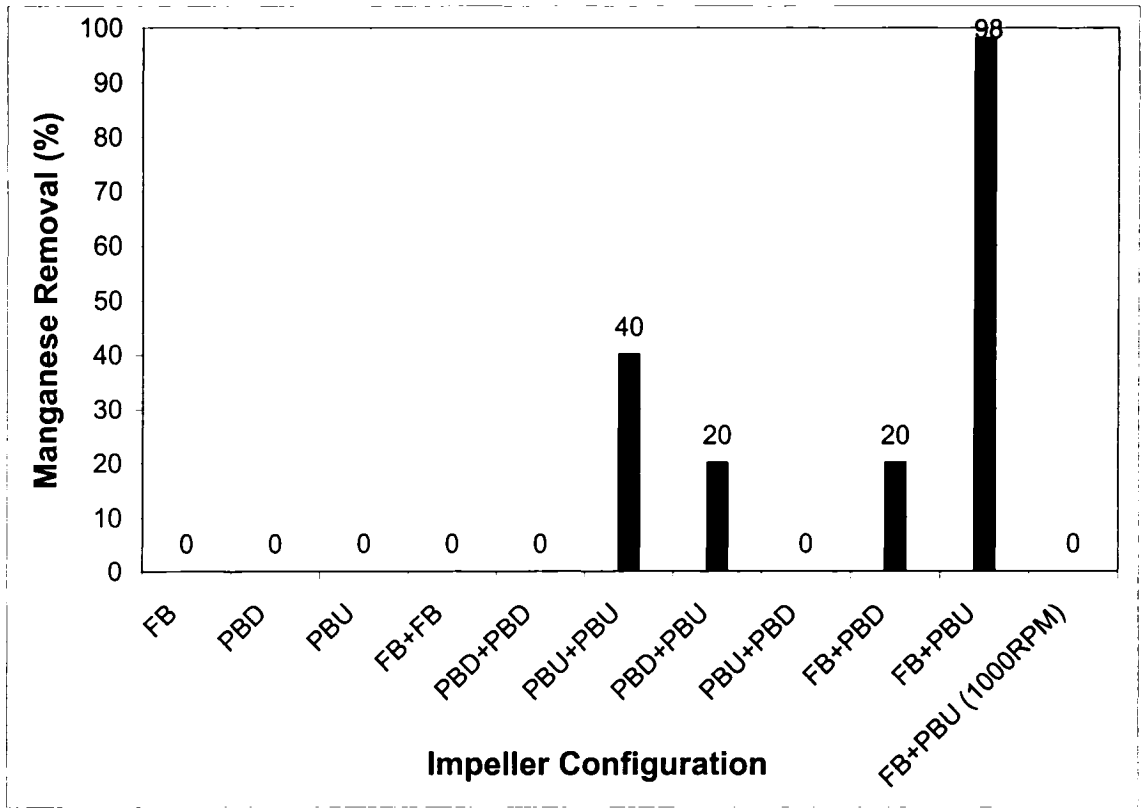

Figure 19: Effect of impeller configuration on manganese removal.

Figure 19 shows that for many of the impeller configurations, manganese did not precipitate at all. This happened because in those cases, the redox potential dropped from 450 mV down to about 200 mV upon injection of SO_2/O_2. The reason for this is that these impeller configurations did not allow sufficient O_2 dissolution to occur in comparison to SO_2, therefore dissolved SO_2 was in excess and reducing conditions prevailed.

For the PBU+PBU, PBD+PBU and FB+PBD configurations, dissolved O_2 was slightly in excess in comparison to SO_2 so only mild oxidizing conditions were obtained.

The best configuration for SO_2/O_2 mixing was using a top flat blade impeller and a bottom 45° upward pitched blade impeller at 2000 RPM. Figure 20 presents the evolution of the manganese concentration and of the ORP during the 2000 RPM test.

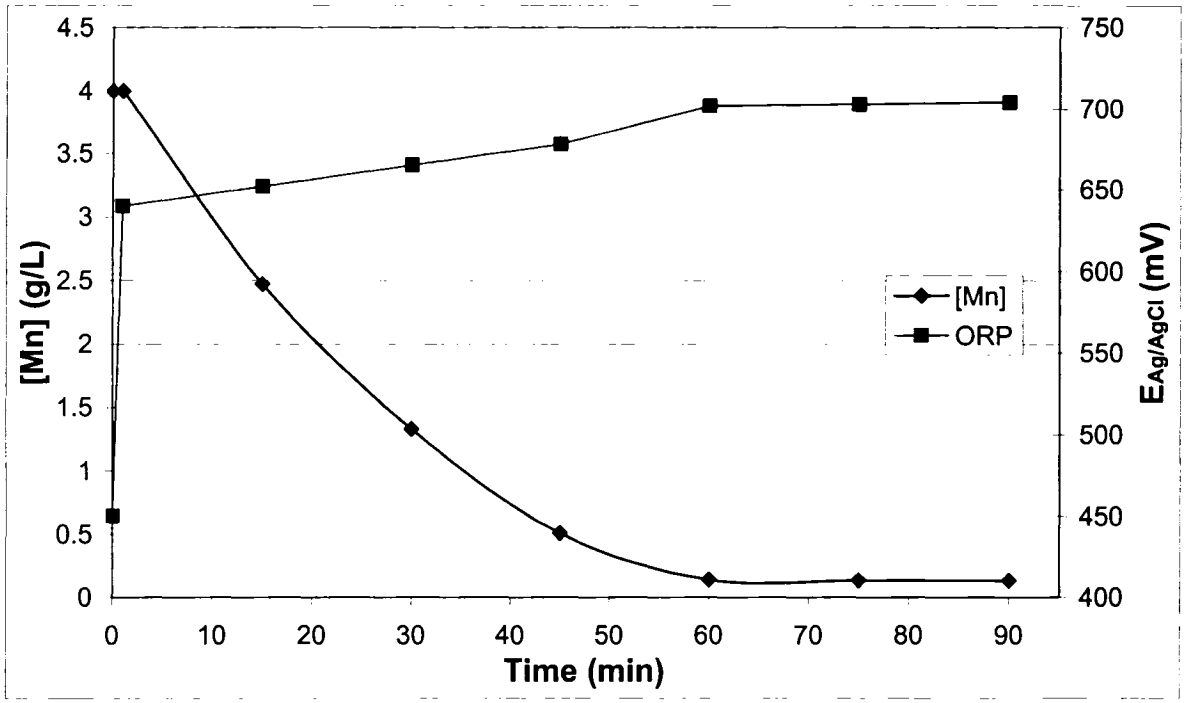

Figure 20: Variation of manganese concentration with time during a typical oxidative precipitation test (Conditions: SO_2/O_2=200/500 sccm; 2000 RPM).

In Figure 20 it can be seen that the redox potential (reported as measured here against the Ag/AgCl reference electrode) of the solution jumped from 450 mV to 640 mV in few seconds as SO_2/O_2 was introduced. Following the introduction of SO_2/O_2, the ORP slowly increased as manganese was oxidatively precipitated. Eventually, the redox potential stabilized around 700 mV which yielded a residual manganese concentration of about 130 ppm. With this configuration, 98% of manganese was precipitated in one hour.

It appears from these tests that the use of an upward 45° pitched bladed impeller on the bottom was the best configuration to handle the gases sparged in the solution. The use of a top flat blade impeller played the role of a surface aerator that created a large additional interfacial area between the solution and the SO_2/O_2 present in the reactor vapour space. However, when the FB+PBU configuration was used at 1000 RPM, the redox potential of the solution dropped as O_2 dissolution and aeration was apparently less effective, rendering the system slightly reducing.

Consequently, the FB+PBU impeller configuration at 2000 RPM was used for all remaining experiments as it appeared to be the most efficient gas sparging configuration.

4.2.3 Effect of SO_2/O_2 Ratio

In order to investigate the effect of the SO_2/O_2 ratio, the SO_2 flowrate was set to 40 sccm while the O_2 flowrate was successively set to 40, 200 and 500 sccm (equipment maximum) giving a SO_2/O_2 volume ratio of 1, 0.4 and 0.16 (or 50%, 16% and 8% SO_2 content). Operating conditions were 80°C, pH 4, slaked $Mg(OH)_2$ at 15% solids, 2000 RPM, "closed" reactor and the FB+PBU impeller configuration.

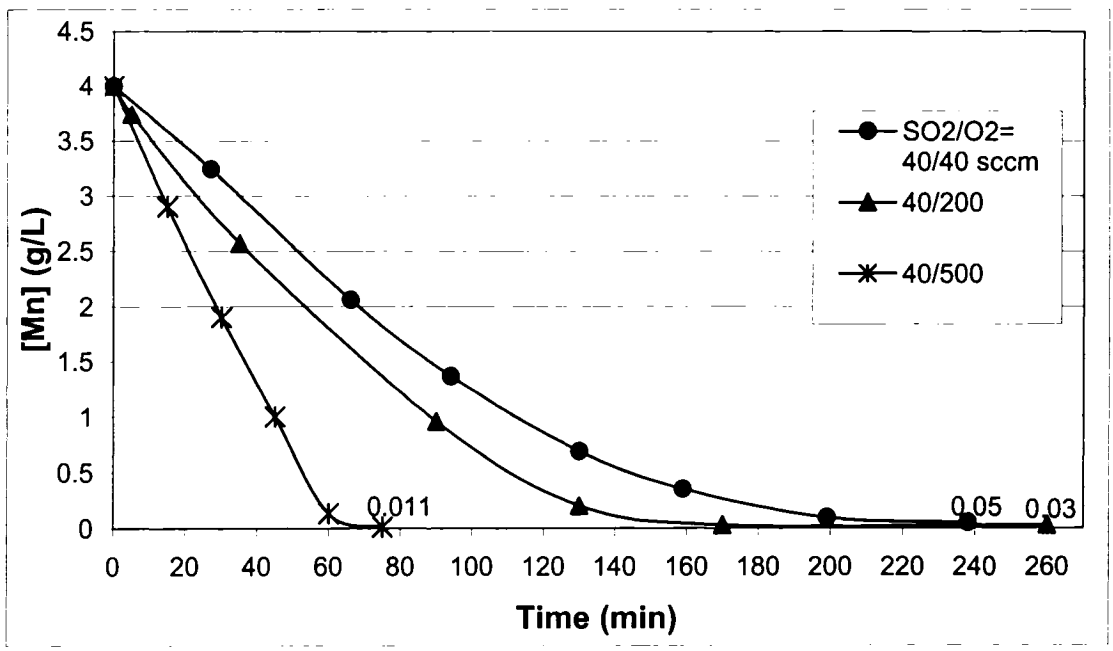

Figure 21: The effect of SO_2/O_2 ratio on manganese removal at fixed SO_2 flowrate equal to 40 sccm.

Although manganese oxidative precipitation was feasible with a SO_2/O_2 ratio of 1, Figure 21 shows that lower ratios offered faster rate. Therefore succeeding experiments were performed using the maximum O_2 flowrate of 500 sccm and variable SO_2 flowrate. It is interesting to comment here that investigations in the past have concluded that the

SO_2/O_2 system is not effective when more than 10% SO_2 is present in the gas mixture [35, 39]. As it can be deduced from the results presented in this section and those in 4.2.2 section, the SO_2 content can be as high as 50%, i.e. SO_2/O_2 ratio of 1 as long as the mixing conditions are satisfactory.

4.2.4 Effect of the SO_2 Flowrate

Several tests were conducted to study the effect of the SO_2 flowrate on manganese oxidative precipitation. For these experiments, the O_2 flowrate was set at 500 sccm while the SO_2 flowrate was varied between 40 sccm and 200 sccm (equipment maximum).

- **Manganese Removal Kinetics:**

Figure 22 presents the manganese removal kinetics for various SO_2 flowrates.

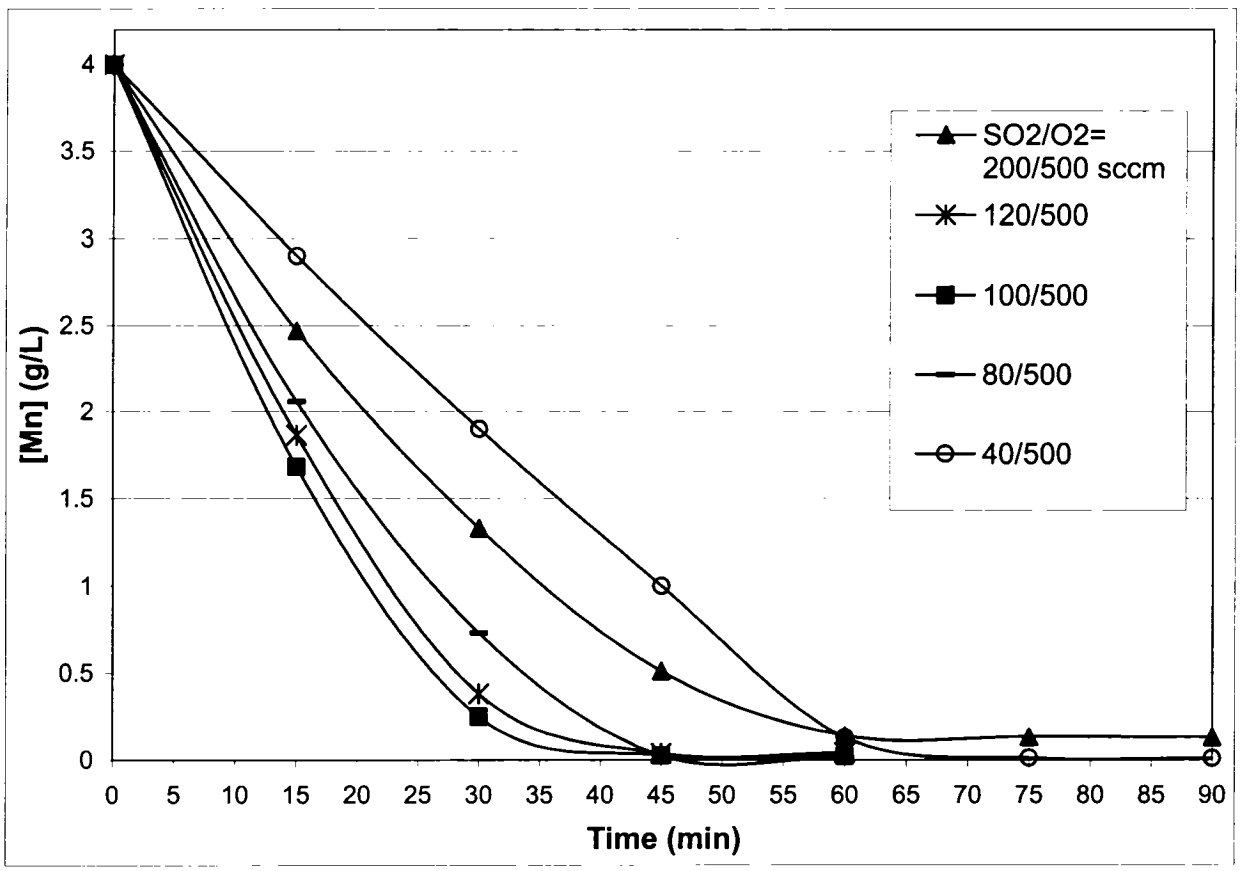

Figure 22: The effect of SO_2 flowrate on manganese removal kinetics at fixed O_2 flowrate equal to 500 sccm.

It appears from Figure 22 that the fastest manganese removal was achieved using 100 sccm of SO_2 with 500 sccm O_2. With these SO_2/O_2 flowrates, 99% of the manganese was removed within 35 minutes while it took about an hour with 200/500 sccm and 40/500 sccm SO_2/O_2 to get the same result.

- **Maximum ORP and Residual Manganese Level:**

Figure 23 presents the lowest manganese concentration obtained for various SO_2 flowrates and SO_2/O_2 ratios. These pseudo-equilibrium manganese concentrations were obtained after 45 to 90 minutes of reaction, depending on the oxidative precipitation rate (refer to Figure 22).

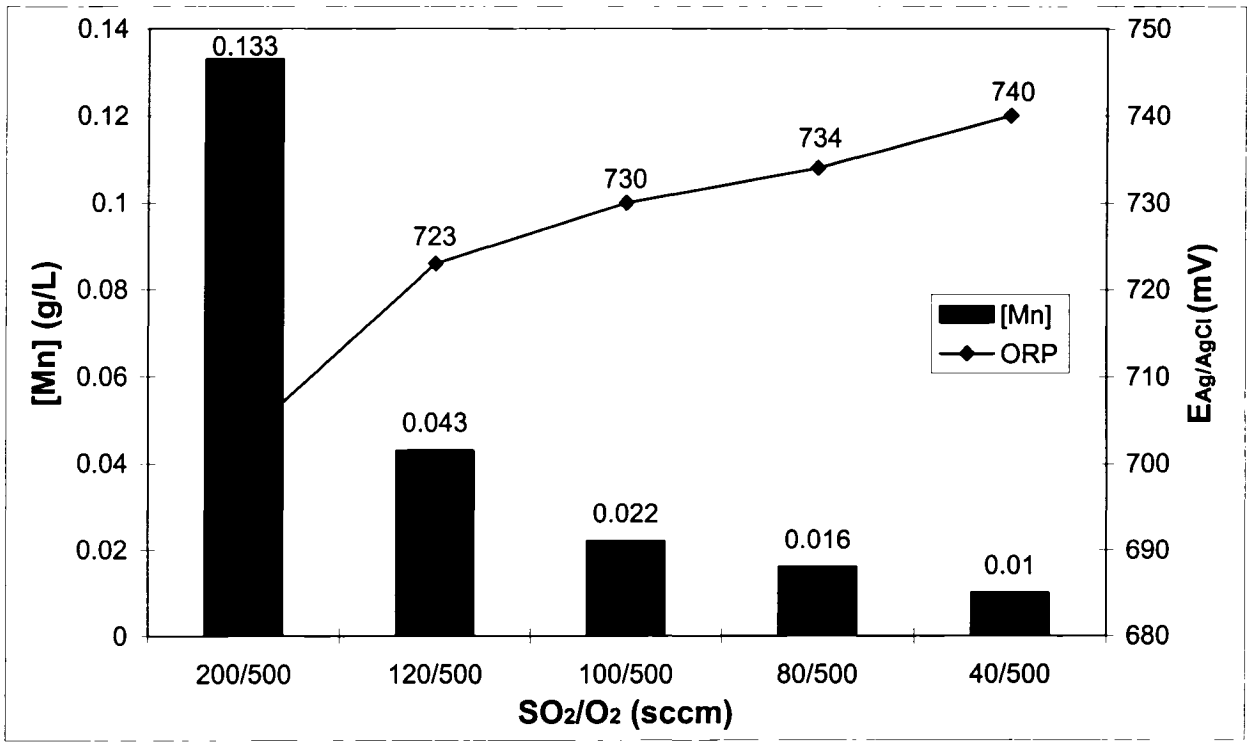

Figure 23: Residual manganese concentration and ORP level as a function of SO_2/O_2 ratio.

Figure 23 shows that, within the range investigated in this work, the lower the SO_2 flowrate and the lower the SO_2/O_2 ratio, the higher the redox potential and the better the total manganese removal although this is achieved at the detriment of slower kinetics.

Consequently, fast and maximum manganese removal could be achieved via a combination of two reactors in series with the first reactor using an elevated SO_2/O_2 ratio for fast removal of the bulk of manganese followed by a second reactor using a lower SO_2/O_2 ratio for lower manganese level (polishing).

- **Manganese Pseudo-Solubility:**

Figure 24 presents the correlation of final manganese concentration with the redox potential for various SO_2 flowrates.

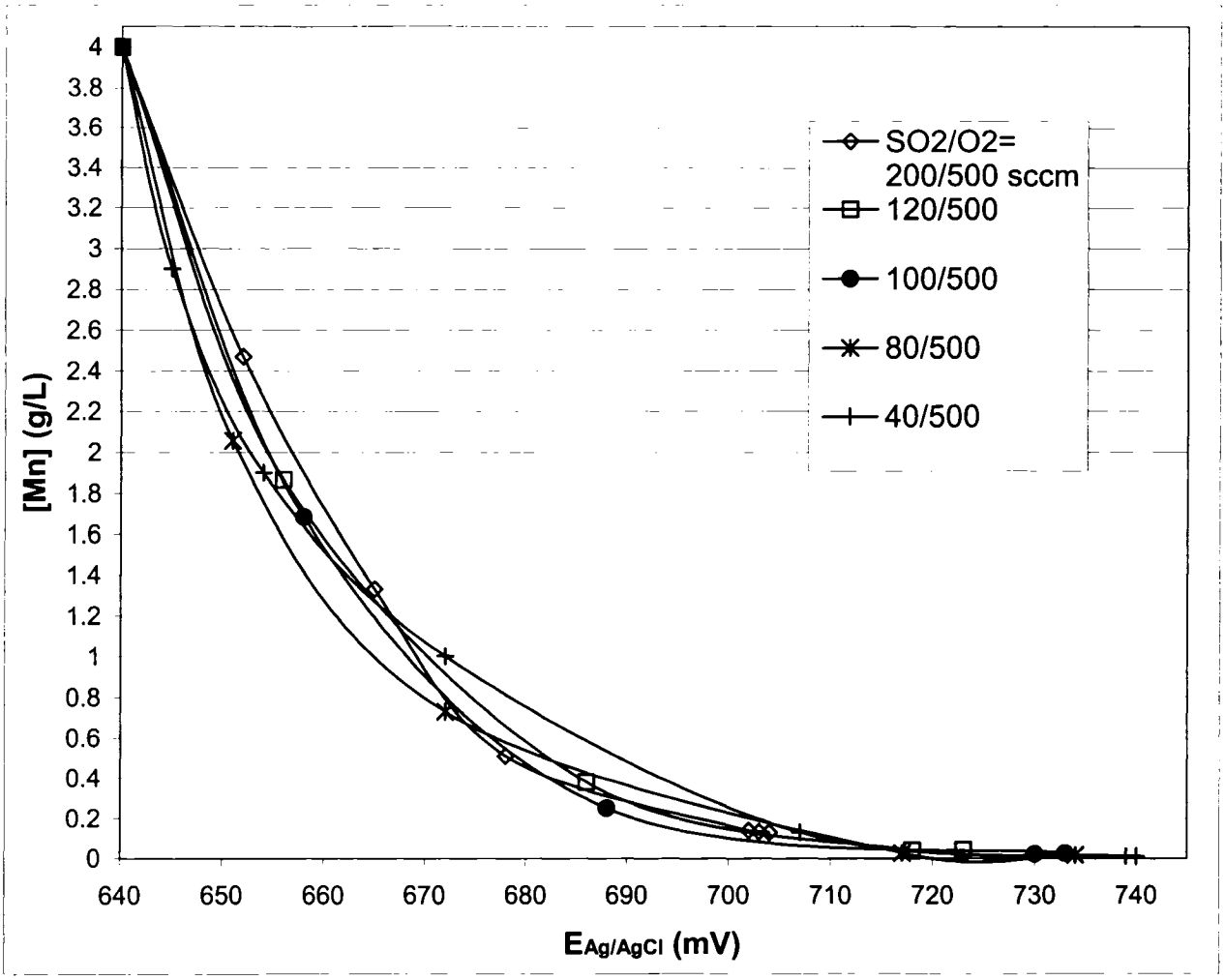

Figure 24: Correlation of final manganese concentration with ORP at various SO_2/O_2 ratios.

It appears from Figure 24 that there was no much difference in pseudo-solubility regarding the SO_2 flowrates, the difference being rather due to experimental uncertainty

on pH, ORP, analysis, etc. Using this figure, it is therefore possible to control the extend of manganese removal using the ORP value.

- **SO_2 Over-Stoichiometry:**

SO_2 was used in excess of its stoichiometric amount determined by reaction 4.2. The excess SO_2 used, denoted here as "over-stoichiometry factor" is the ratio of actual SO_2 consumption to the stoichiometric amount of SO_2 (refer to reaction 4.2). Figure 25 presents the over-stoichiometry factor as a function of the time and the SO_2 flowrates employed.

$$Mn^{2+} + SO_{2(aq)} + O_{2(aq)} + 2H_2O \rightarrow MnO_{2(s)} + H_2SO_4 + 2H^+ \qquad (4.2)$$

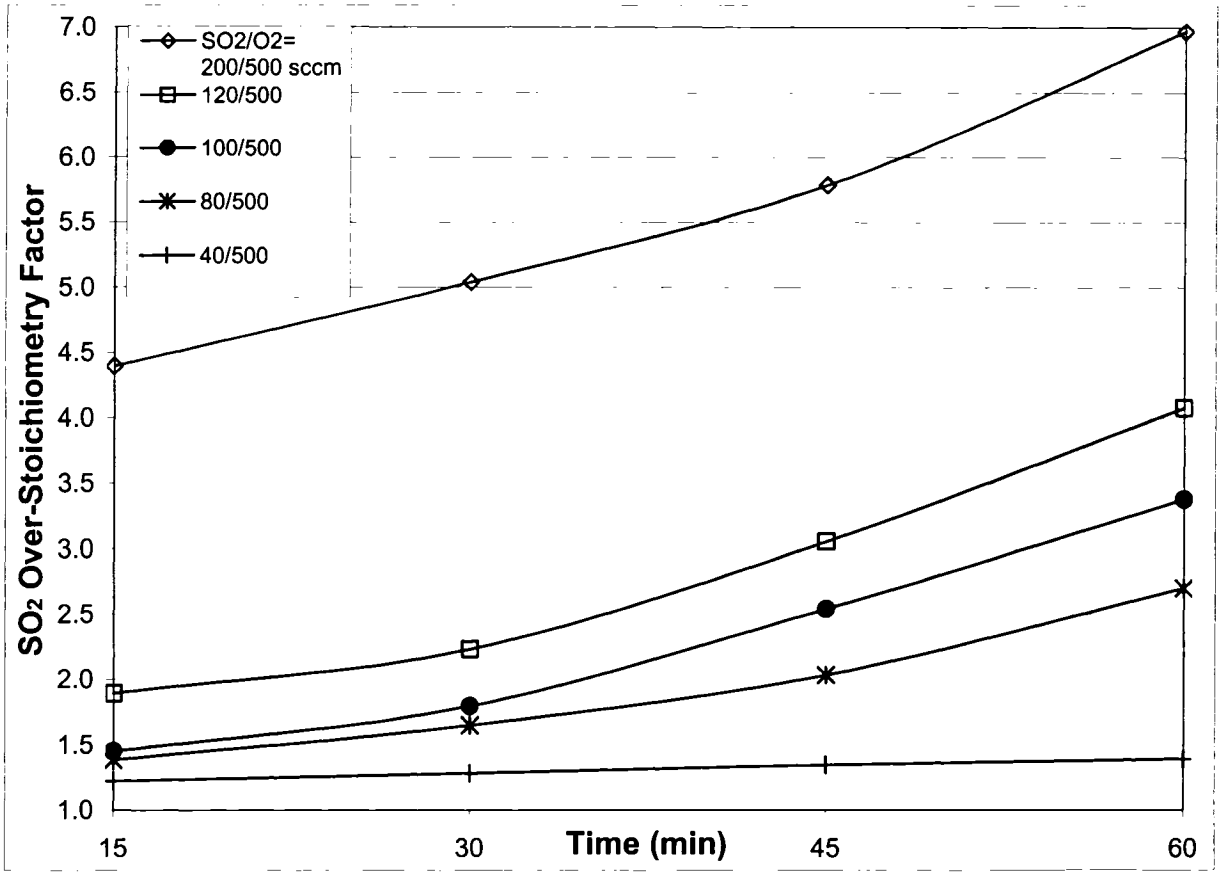

Figure 25: Variation of the SO_2 over-stoichiometry factor with time at various SO_2 flowrates.

According to Figure 25, the higher is the SO_2 flowrate (and SO_2/O_2 ratio), the higher the SO_2 over-stoichiometry factor. This means that with increasing SO_2 flowrate the utilization efficiency decreases. This is apparently so because of the parasitic

production of sulphuric acid, cf. equation 4.3, that competes with the manganese oxidative precipitation reaction.

$$SO_2(aq) + \frac{1}{2} O_{2(aq)} + H_2O \rightarrow H_2SO_4 \qquad (4.3)$$

It can also be noticed that the over-stoichiometry factor increased with the progress of the test. The reason was that the manganese concentration decreased with time hence a larger excess of SO_2 was consumed by the parasitic reaction of sulphuric acid production.

- **<u>$Mg(OH)_2$ Over-Stoichiometry:</u>**

Similarly to the SO_2 over-stoichiometry factor, the $Mg(OH)_2$ over-stoichiometry factor was determined and considered. Figure 26 presents the $Mg(OH)_2$ over-stoichiometry factor for various SO_2 flowrates. Not surprisingly, the consumption of $Mg(OH)_2$ parallels that of SO_2 as the excess of SO_2 is converted to acid which needs to be neutralized hence the large over-stoichiometry factor of $Mg(OH)_2$.

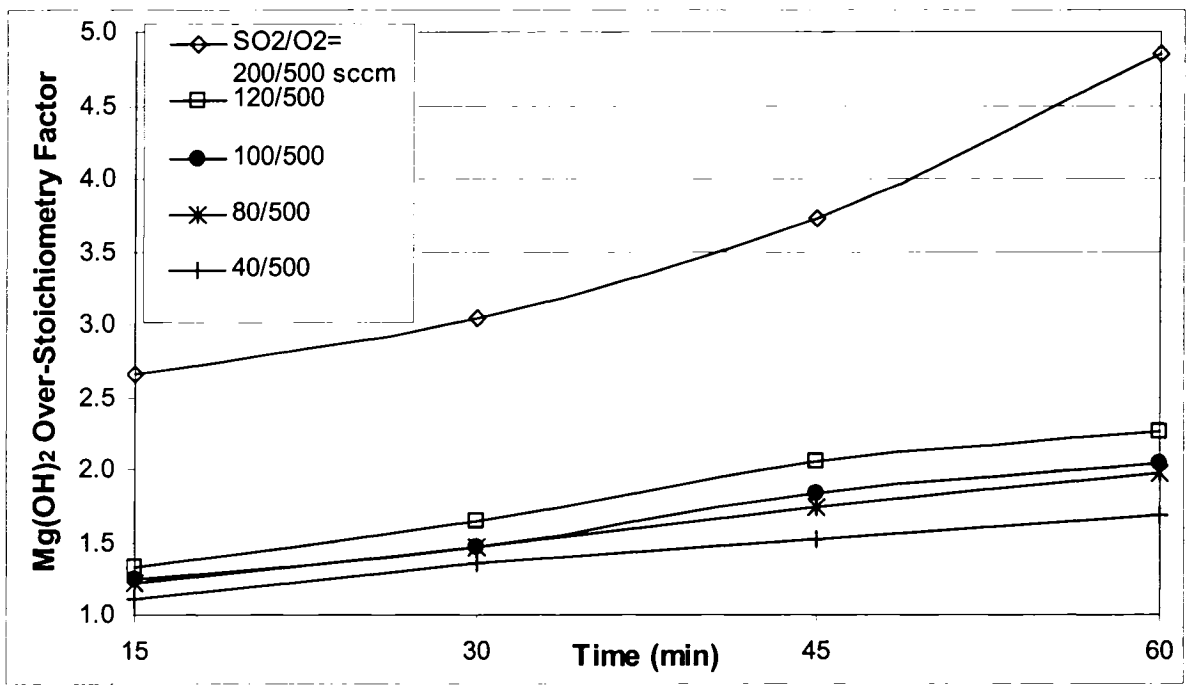

Figure 26: Variation of $Mg(OH)_2$ over-stoichiometry factor with time for various SO_2 flowrates.

The direct relationship between the two over-stoichiometry factors is better described with curves plotted in Figure 27.

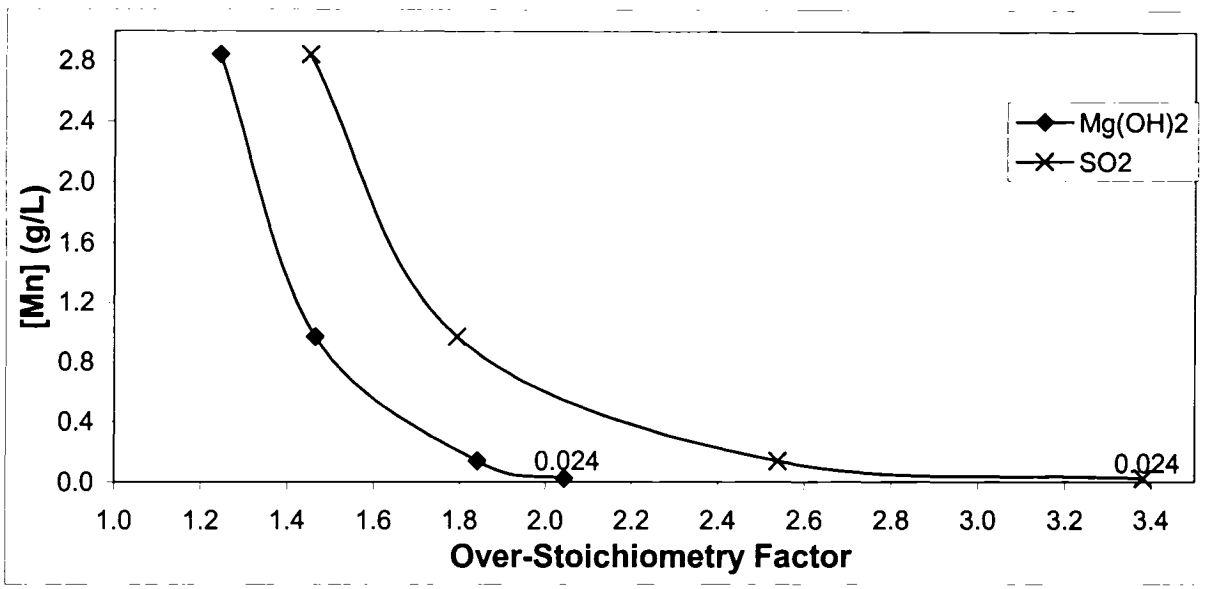

Figure 27: The relationships between final manganese concentration and $Mg(OH)_2$ and SO_2 consumption (expressed as over-stoichiometric factors) for the case of SO_2/O_2=100/500 sccm.

4.2.5 Effect of Closed vs. Open Reactor

Several tests were performed in order to determine if there was a difference between performing manganese oxidative precipitation in an "open" or "closed" reactor. The closed reactor consisted of the regular reactor except that efforts were made to minimize gas escape from the reactor vapour space to the exterior. However, gas leaks were unavoidable so no significant pressure build-up was recorded with a pressure gauge and the internal reactor pressure remained slightly over 1 bar. On the other hand, the open reactor consisted of the same reactor except that some of the cover stoppers were removed to let unreacted gasses escape freely (this situation is similar to an industrial reactor fitted with a gas vent). Figure 28 presents the effect of "closed" or "open" reactor on manganese removal kinetics using different SO_2 flowrates.

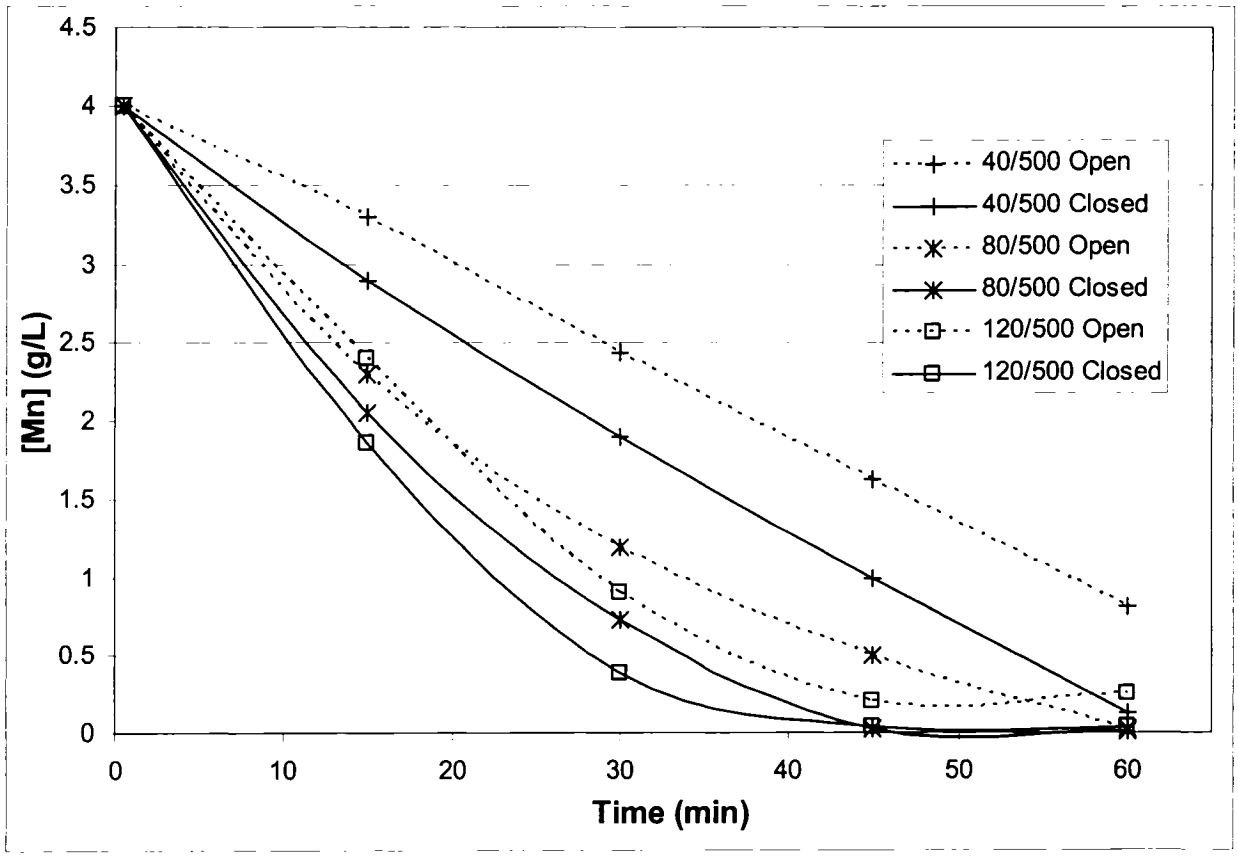

Figure 28: The effect of closed vs. open reactor configuration on manganese removal kinetics at various SO_2 flowrates.

It is clear from Figure 28 that the kinetics and maximum manganese removal were significantly enhanced using a closed reactor. Actually, as the solubility of O_2 is very low, a large part of the oxygen did not dissolve directly into the solution and escaped to the reactor vapour space. With an "open" reactor, this unreacted O_2 is lost directly to the outside air thus increasing the actual SO_2/O_2 ratio which as previously demonstrated is detrimental to manganese oxidative precipitation. On the other hand, with a "closed" reactor, the unreacted O_2 was retained in the vapour space from where it was pumped back into the solution by the top impeller. Hence, a "closed" reactor offers a better O_2 utilization so a lower SO_2/O_2 ratio and a faster manganese oxidative precipitation results.

4.2.6 Effect of Seed

To investigate the effect of seed addition on manganese oxidative precipitation, seed was prepared by running a typical manganese oxidative precipitation experiment (80°C, pH 4.0, $Mg(OH)_2$ at 15% solids, 2000 RPM, SO_2/O_2=40/500 sccm) for one hour. The resultant slurry was settled in a beaker for 30 minutes, the supernatant liquor was discarded and the remaining thickened pulp containing the precipitates was immediately introduced as "is" in a second reactor where the seeding test took place. Consequently, there was about one gram of seed for each gram of manganous ions in solution. Figure 29 presents the effect of seed during a standard manganese oxidative precipitation experiment (80°C, pH 4.0, $Mg(OH)_2$ at 15% solids, 2000 RPM, SO_2/O_2=40/500 sccm).

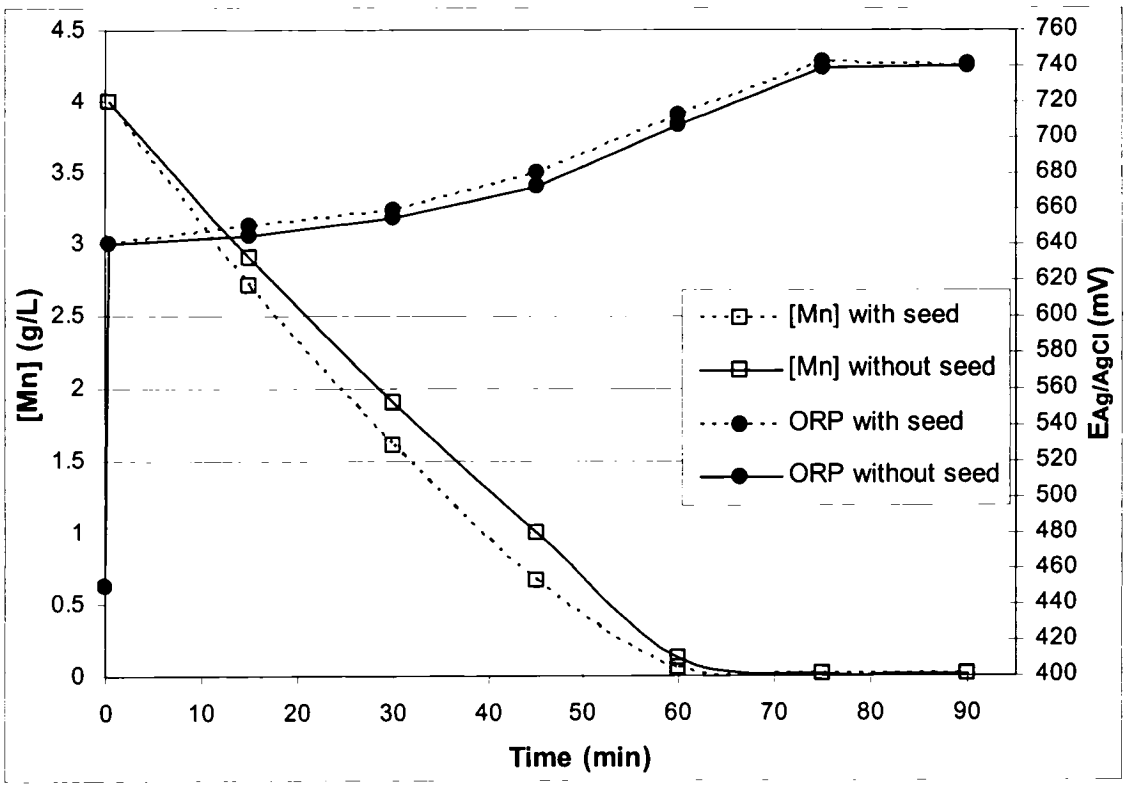

Figure 29: The effect of seed addition on manganese removal kinetics.

As it can be seen in Figure 29 the use of seed yielded a slightly higher redox potential and consequently slightly improved manganese removal kinetics. However, the final manganese concentration was the same, i.e. around 10 ppm, independent of the presence or not of seed.

4.2.7 Summary

The various tests conducted in semi-batch mode permitted to determine the optimum conditions for fast and efficient manganese removal. These optimum conditions (at 80°C) are listed below:

- **pH:** It was demonstrated that zinc undergoes precipitation at pH 4.3. Therefore, the semi-batch tests were performed at pH 4.0.
- **Agitation:** The best configuration for SO_2/O_2 gas dispersion was using two impellers turning at 2000 RPM: an upward pitched-blade impeller on the bottom and a flat blade impeller on the top.
- **SO_2/O_2 ratio:** Manganese removal was faster and more efficient using low SO_2/O_2 ratio.
- **SO_2/O_2 flowrate:** The fastest manganese removal was attained using a SO_2/O_2 flowrates equal to 100/500 sccm. Using these SO_2/O_2 flowrates, ORP (vs. Ag/AgCl) reached 730 mV so manganese could be removed from 4 g/L down to 22 ppm in about 40 minutes.
- **SO_2 and $Mg(OH)_2$ over-stoichiometry factors:** It was shown that the SO_2 and $Mg(OH)_2$ over-stoichiometry factor increased when the SO_2/O_2 ratio increased and/or the manganese concentration decreased. From an industrial point of view, it could therefore be advantageous to conduct the oxidative precipitation of manganese in two steps in order to save on reagents: The first step would consist in removing manganese down to about 1 g/L using a relatively high SO_2/O_2 ratio while the second step would bring the manganese concentration down to few ppm using a lower SO_2/O_2 ratio.
- **Closed/Open reactor:** Manganese removal using SO_2/O_2 was shown to be faster and more efficient when conducted in a "closed" reactor.
- **Seed:** Use of seed slightly improved manganese removal.

Finally, these optimum conditions were used for the investigation of manganese removal using SO_2/O_2 in continuous-mode.

4.3 Continuous-mode Tests

In order to compare the standard oxidative precipitation technique with the S.W.O.P technique for manganese removal using SO_2/O_2, three continuous-mode tests were performed. All these tests were performed at 80°C, pH 4.0, 2000 RPM, using $Mg(OH)_2$ at 15 w/w % solids, "closed" reactors, and the FB+PBU impeller configuration (refer to section 4.2.2). The main variables were the SO_2/O_2 flowrate (and consequently ORP) in the two reactors and the utilization or not of a recycle from the thickener underflow to the reactor 1 for seeding purposes.

These tests were carried out for 12 hours during which the operating conditions were constantly monitored and adjusted. Complete aqueous and solid stream sampling and analysis and measurement of settling rates was performed every 4 hours. Due to difficulties in controlling accurately the continuous-mode set-up for an extended period of time (the author was the sole operator) and that 12 hours of operation was not sufficient to reach steady-state, the results presented are considered as semi-quantitative only.

4.3.1 Non-Staged, Non-Seeded Operation at 715 mV

The first continuous-mode test consisted of manganese removal using the standard oxidative precipitation technique where most of the manganese was removed in the first reactor and where no seed was used. As the semi-batch tests showed, SO_2/O_2 flowrate equal to 100/500 sccm gave the fastest manganese removal. Consequently, SO_2/O_2 was introduced at 90/450 sccm in R1 and at 10/50 sccm in R2. These settings permitted to reach **715** mV in R1 and to maintain it around **715** mV in reactor 2. **No Recycling** from the thickener underflow was used so this test was consequently called **715/715/NR**.

4.3.1.1 Mass Balance

Figure 30 summarizes the mass balance of the 715/715/NR test where the average flowrates are indicated in sccm. Although no recycling of the thickener underflow was used, Percol 351 flocculant was still added to the thickener feedwell as a 1 g/L solution dosed around 600 g/t of precipitate (the dosage was set quite high to compensate for the

poor mixing of the flocculant with the slurry). The thickener underflow was roughly comprised of a 8 w/w % solids slurry.

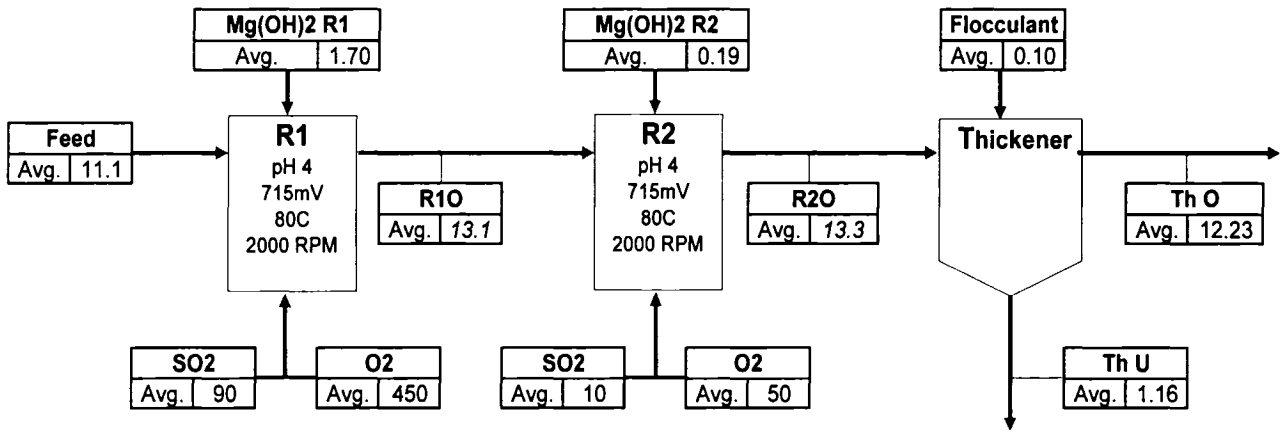

Figure 30: Mass balance of the 715/715/NR test.
(Flowrates are in sccm)

With reactors containing about 900 mL of slurry and a feed flowrate around 13.2 sccm (equivalent to mL/min), the retention time in each of the reactors was approximately 68 minutes. With a thickener containing 2 litres of slurry and a thickener overflow flowrate of 12.2 sccm, the retention time of the aqueous phase was about 155 minutes. Considering the average precipitate's settling rate, the bed volume (100 mL) and the thickener underflow flowrate, the solids retention time was estimated at 90 minutes.

4.3.1.2 Manganese Removal

Figure 31 presents the evolution of the ORP and the residual manganese in R1 and R2 throughout the test.

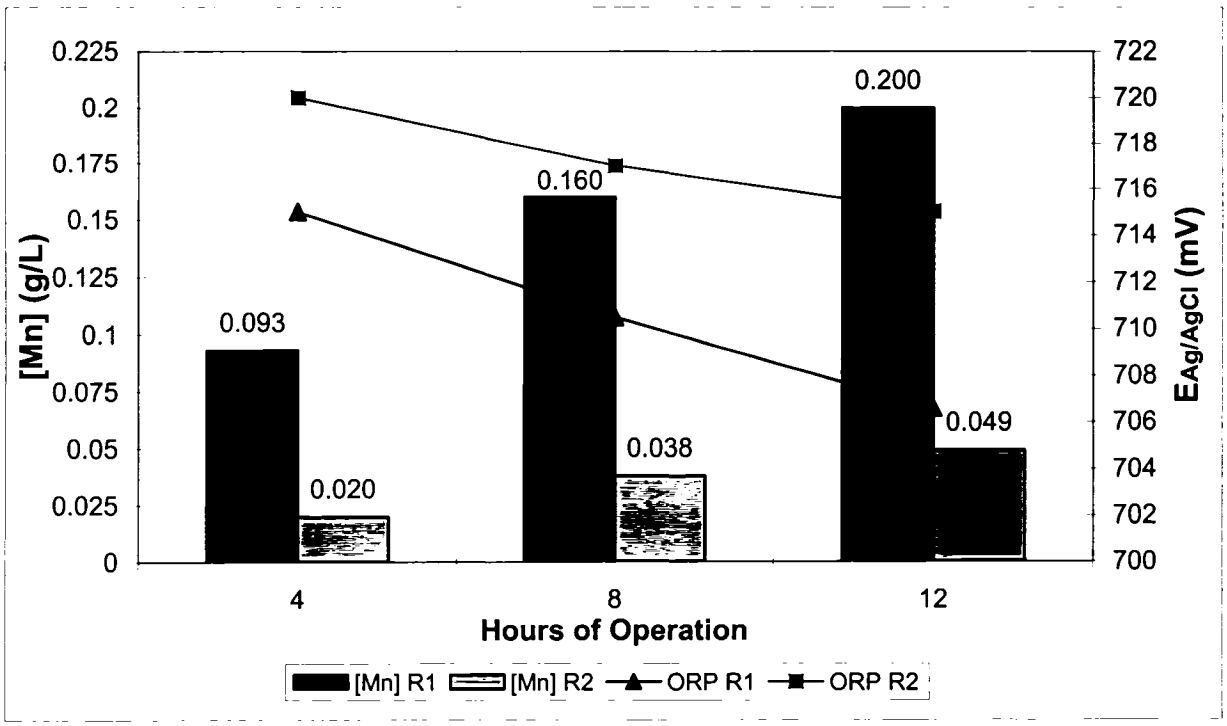

Figure 31: ORP and residual manganese during the 715/715/NR test.

The ORP was always higher in R2 than in R1 as a bit of SO_2/O_2 was also injected in R2. Consequently, the residual manganese was always lower in R2 than R1. It can be noticed that the ORP in R1 and R2 decreased throughout the test and the residual manganese increased up to 200 ppm and 49 ppm in R1 and R2 respectively. Short-circuiting in the reactor is suspected to be mainly responsible of this phenomenon as the circuit switched from batch-mode at the very beginning of the test (start-up period) to continuous-mode. Consequently, the overall retention time in the reactors was shortened hence manganese removal decreased. As an example, if only 2% v/v of the feed solution containing 4 g/L Mn short-circuited R1, which contained 0.9 L of process solution, this would have caused the R1 outlet manganese concentration to rise from 0.02 g/L to ((0.9*2%)*4+(0.9-(0.9*2%))*0.02)/0.9= **0.1 g/L**. Therefore, minor reactor short-circuiting in continuous-mode operation can have a major impact on manganese removal compared to batch-mode operation.

Despite the fact that the extent of manganese removal decreased throughout the test, Figure 32 shows that, considering a feed solution containing 4 g/L of manganese, it

took less than an hour to remove 95% of manganese in R1 and less than 2 hours to remove 99% of manganese, an excellent performance indeed.

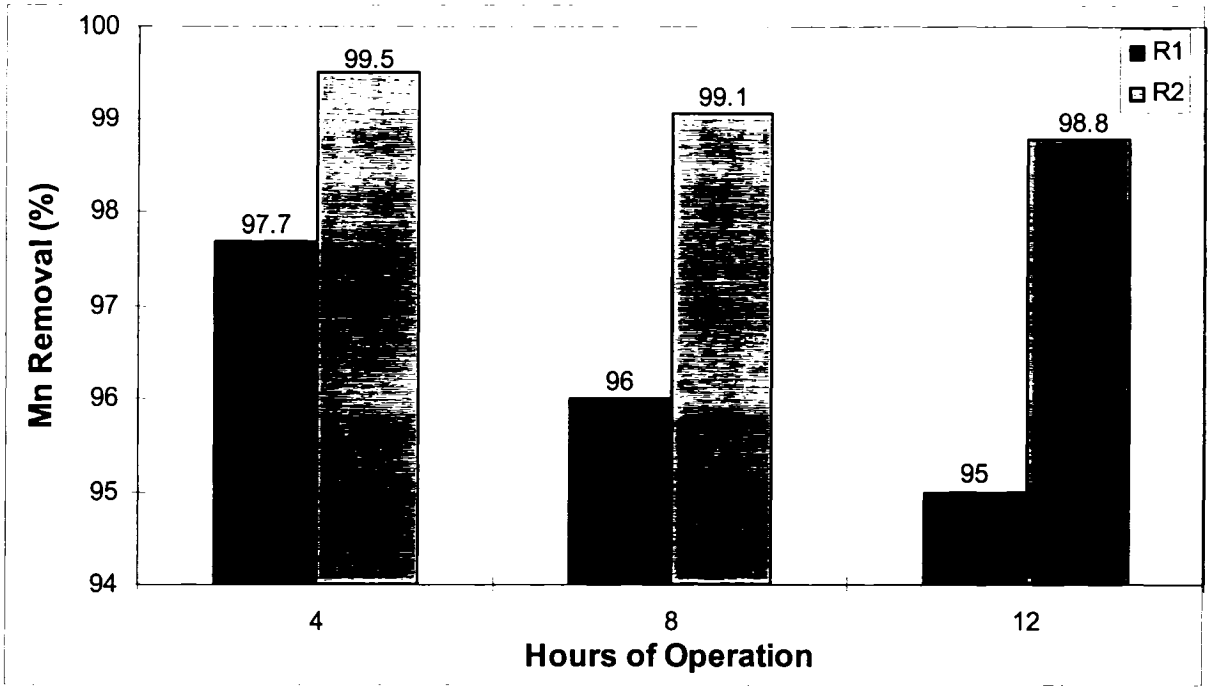

Figure 32: Manganese removal during the 715/715/NR test.

These figures clearly demonstrate also that 12 hours of operation was not enough to reach steady-state. Unfortunately, it was not possible to prolong the operation due to time constraints.

4.3.1.3 Reagent Over-Stoichiometry

Figure 33 shows that 3.5, 5.4 and 26.7 times the stoichiometric amount of $Mg(OH)_2$, SO_2 and O_2 respectively were consumed on average under the selected experiment operating conditions.

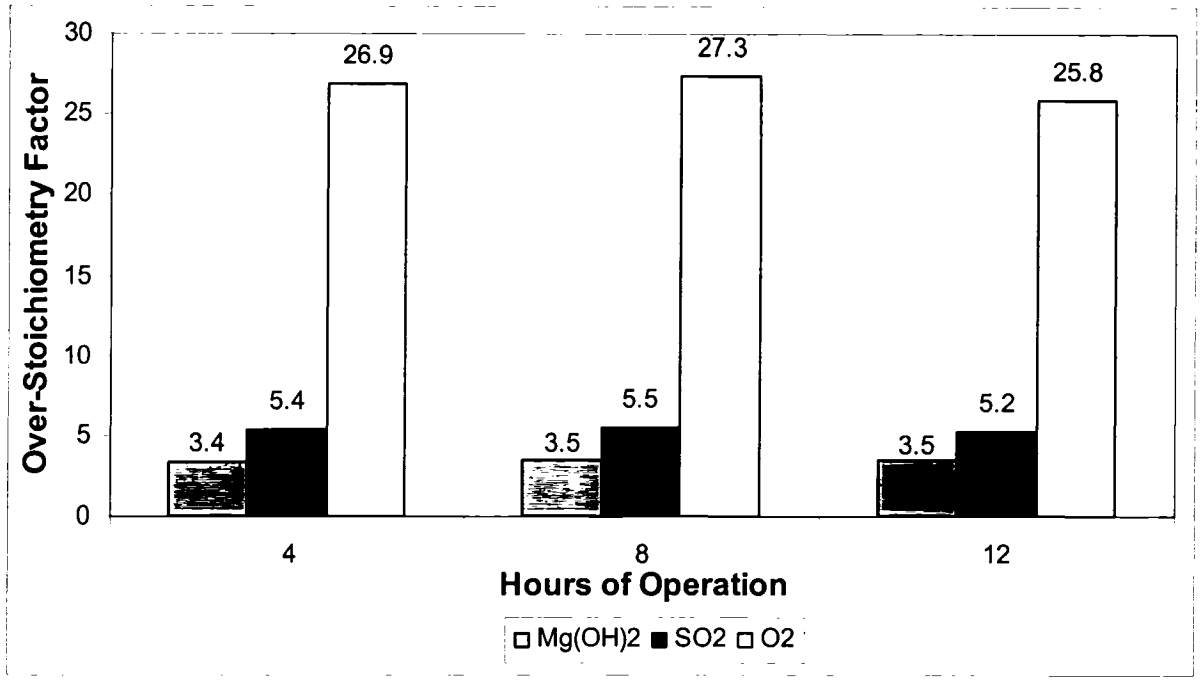

Figure 33: Reagent over-stoichiometry factors for the 715/715/NR test.

The high over-stoichiometry factors were the consequence of the detrimental side-reaction of sulphuric acid generation. This is especially detrimental in industrial practice as it would increase significantly the operating cost. Undoubtedly, further work is required to bring the utilization efficiency of the reagents closer to those obtained with the semi-batch tests.

4.3.1.4 Precipitate Characterization

- **Composition:** Table 4 presents the main composition of the precipitates obtained throughout the test.

Table 4: Composition of the precipitates obtained from the 715/715/NR test.

Hours of Operation	% Solids	% Mn	% Zn	% S	% Cu	% Mg	% Na	% Ca	% Fe
4	1.1	26.1	13.3	3.6	2.4	0.9	1.6	0.12	0.055
8	1.1	25.7	17.6	5.8	2.0	1.5	1.6	0.23	0.048
12	1.1	25.5	22.2	8.1	1.8	2.2	0.9	0.21	0.063
Avg.	1.1	25.8	17.7	5.8	2.1	1.5	1.3	0.19	0.056

Table 4 shows that manganese represented only 26 % w/w on average of the precipitate while the average zinc content was approximately 18%. It can be noticed also that the precipitate's zinc and sulphur content was rising throughout the test leading to an increase of the zinc losses. Figure 34 shows that the zinc entrained in the precipitate represented up to 2.2 % of the zinc contained in the feed solution. Such zinc losses would have to be reduced to enhance the industrial feasibility of the process.

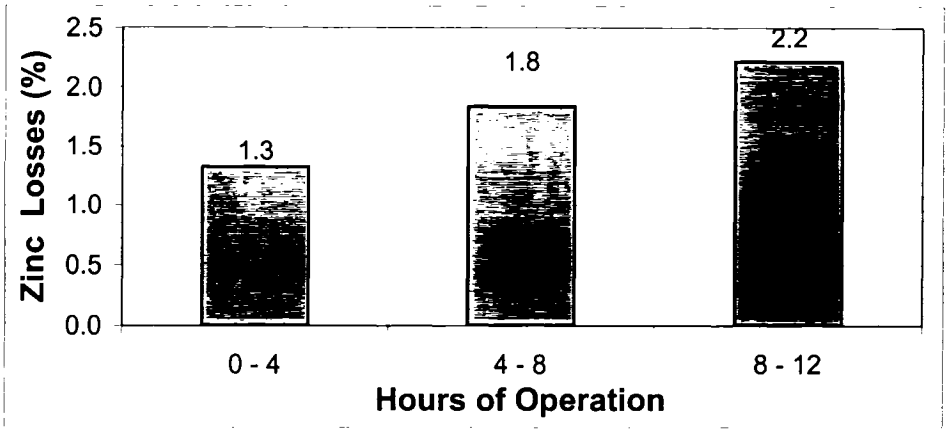

Figure 34: Zinc losses during the 715/715/NR test.

- **Particle Size Distribution (PSD):** Particle size analysis of the precipitate as a function of operating time is presented in Figure 35 and Figure 36. It appears from the analysis that the mean diameter of the precipitates was around 12 μm and was increasing throughout the test.

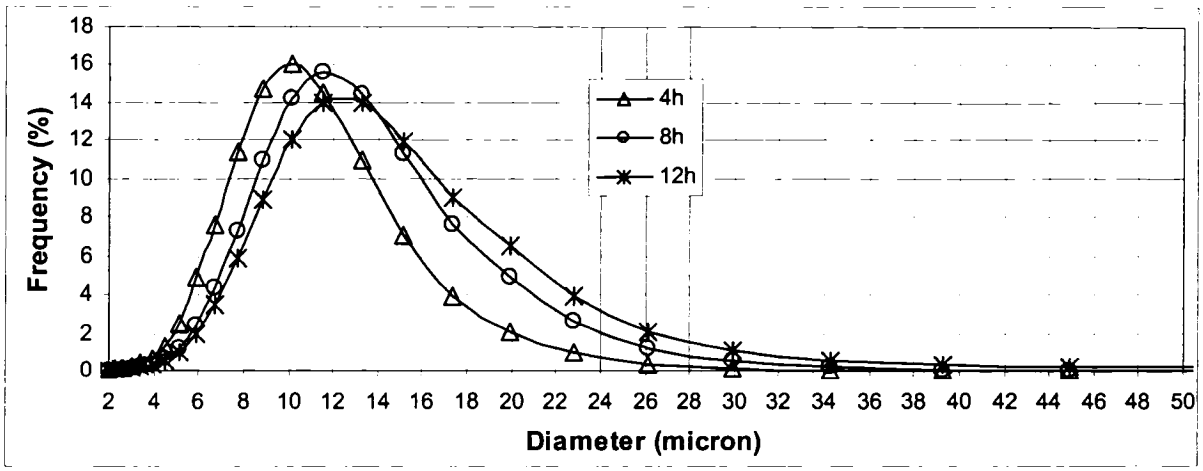

Figure 35: Precipitate's particle size distribution by volume (715/715/NR).

The smallest and largest particles in significant amount, i.e. ≈ 1% frequency, were respectively around 4 μm and 30 μm irrespective of the operating time. It can be noticed also that the particle size distribution became broader with the progress of the test.

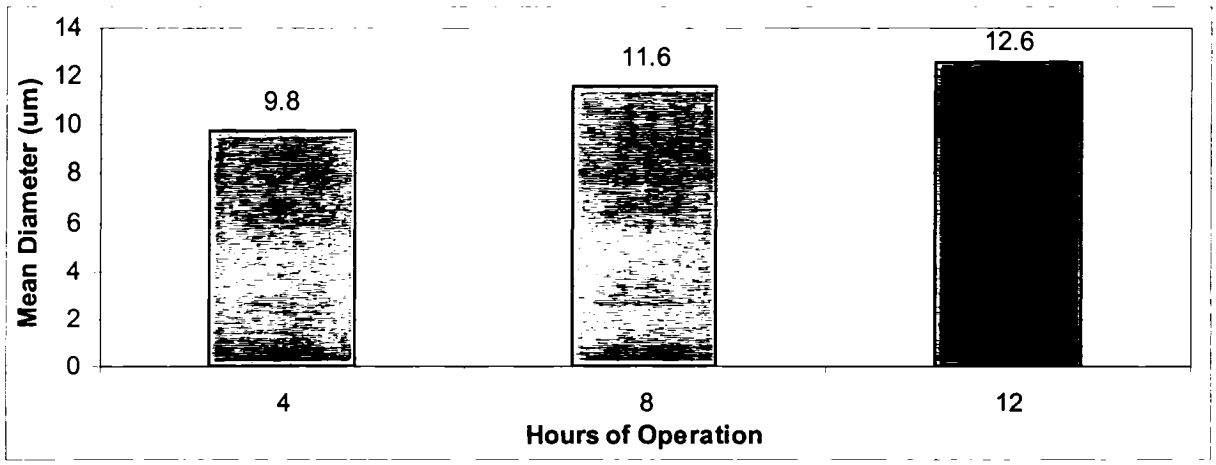

Figure 36: Precipitate mean diameter from the 715/715/NR test.

- **X-Ray Diffraction (XRD):** Because of the numerous oxidation states of manganese and the complex composition of the feed solution, phase determination of the precipitates using XRD was difficult. Figure 37 presents the XRD patterns of the precipitates produced after 4, 8 and 12 hours of continuous-mode operation along the XRD reference patterns for materials: MnO_2-$MnO{\bullet}H_2O$ (JCPDS 02-1070), $(Na_{0.7}Ca_{0.3})Mn_7O_{14}{\bullet}2.8H_2O$ a birnessite-like phase (JCPDS 13-0105), and for $ZnSO_4{\bullet}H_2O$ (JCPDS 01-0621).

It appears from this figure that the precipitates are poorly crystalline with a background located around 300 counts and a highest peak around 700 counts only. However, one can notice that the precipitate produced after 4 hours of operation exhibits some distinct peaks at 1.41Å and 2.43Å and a very broad peak around 7.3Å. The only materials found to have a similar XRD pattern are MnO_2-$MnO{\bullet}H_2O$ and birnessite. The reference for MnO_2-$MnO{\bullet}H_2O$ is controversial as it does not exhibit a peak around 7.3Å and dates from 1929. Given that no other compound was found to have peaks at 1.41Å and 2.43Å simultaneously, this phase was retained as a best guess. However, the

precipitates are more likely to be of birnessite type. Birnessite belongs to the jianshuiite-birnessite series which consist of poorly crystallized manganese oxide hydrates characterized by a two-dimensional layered structure made of edge shared MnO_6 octahedra with cations and water molecules occupying the interlayer region [60]. The jianshuiite-birnessite series can be represented by the general formula $AMn_xO_y \bullet zH_2O$ in which A represents a cation or a group of cations. The XRD reference shown in Figure 37 corresponds to a birnessite phase that can be written as $(Na_{0.7}Ca_{0.3})Mn_7O_{14} \bullet 2.8H_2O$; $(Na_{0.3}Ca_{0.1}K_{0.1})Mn^{4+}Mn^{3+}O_4 \bullet 1.5H_2O$ (JCPDS 23-1046) has a similar X-Ray pattern. Although Na, Ca, K, Li and Mg are the most common cations present in the birnessite structure, other metal cations like Mn and Ni have also been reported [61, 62]. In addition to birnessite, the jianshuiite-birnessite series include $(Mg,Mn)Mn_3O_7 \bullet 3H_2O$ also called jianshuiite, $(Mg,Ag,Ca)Mn_3O_7 \bullet 3H_2O$ (aurorite), $NiMn_3O_7 \bullet 3H_2O$ (ernienickelite) and $(Zn,Fe,Mn)Mn_3O_7 \bullet 3H_2O$ (chalcophanite) [63, 64]. Although these latter minerals exhibit different XRD patterns than the present precipitates, they do demonstrate that manganese oxide hydrate has a great ability to pick-up a wide variety of cations.

XRD patterns of the precipitates produced after 4, 8 and 12 hours of operation show also the presence of a second phase characterized by peaks at 3.08Å, 3.4Å and 4.8Å which are characteristic of $ZnSO_4 \bullet H_2O$. It must be noted here this phase was not expected as the precipitate were thoroughly washed with hot water (refer to section 3.4.3) and that zinc sulphate monohydrate is highly soluble in water [65, 66]. Its appearance here may signify that the phase is coprecipitated within the manganese oxide particle structure.

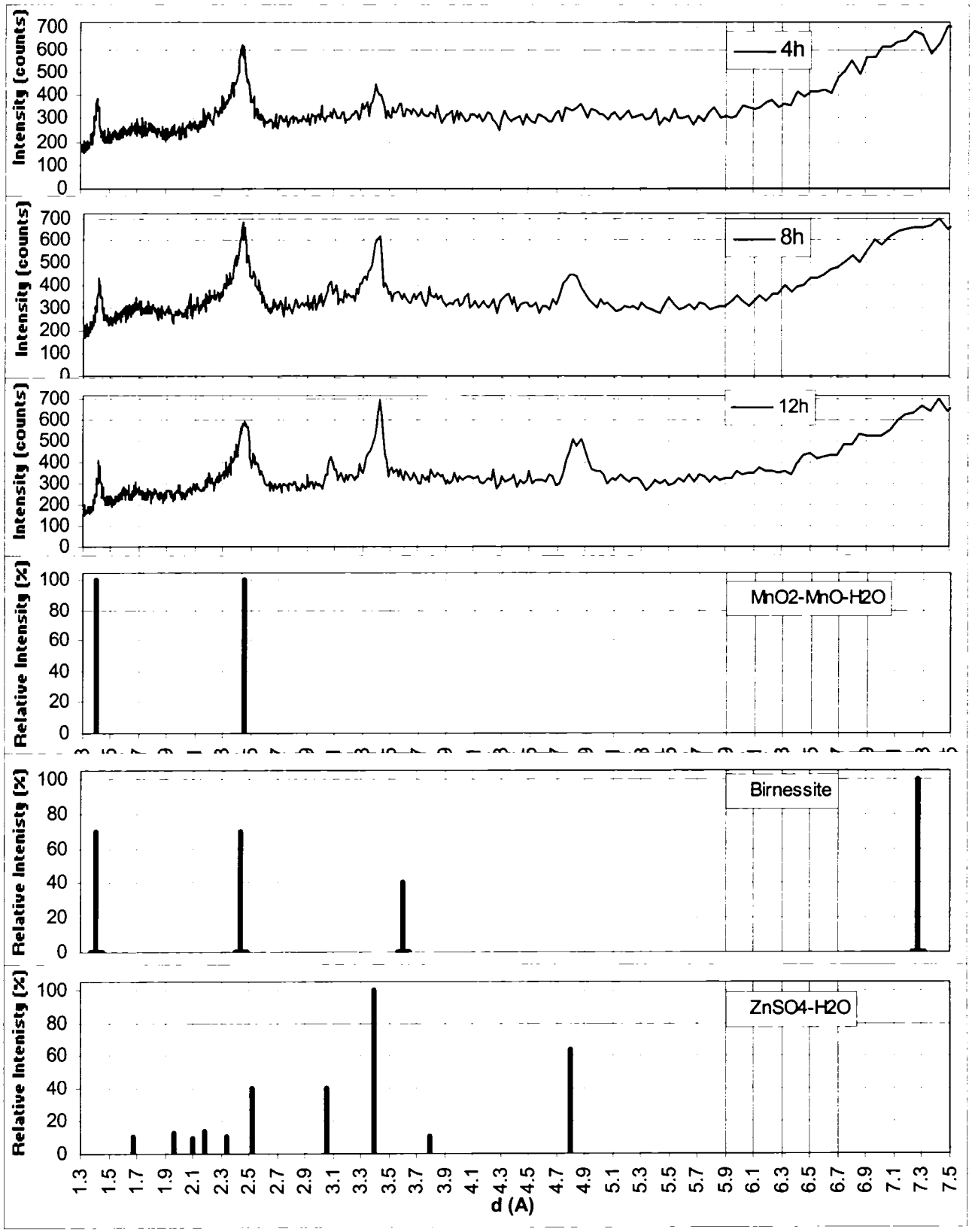

Figure 37: XRD patterns of the 715/715/NR product.

- **Scanning Electron Microscopy (SEM):** Figure 38 shows some pictures of the precipitate with two different magnifications.

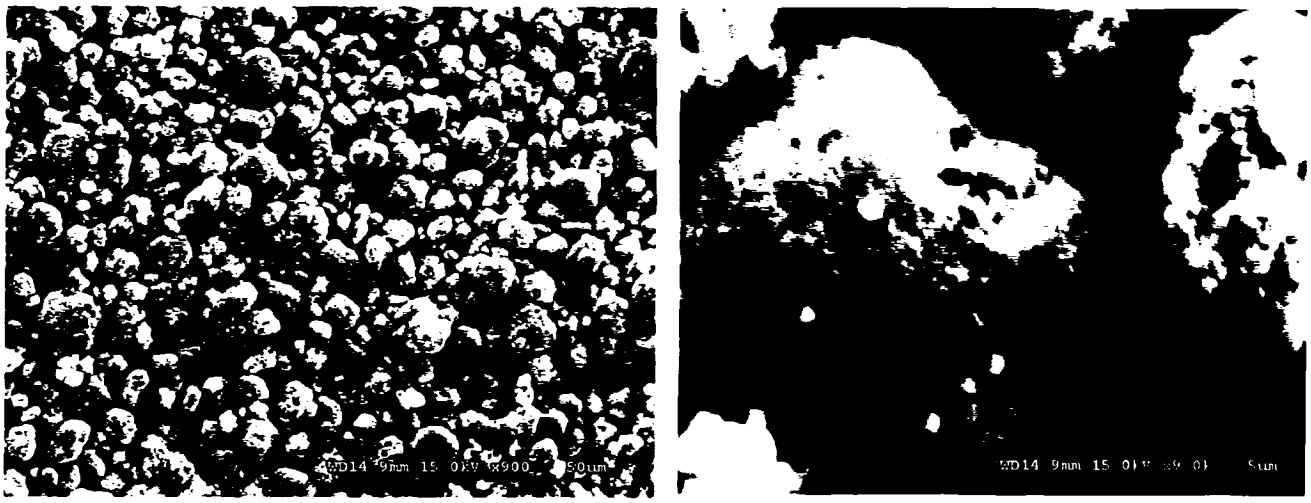

Figure 38: SEM images of the 715/715/NR product.

These pictures show that the precipitates were mainly composed of fairly rounded particles having a rough surface and average size of 10μm confirming the particle size analysis data presented earlier.

- **Cross-section Imaging and Mapping:** Figure 39 is a picture of the cross-section of some precipitates produced after 12 hours of operation.

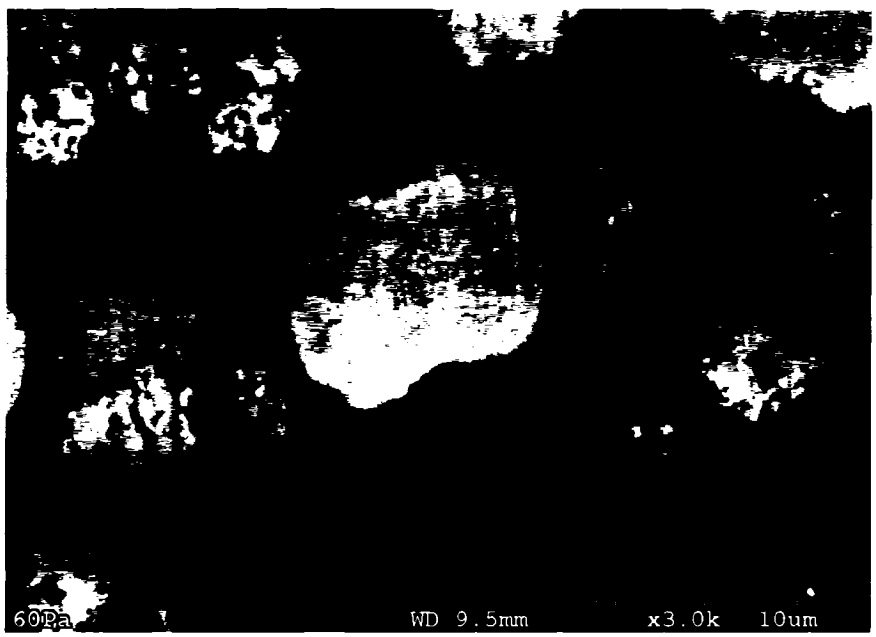

Figure 39: Precipitate's cross-section imaging (715/715/NR).

In this picture, it appears that the precipitates consisted mainly of cauliflower-type particles having significant porosity (ideal for inclusion of aqueous solution) but also of larger and denser homogeneous particles. No layers were apparent in the precipitates indicating the absence of significant epitaxial growth by surface nucleation. Significant inclusion of aqueous solution containing 150 g/L of Zn is detrimental as it is a source of zinc losses.

Figure 40 shows the elemental mapping of some precipitate's cross-section. According to these images, Mn, O, Zn and Na were evenly distributed. Sulphur, copper, magnesium, calcium and iron did not exhibit discernable signals.

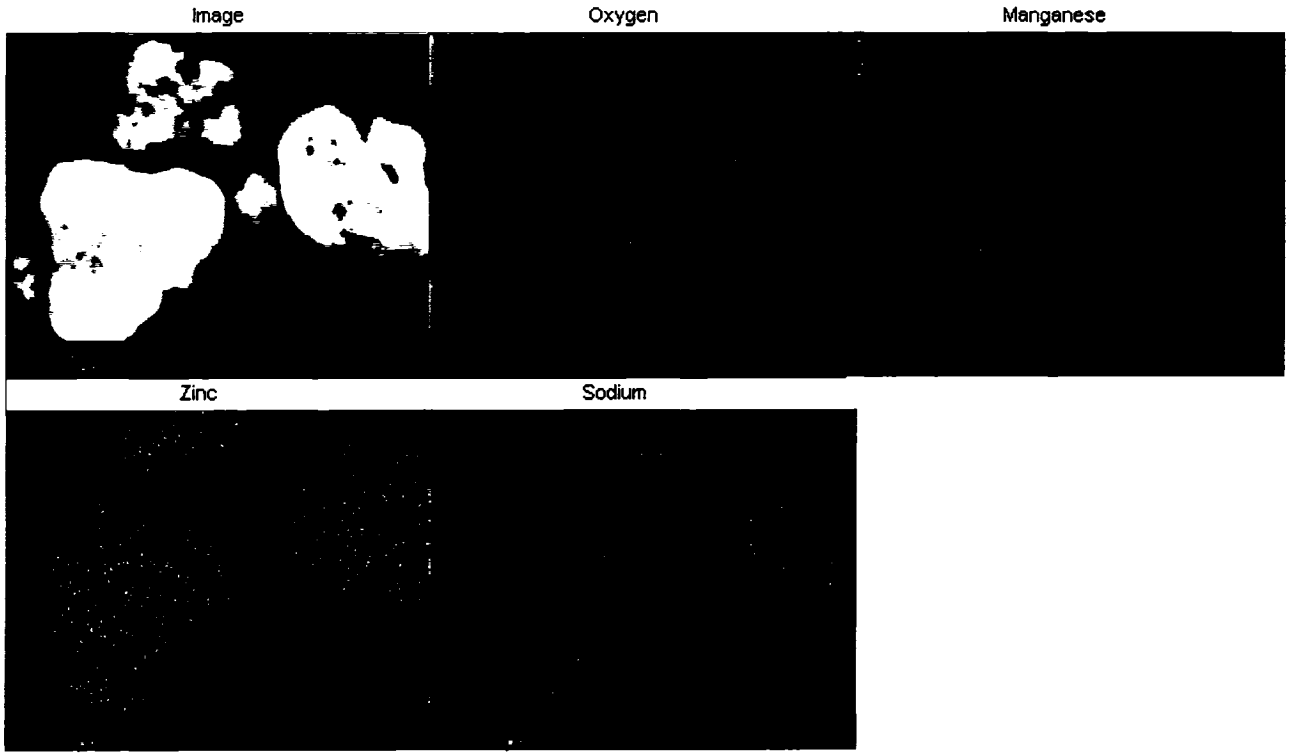

Figure 40: Mapping of precipitate's cross-section (715/715/NR).

Although the zinc signal was very weak, the even distribution of zinc in the precipitates and the fact that no discrete zinc sulphate hydrate particles were found would tend to prove that zinc sulphate hydrate would be rather co-precipitated within the birnessite-like phase rather than adsorb on its surface or precipitated as distinct particles. Alternatively, the birnessite phase may be thought to have incorporated zinc via sustitution.

Hence, considering the precipitate's composition and previous characterization, the precipitates are likely to be mostly composed of a birnessite-like phase similar to $(Na_{0.7}Ca_{0.3})Mn_7O_{14}\bullet 2.8H_2O$ with manganese having an oxidation state close to 3.8 intimately co-precipitated with zinc sulphate hydrate. The existence of more complicated phases having extensive cations and sulphate insertion in a birnessite-like structure like $(Ca, Cu, Mg, Na, Zn)(SO_4)Mn_xO_y\bullet_zH_2O$ is also very probable.

- **Settling:** Figure 41 and Figure 42 presents the settling behaviour and the corresponding settling rate of the precipitates in a 100 mL graduated cylinder. It appears that there was no significant change in precipitate's settling throughout the test.

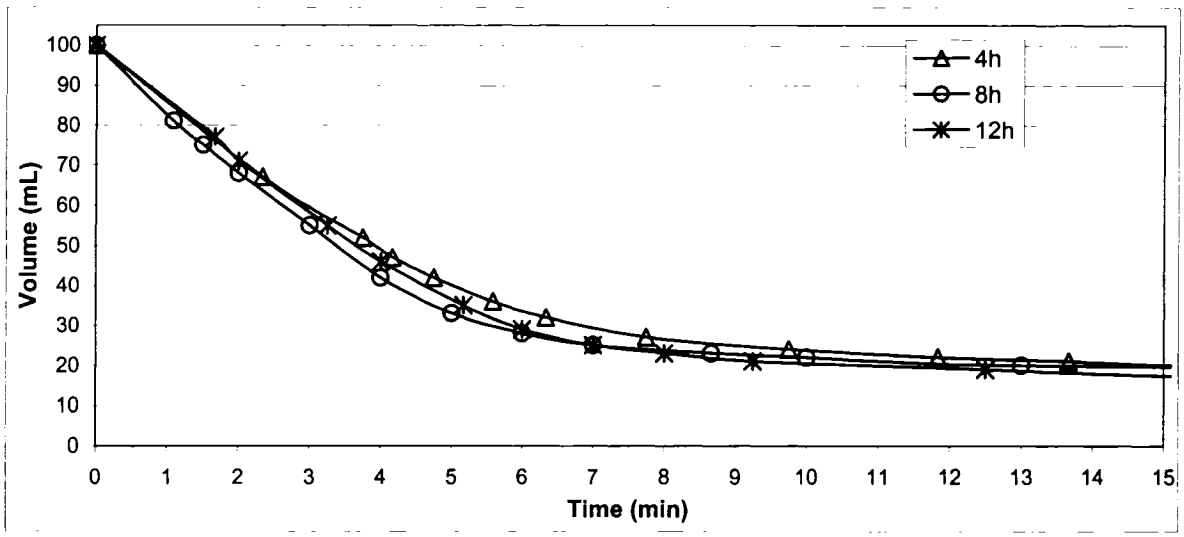

Figure 41: Settling behaviour of the 715/715/NR product.

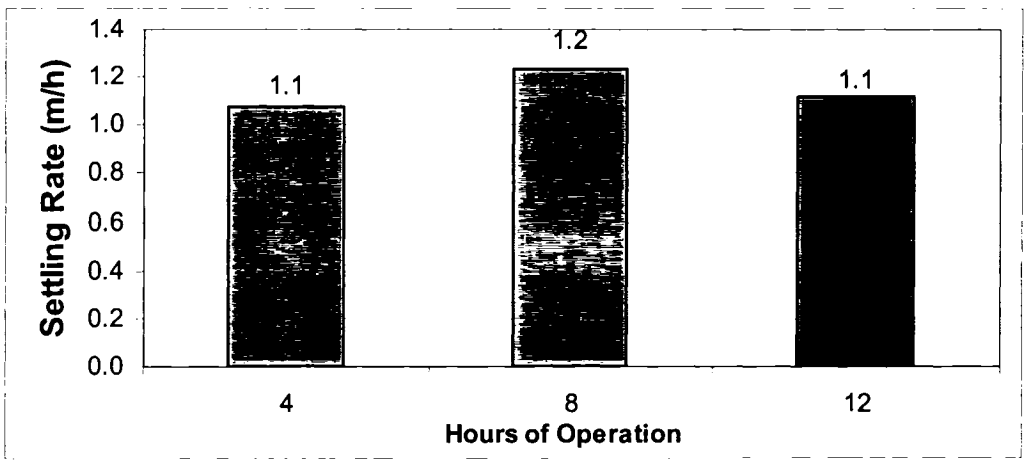

Figure 42: Settling rate of the 715/715/NR product.

Figure 43 shows that the solids flux was constant throughout the test around 16.4 $kg/m^2/h$. This parameter would become particularly relevant in the next continuous-mode tests where the percentage of solids was increasing upon solids recycling which is known to hinder the settling of particles [67].

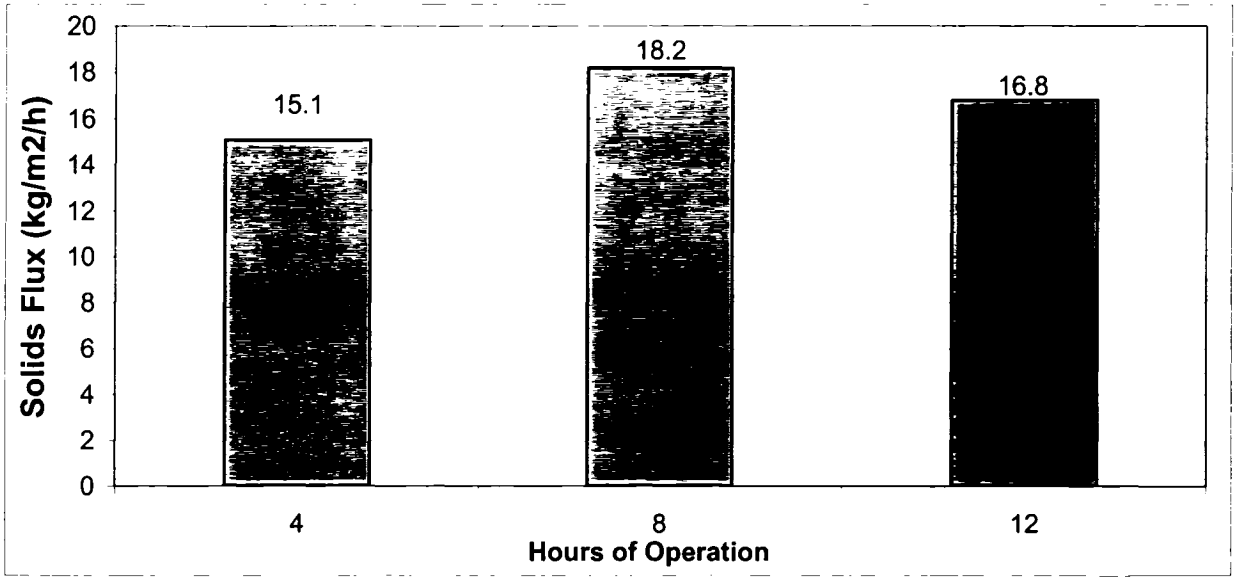

Figure 43: Solids flux (715/715/NR)

- **Scaling:** It was noticed during this test that scaling of the reactors walls, pH/ORP probes, impellers, etc. was very significant. The scale consisted of a thin black and hard layer of precipitates that could not be removed easily. Scaling of the probes was problematic as it altered the accuracy of the pH and ORP controls. Deviation from calibration of approximately 0.3 pH unit and 30 mV were regularly recorded after 3-4 hours of operation. Consequently, probes were chemically and physically cleaned every 2 hours.

4.3.2 Non-Staged Seeded Operation at 715 mV

The second continuous-mode test consisted of the oxidative precipitation of manganese mainly in the first reactor concurrently with the usage of seed coming from the thickener underflow. Like the first continuous-mode test, SO_2/O_2 was introduced at 90/450 sccm in R1 and at 10/50 sccm in R2. These settings permitted to reach **715** mV in R1 and to maintain it around **715** mV in reactor 2. All the precipitate was **R**ecycled back from the thickener underflow to the first reactor so this test was called **715/715/R**.

4.3.2.1 Mass Balance

Figure 44 summarizes the mass balance of the 715/715/R test. Final flowrates are the flowrates at the end of the test. As with the 715/715/NR test, the thickener underflow also consisted of an approximately 8 w/w % solids slurry.

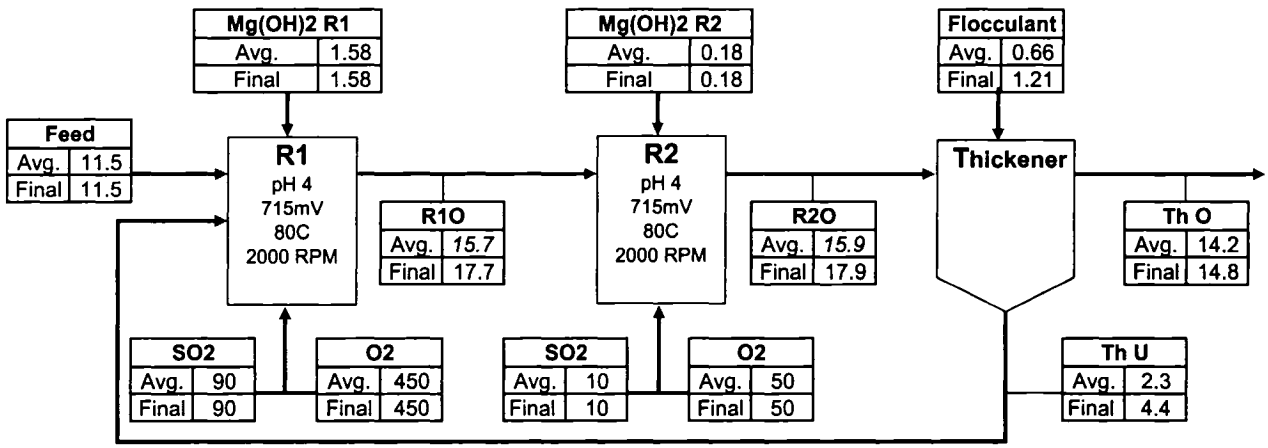

Figure 44: Mass balance of the 715/715/R test.

(Flowrates are in sccm)

The average retention time was approximately 57 minutes for the slurry in each of the two reactors, 130 minutes and 40 minutes for the aqueous and solid phases respectively in the thickener.

4.3.2.2 Manganese Removal

Figure 45 presents the evolution of the ORP and the residual manganese in R1 and R2 throughout the test.

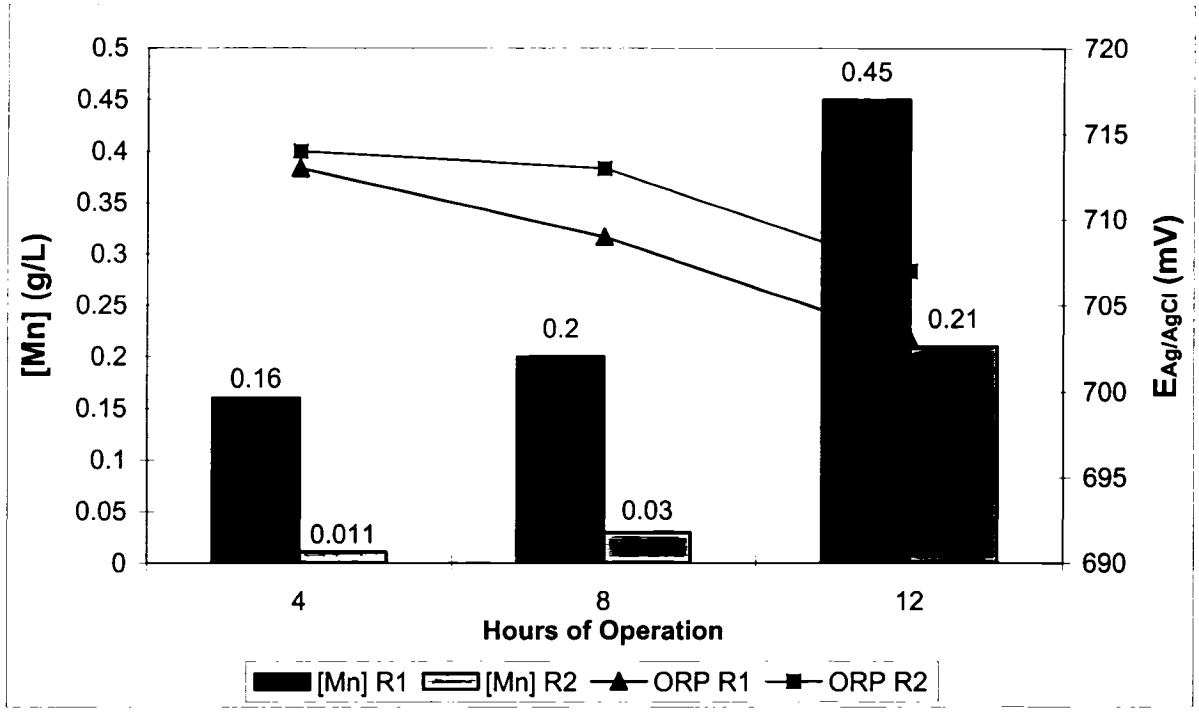

Figure 45: ORP and residual manganese during the 715/715/R test.

It can be noticed that the ORP in R1 and R2 decreased throughout the test and the residual manganese increased up to 0.45 g/L and 0.210 g/L in R1 and R2 respectively. Hence, residual manganese in R2 in the 715/715/R test was four times larger than in the 715/715/NR test after 12 hours of operation. This is probably due to larger short-circuiting and shorter retention time due to larger flowrates dictated by recycling.

Despite the decreasing degree of manganese removal with operation time, Figure 46 shows that, considering a feed solution containing 4 g/L of manganese, 95% of manganese was still removed in R2 after 12 hours of operation compared to 99% in the 715/175/NR test.

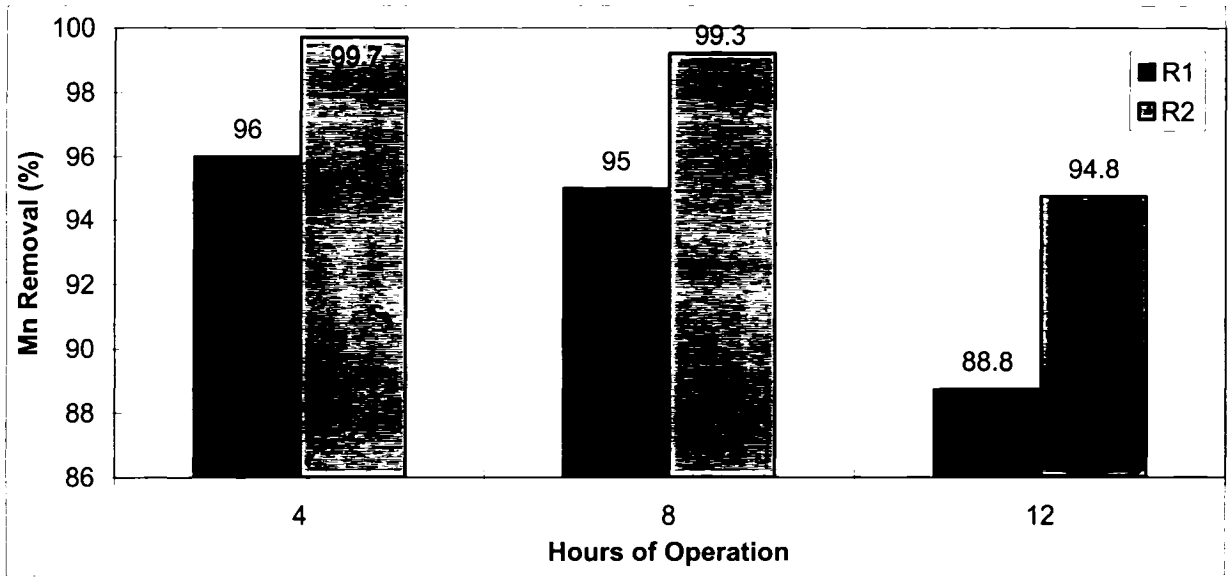

Figure 46: Manganese removal during the 715/715/R test.

4.3.2.3 Reagent Over-Stoichiometry

Figure 47 shows that 3.4, 5.0 and 25.4 times the stoichiometric amount of $Mg(OH)_2$, SO_2 and O_2 respectively were consumed on average under the selected experiment operating conditions.

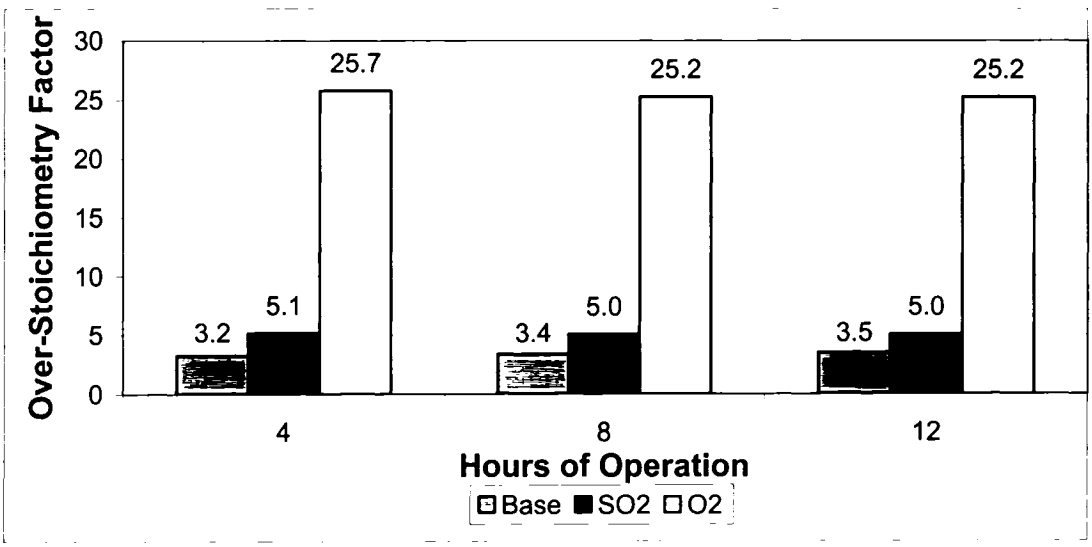

Figure 47: Reagent over-stoichiometry factors for the 715/715/R test.

After comparing the results of Figure 47 with those of Figure 33, it is deduced that seeding did not have much effect on reagent consumption.

4.3.2.4 Precipitate Characterization

- **Composition:** Table 5 presents the variation in composition of the precipitates with operation time.

Table 5: Composition of precipitates obtained from the 715/715/R test.

Hours of Operation	% Solids	% Mn	% Zn	% S	% Cu	% Mg	% Na	% Ca	% Fe
4	1.3	25.0	18.0	4.2	2.6	1.0	0.7	0.09	0.05
8	2.5	27.6	23.0	7.2	2.0	2.5	1.6	0.08	0.09
12	4.2	32.0	21.7	1.8	2.5	0.4	1.2	0.09	0.11
Avg.	2.7	28.2	20.9	4.4	2.3	1.3	1.2	0.09	0.08

Table 5 shows that manganese represented up to 28 % w/w on average of the precipitate's composition while the average zinc content was approximately 21 % w/w which is similar to the precipitate's composition in the 715/715/NR test (refer to Table 2). After 4 hours of operation, the percentage of solids was 1.3 % w/w which corresponds roughly to the amount of solids precipitated in the first pass. Therefore, 4.3 % w/w of solids after 12 hours of operation corresponds to 2.3 times the recycling of solids.

Figure 48 shows that the zinc contained in the precipitates increased from 2.2 % up to 3.2 % of the zinc fed to the reactor 1, i.e. the aqueous zinc contained in the feed solution and in the recycle. This increase may be partly due to the increased mass of the precipitates due to solids recycling and consequently to the increased probability of zinc uptake (refer to Table 5).

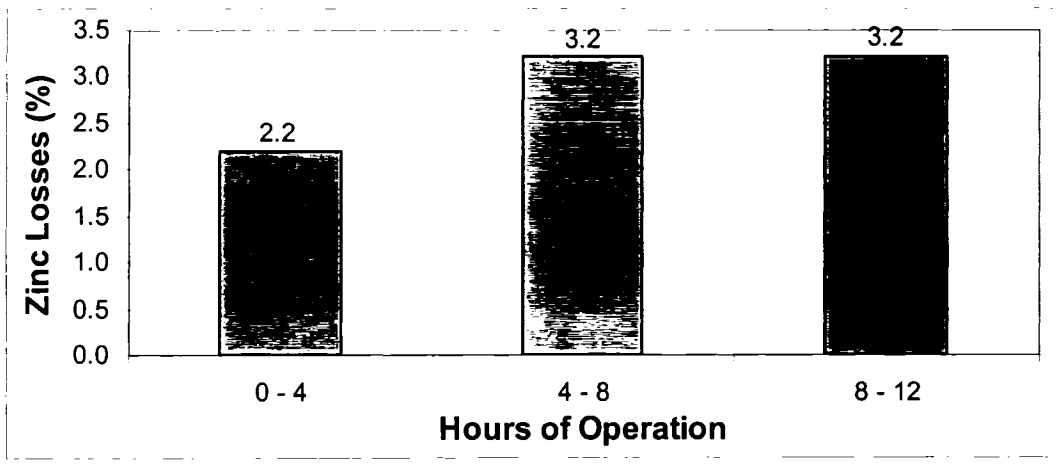

Figure 48: Zinc losses incurred during the 715/715/R test.

- **Particle Size Distribution (PSD):** Particle size distribution of the precipitates as a function of operating time is presented in Figure 49 and Figure 50. It appears that the mean diameter by volume of the precipitates was around 16 μm and was increasing throughout the test. This mean diameter was larger than the one obtained in the unseeded test (12.6 μm).

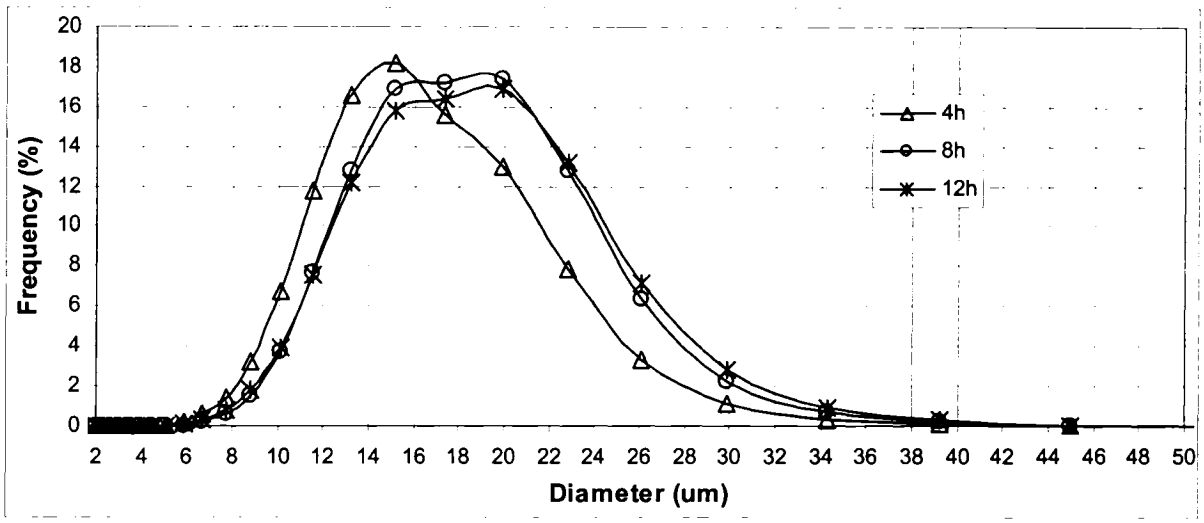

Figure 49: Particle size distribution by volume of the 715/715/R product.

The smallest and largest particles in significant amount were respectively around 8 μm and 32 μm independent of the operating time.

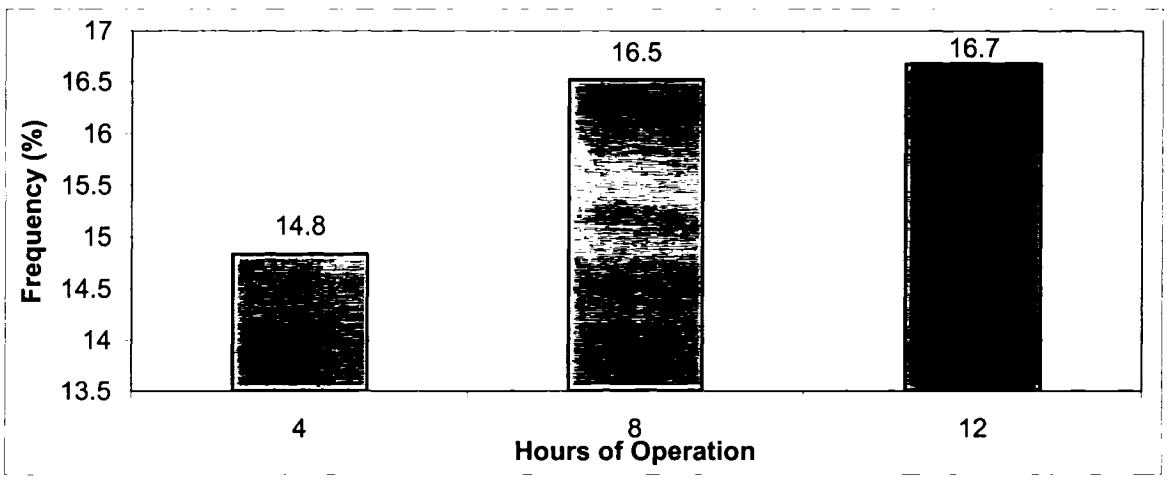

Figure 50: Mean diameter of the 715/715/R product.

- **X-Ray Diffraction (XRD):** Figure 51 presents the XRD patterns of the precipitates produced after 4, 8 and 12 hours of continuous-mode operation and the XRD reference patterns for birnessite-like material and $ZnSO_4 \bullet H_2O$.

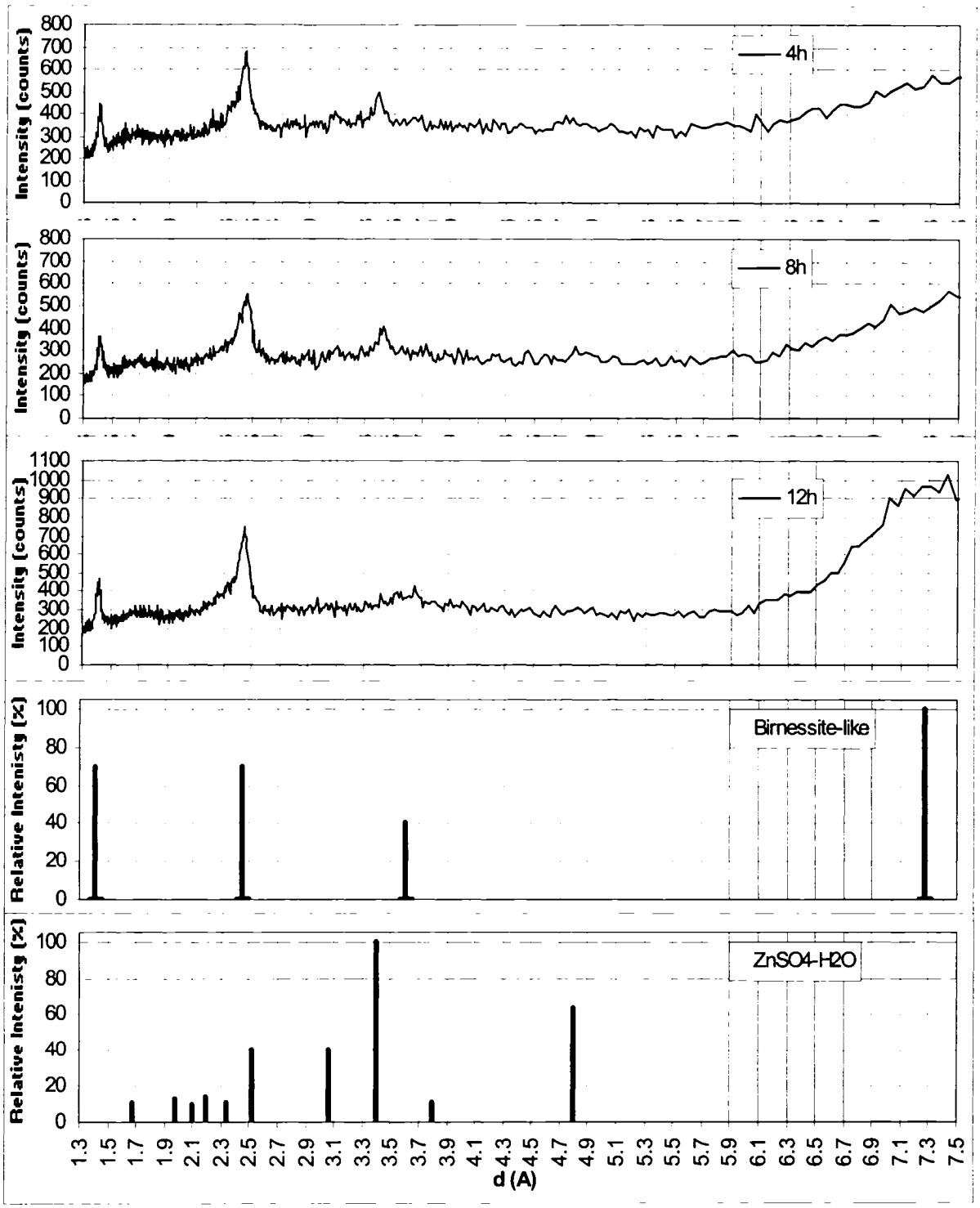

Figure 51: XRD patterns of the 715/715/R product.

The precipitates were once more poorly crystalline with a background located around 300 counts and a highest peak around 1000 counts only. In comparison to the 715/715/NR test, it can be noticed that the $ZnSO_4 \bullet H_2O$ phase was not as significant although the uptake of zinc is slightly superior with 21% of contamination vs. 18% in the 715/715/NR test. The precipitates produced after 12 hours of operation exhibited clearly the birnessite-like XRD pattern with the highest peak located around 7.3Å, two distinct peaks at 1.41 Å and 2.44 Å as well as a small peak at 3.6 Å.

- **Scanning Electron Microscopy (SEM):** Figure 52 shows SEM pictures of the precipitate with two different magnifications.

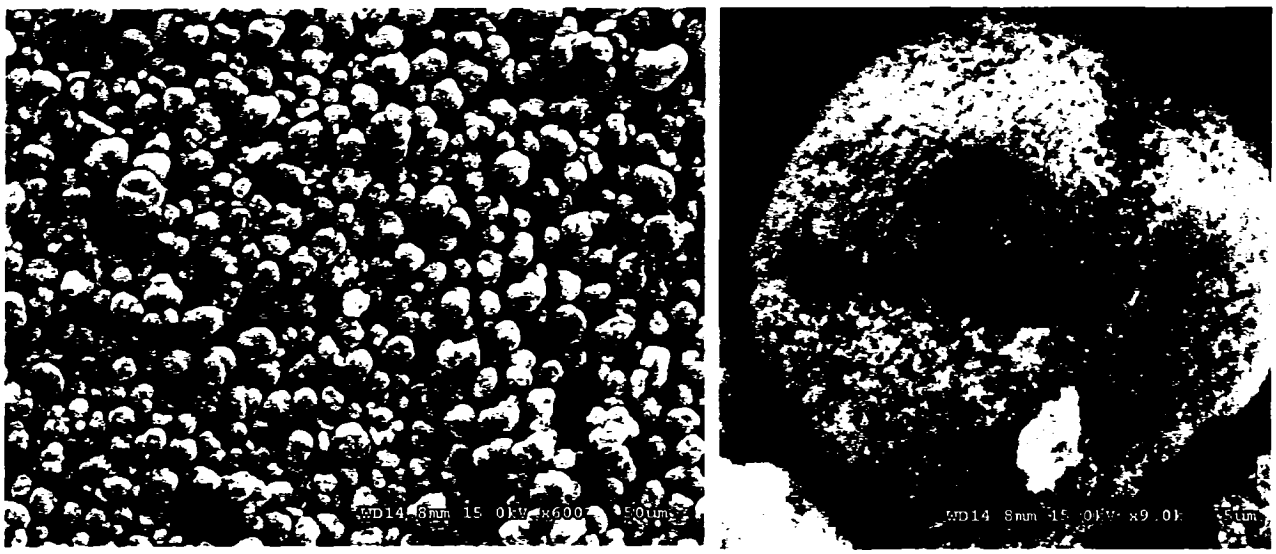

Figure 52: SEM image of the 715/715/R product.

- **Cross-section Imaging and Mapping:** Figure 53 is a picture of the cross-section of the precipitate produced after 12 hours of operation. In comparison to the precipitate produced in the 715/715/NR test, there was no cauliflower-type particle as the precipitates consisted only of dense homogeneous particles indicating better growth and densification characteristics.

Figure 53: Cross-section imaging of the 715/715/R product.

Similarly, mapping indicated a homogeneous distribution of the elements in the precipitates (Figure 54). This suggests that the zinc contamination is not in the form of a discrete phase but part of the birnessite structure.

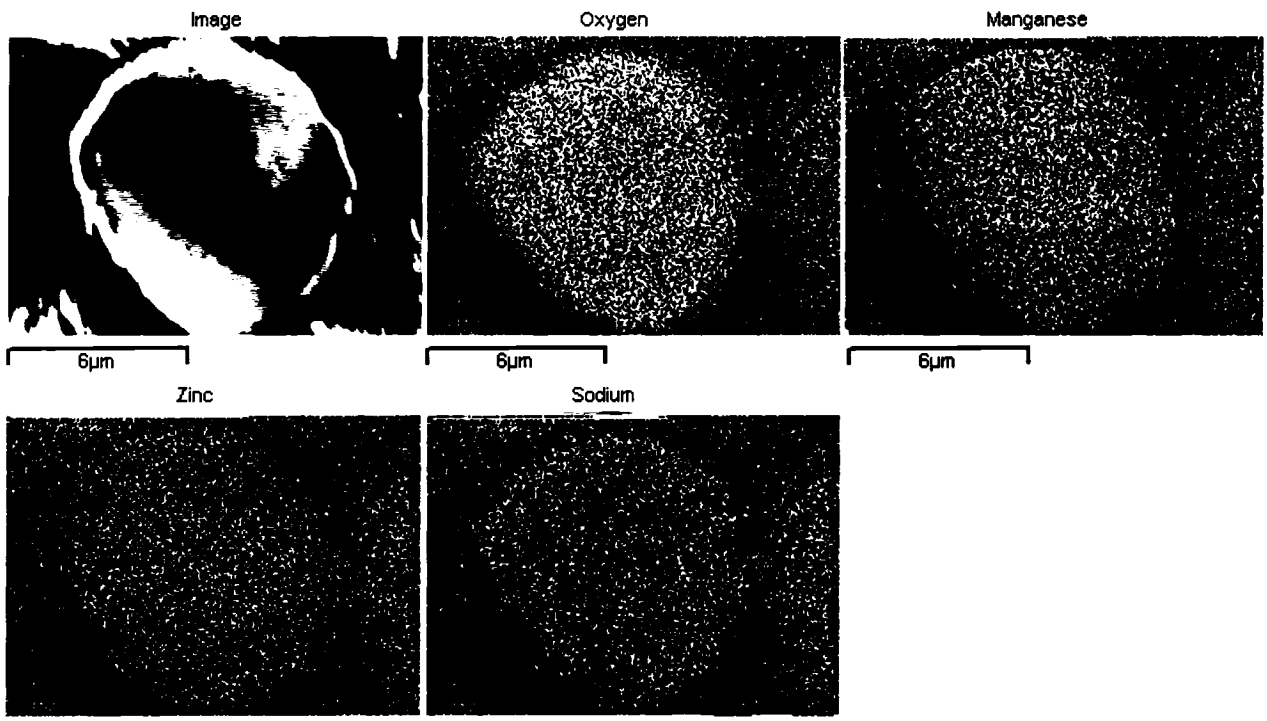

Figure 54: Mapping of precipitate's cross-section (715/715/R).

- **Settling:** Figure 55 and Figure 56 summarize the settling behaviour and the corresponding settling rate of the precipitates in a 100 mL graduated cylinder.

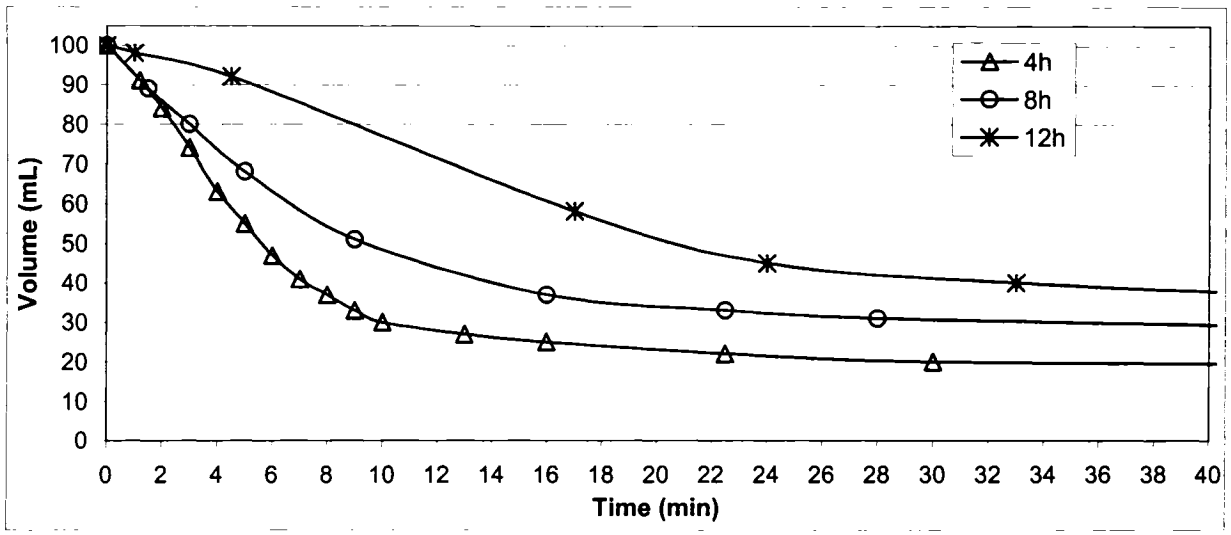

Figure 55: Precipitate's settling behaviour (715/715/R).

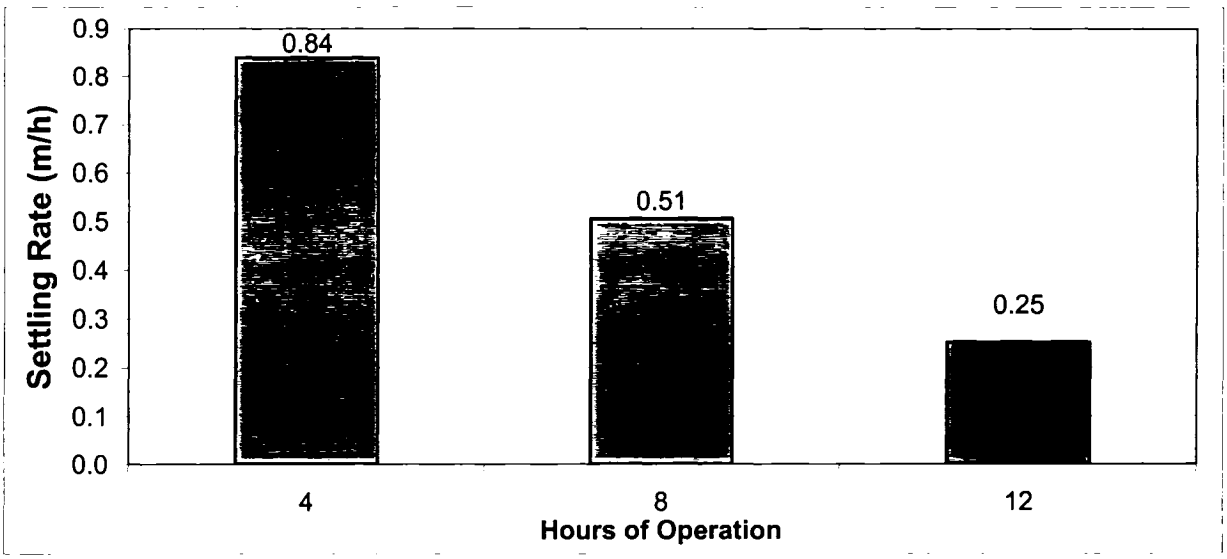

Figure 56: Precipitate's settling rate (715/715/R).

It appears that the settling rate of precipitates was significantly slower than the one measured with the non-seeded test (715/715/NR). This was surprising since the particles were found to be coarser and denser as a result of seeding and recycling. However, Figure 57 shows that the solids flux was fairly constant around 15.1 $kg/m^2/h$.

This suggests that the slower settling rate was mainly due to the increase in the percentage of solids and consequently to the interaction between particles.

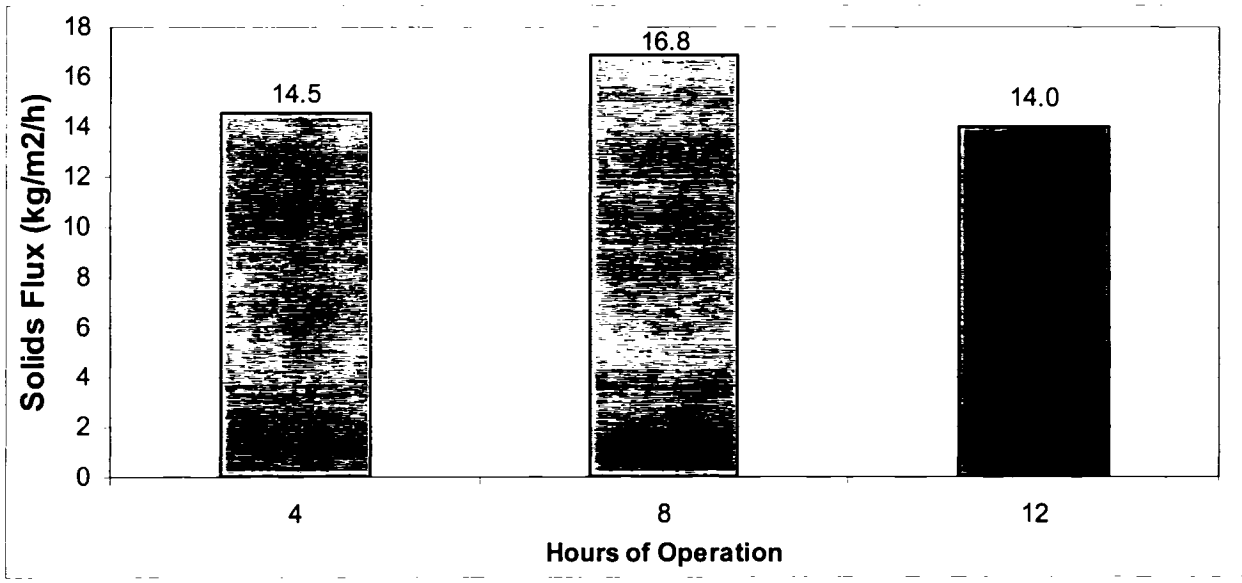

Figure 57: Solids flux of the 715/715/R product.

- **Scaling:** Scaling of the reactor's walls, pH/ORP probes, impellers, and other internal parts was not as extensive as in the 715/715/NR test. Scaling consisted also of a thin black but relatively soft layer of precipitate deposit that could be easily removed. pH/ORP control was consequently significantly improved as deviation from calibration was less than 0.2 pH unit and 20 mV after 3-4 hours of operation.

4.3.3 Staged and Seeded Operation at 665 mV and 715mV

The aim of the third continuous-mode test was to assess the efficiency of the manganese step-wise oxidative precipitation process. Hence, the process was designed to precipitate about 50% of manganese in the first reactor (concurrently with the usage of seed) and the manganese remaining to be precipitated in the second reactor. It turned out from preliminary continuous tests that the appropriate settings to meet the 50% manganese removal specification was to introduce SO_2/O_2 at 30/150 sccm in R1 and at 70/350 sccm in R2. These settings permitted to reach **665** mV in R1 and around **715** mV in reactor 2. All the precipitates were **R**ecycled back from the thickener underflow to the first reactor so this test is called **665/715/R**.

4.3.3.1 Mass Balance

Figure 58 summarizes the mass balance of the 665/715/R test where the average and final flowrates are indicated in sccm. Like with the previous continuous tests, the thickener underflow also consisted of an approximately 8 % w/w solids slurry.

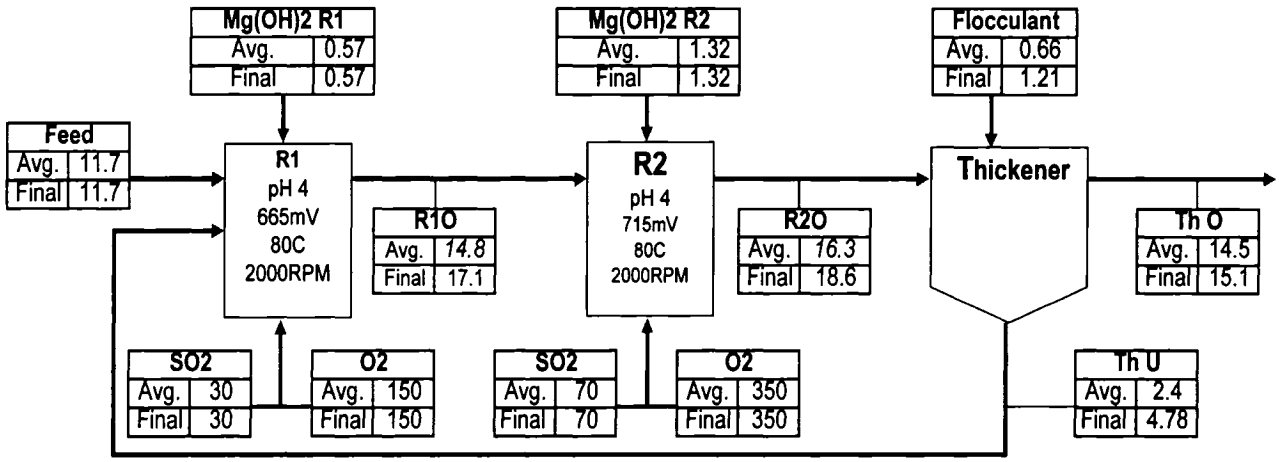

Figure 58: Mass balance of the 665/715/R test.
(Flowrates are in sccm)

Similarly to the 715/715/R test, the average retention time was approximately 58 minutes for the slurry in each of the two reactors, and 130 minutes and 40 minutes for the aqueous and solid phases respectively in the thickener.

4.3.3.2 Manganese Removal

Figure 59 presents the evolution of the ORP and the residual manganese in R1 and R2 throughout the test.

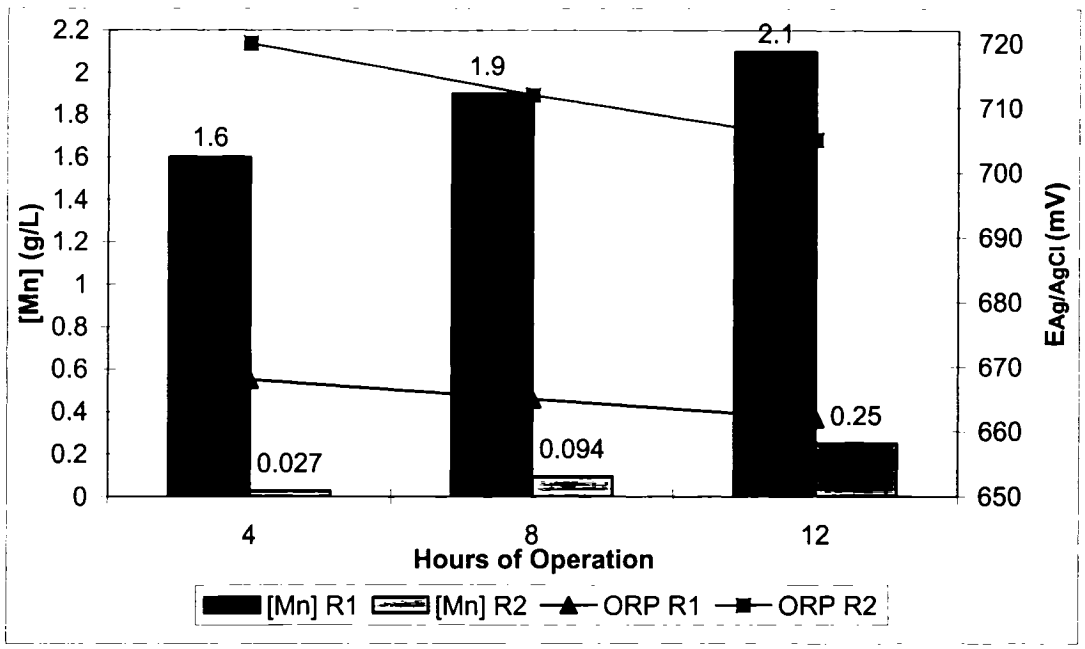

Figure 59: ORP and residual manganese (665/715/R).

Due to a reduced retention time, the ORP in R1 and R2 decreased throughout the test so the residual manganese increased up to 2.1 g/L and 0.25 g/L respectively. However, Figure 60 shows that 94% of manganese was still removed in R2 after 12 hours of operation which is similar to the 715/715/R test.

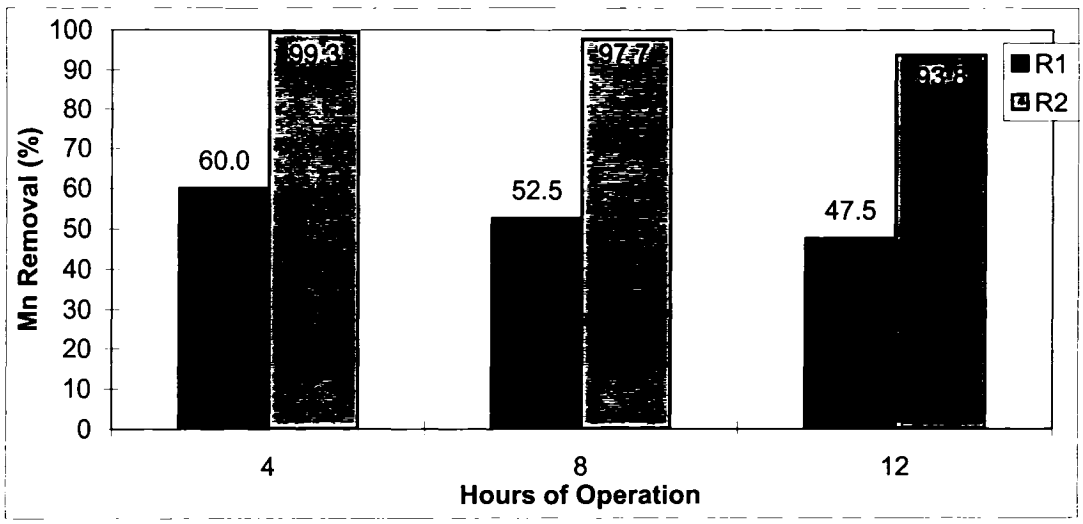

Figure 60: Manganese removal during the 665/715/R test.

4.3.3.3 Reagent Over-Stoichiometry

Figure 61 shows that 3, 5.2 and 25.9 times the stoichiometric amount of $Mg(OH)_2$, SO_2 and O_2 respectively were consumed on average under the selected experiment operating conditions.

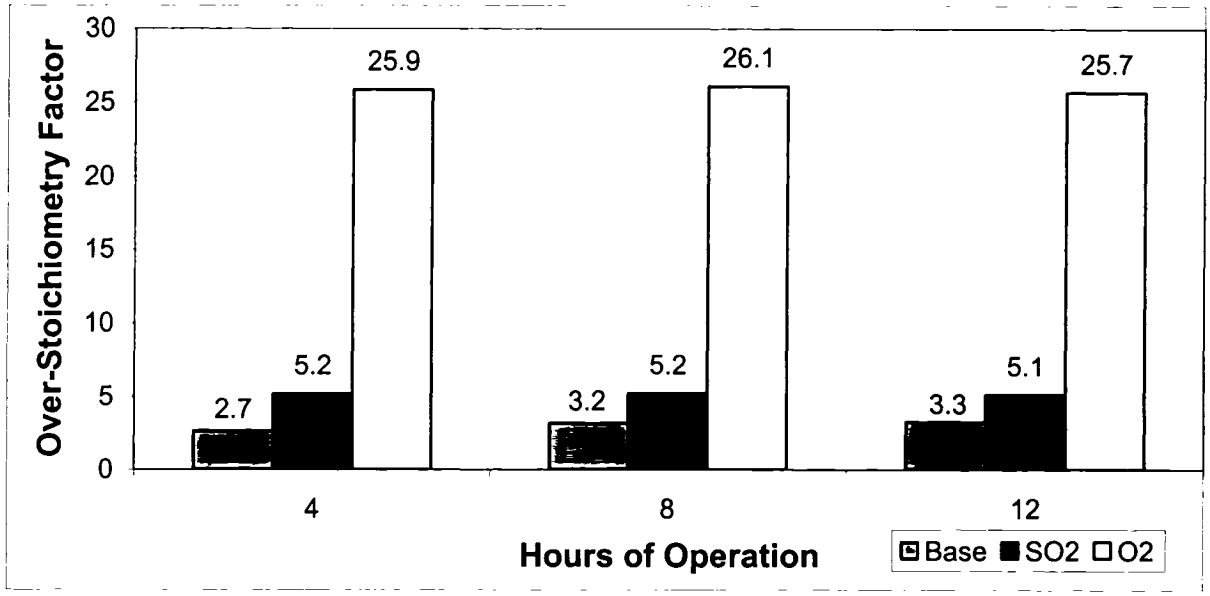

Figure 61: Reagent over-stoichiometry factors for the 665/715/R test.

Step-wise oxidative precipitation does not appear to have much effect on reagent consumption as it was similar to the 715/715/NR and 715/715/R tests.

4.3.3.4 Precipitate Characterization

- **Composition:** Table 6 presents the variation in composition of the precipitates throughout the test.

Table 6: Composition of precipitates obtained from the 665/715/R test.

Hours of Operation	% Solids	% Mn	% Zn	% S	% Cu	% Mg	% Na	% Ca	% Fe
4	1.3	23.2	15.0	11.0	1.6	3.7	0.47	0.09	0.07
8	2.5	29.7	18.0	4.3	2.8	1.0	0.79	0.09	0.05
12	4.3	25.0	17.0	5.4	2.1	1.6	0.84	0.23	0.05
Avg.	2.7	26.0	16.7	6.9	2.2	2.1	0.70	0.14	0.05

Table 6 shows that manganese represented only 26 w/w % on average of the precipitate's composition while the average zinc content is approximately 17 %. Figure 62 shows that the zinc contained in the precipitates represented up to 2.7 % of the total zinc fed to the reactor 1, i.e. aqueous zinc contained in the feed solution and in the recycle, compared to 2.2% and 3.2% for the 715/715/NR and 715/715/R tests respectively.

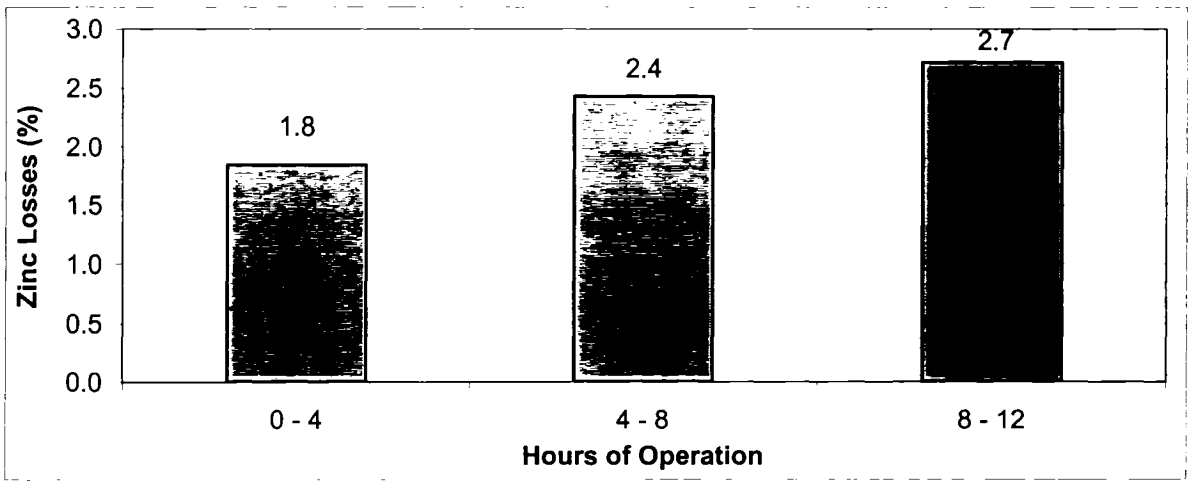

Figure 62: Zinc losses incurred during the 665/715/R test.

- **Particle Size Distribution (PSD):** Particle size analysis of the precipitate as a function of operating time is presented in Figure 63 and Figure 64. It is clear from this analysis that the mean diameter by volume of the precipitates was around 12 μm and was increasing throughout the test. The smallest and largest particles in significant amount were respectively around 6 μm and 30 μm irrespective of the operating time. The precipitate's mean diameter after 12 hours of operation was 13.2 μm in comparison to 12.6 μm and 16.7 μm in the 715/715/NR and the 715/715/R test respectively.

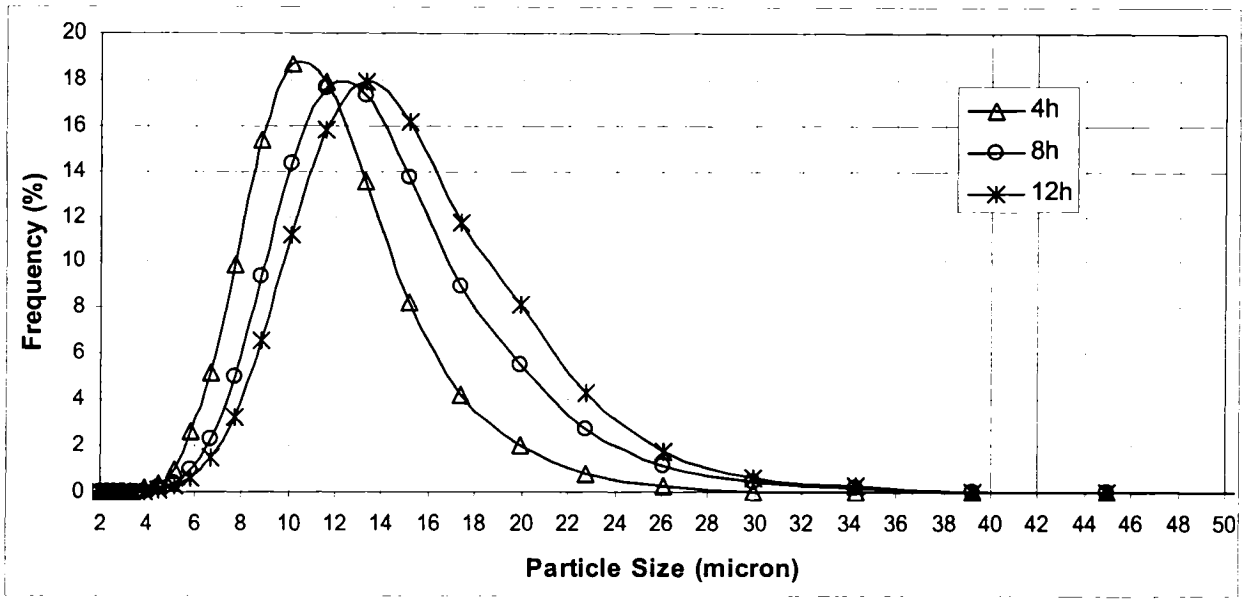

Figure 63: Precipitate's particle size distribution by volume (665/715/R).

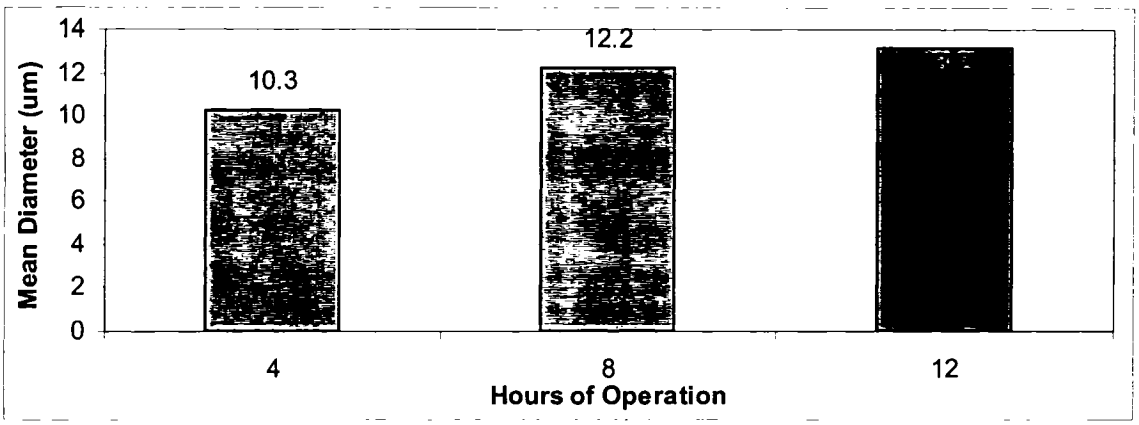

Figure 64: Precipitate's mean diameter (665/715/R).

- **X-Ray Diffraction (XRD):** Figure 65 presents the XRD patterns of the precipitates produced after 4, 8 and 12 hours of continuous-mode operation and the XRD references for MnO_2-$MnO{\bullet}H_2O$, birnessite-like material and $ZnSO_4{\bullet}H2O$. The precipitates exhibited very similar XRD patterns with those of the 715/715/R test. Precipitates were still quite amorphous with a background located around 300 counts and a highest peak around 700 counts only. The $ZnSO_4{\bullet}H_2O$ phase was quite significant at the beginning of the test while there was no peak around 7.27Å. However, after 12 hours of operation, the

$ZnSO_4 \bullet H_2O$ phase disappeared while the peak around 7.27Å appeared indicating formation of the birnessite-like structure.

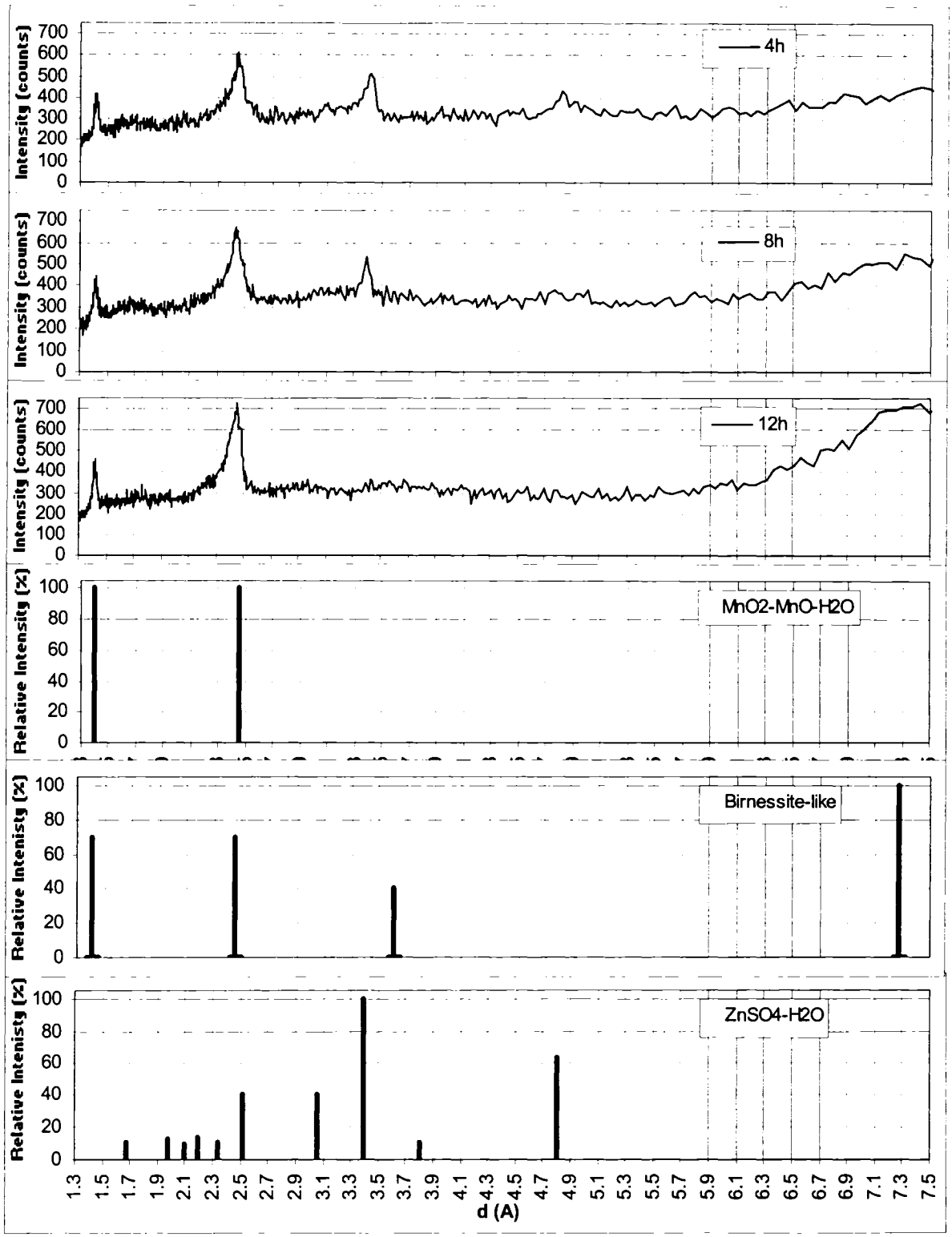

Figure 65: XRD patterns of the 665/715/R product.

- **Scanning Electron Microscopy (SEM):** Figure 66 shows pictures of the precipitate that was produced after 12 hours of operation at two different magnifications.

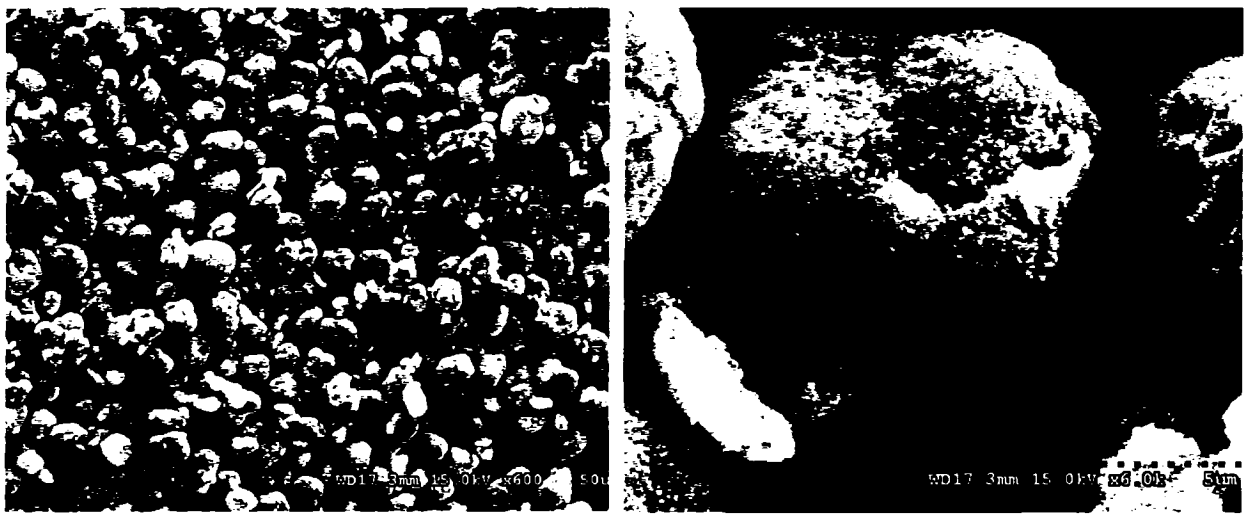

Figure 66: SEM images of the 665/715/R product.

The precipitate morphology was similar with that of the precipitates of the 715/715/NR and 715/715/R tests.

- **Crosse-section Imaging and Mapping:** The Figure 67 is a picture of the cross-section of some precipitate produced after 12 hours of operation.

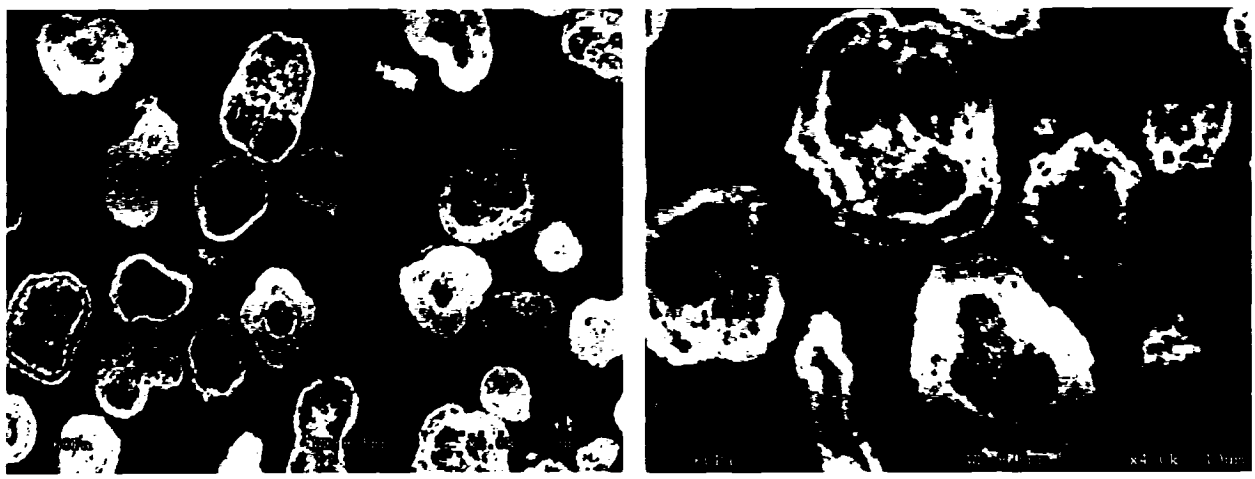

Figure 67: Precipitate's cross-section imaging (665/715/R).

Although Figure 66 showed that the precipitate's particle morphology was similar to that of the product obtained from the 715/715/NR and 715/715/R tests, Figure 67 shows that its internal structure was quite different. In this test, the precipitates exhibited a layered structure with a darker core coated with a brighter layer. In some instance, several superimposed darker and brighter layers were visible.

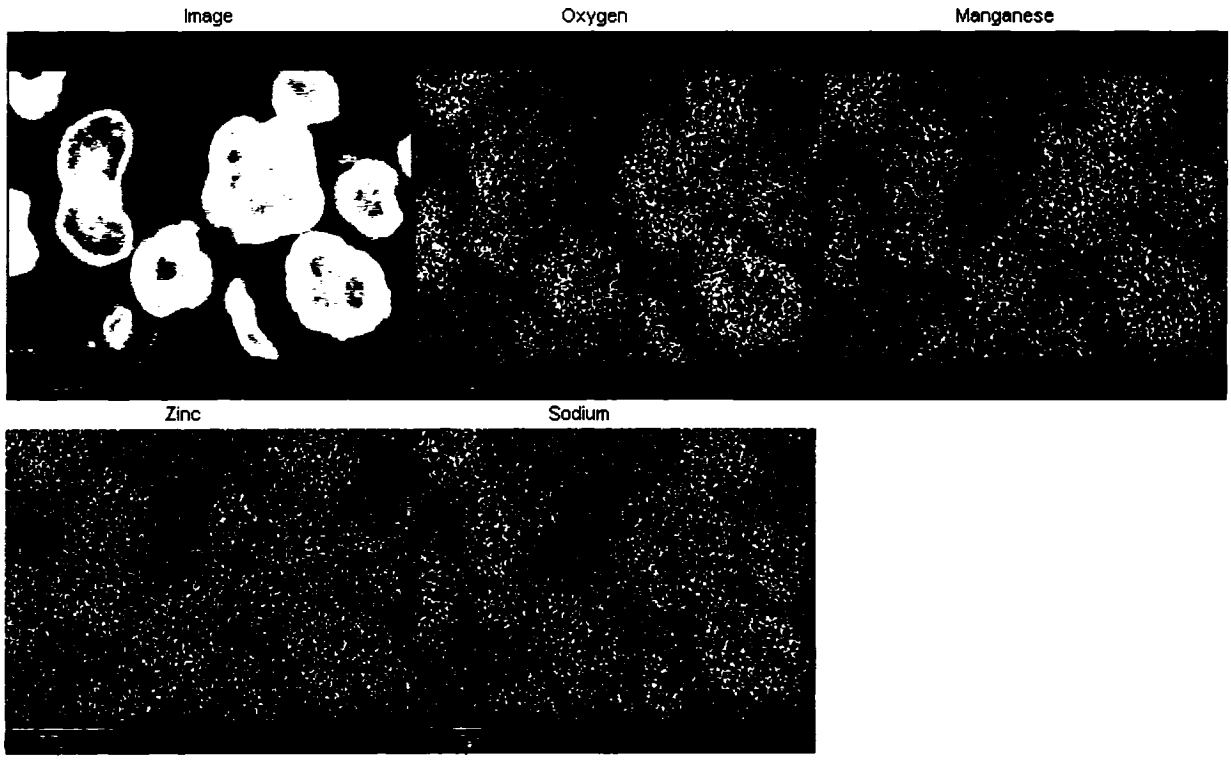

Figure 68: Mapping of precipitate's cross-section (665/715/R).

Although Figure 67 showed a layered structure, elemental mapping images (Figure 68) failed to show a clear difference in composition between the darker and the brighter layers. One of the reasons is that the layers were only 1-2 μm wide while the beam's interaction volume used for mapping was about 3 μm. The other reason is that the brighter material has apparently similar composition with that of the darker material. Actually, because the ORP was raised in two steps in this test and that the particle's core was always made of the darker material, it is suspected that the darker material was synthesized in the first reactor at 665mV while the brighter material was synthesized in the second one at 715mV. The several darker and brighter layers reflect apparantly the corresponding precipitate recycles. The darker and brighter materials were probably both

manganese oxide hydrates contaminated with foreign cations with the darker material having a phase closer to MnO_2-MnO-H_2O and manganese in a lower oxidation state, i.e. around 3, while the brighter material having a phase closer to birnessite with manganese in a higher oxidation state, i.e. around 3.8.

- **Settling:** Figure 69, Figure 70 and Figure 71 summarize the precipitate's settling characteristics in a 100 mL graduated cylinder.

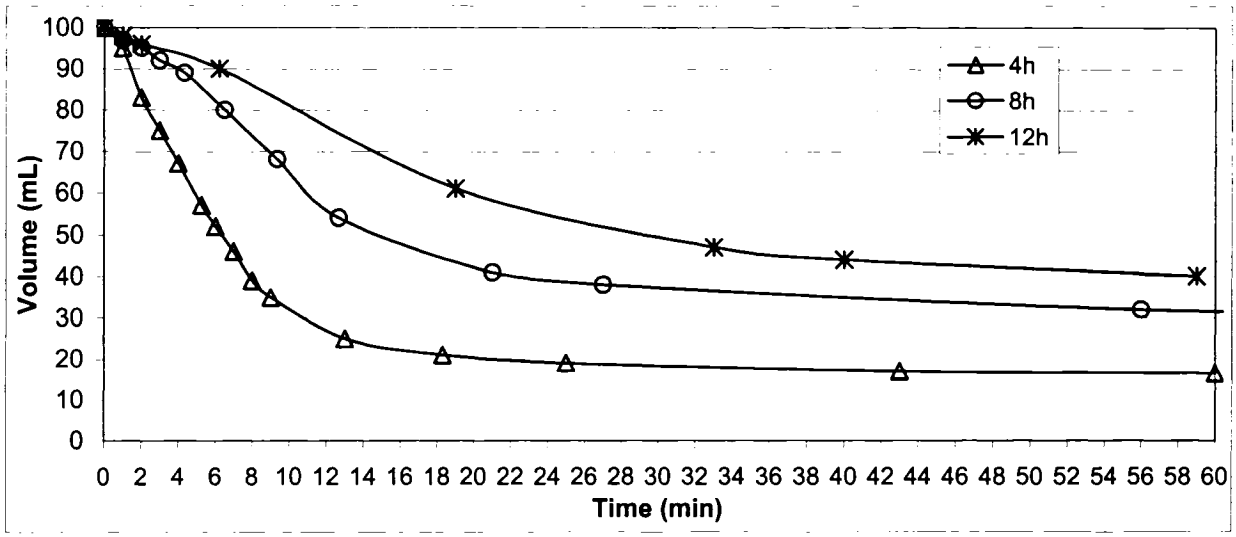

Figure 69: Precipitate's settling behaviour (665/715/R).

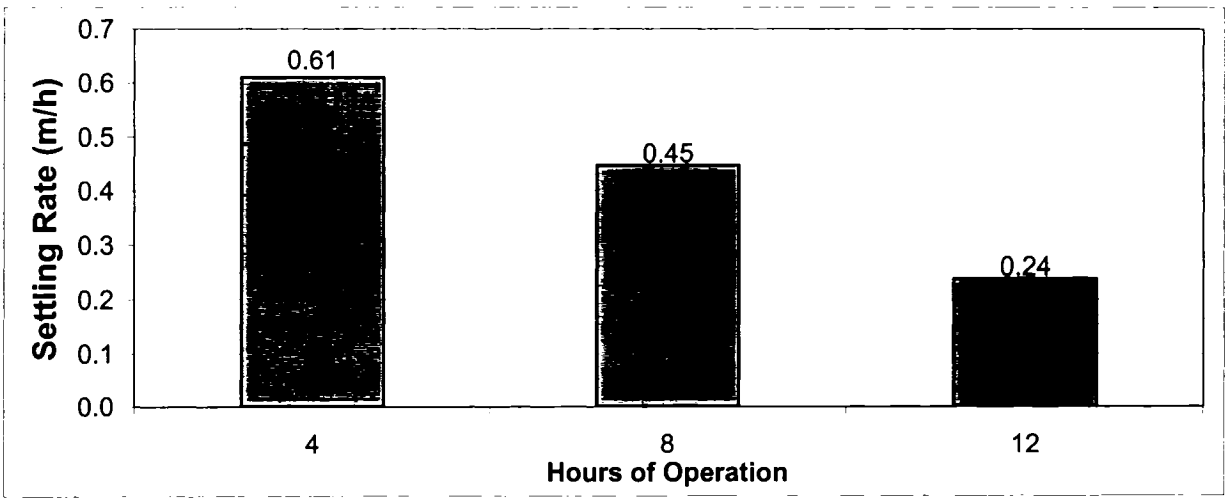

Figure 70: Precipitate's settling rate (665/715/R).

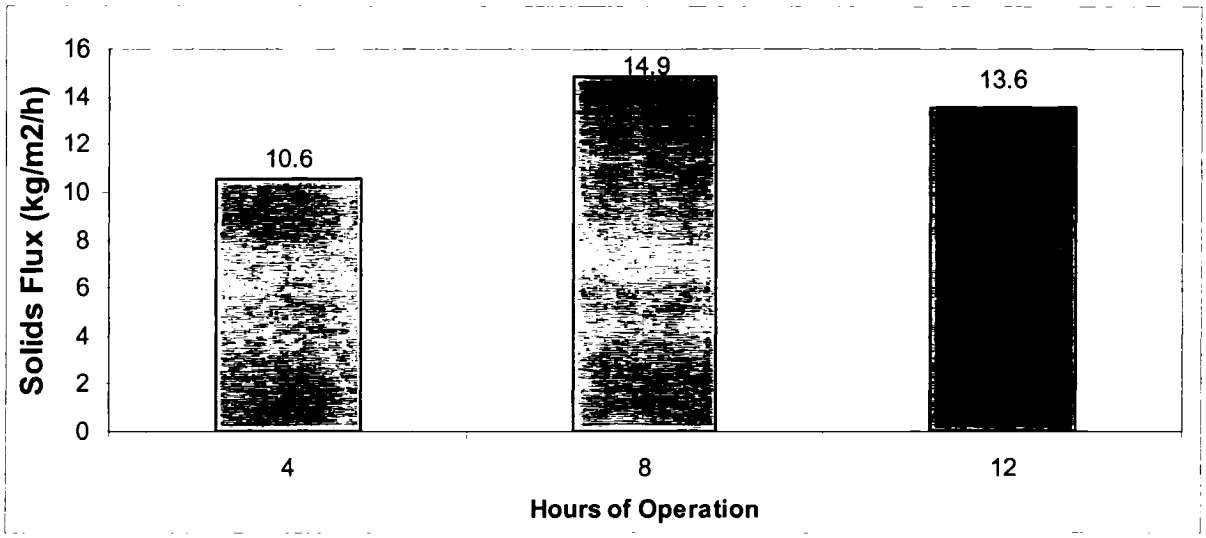

Figure 71: Solids flux (665/715/R)

The precipitate's settling characteristics were quite similar to those of the 715/715/R test except for the 4 hours of operation sample. With an average value of 13 $kg/m^2/h$ compared to 16.4 $kg/m^2/h$ and 15.1 $kg/m^2/h$, the present solids flux was lower than the corresponding ones for 715/715/NR and 715/715/R tests.

- **Scaling:** Scaling of the reactor's walls, pH/ORP probes, impellers, and other external parts was negligible. pH/ORP control was therefore excellent and deviation from calibration was under 0.2 pH unit and 20 mV even after 12 hours of operation.

4.3.4 Summary

Three continuous-mode tests were performed in order to investigate the effect of step-wise oxidative precipitation on manganese removal using SO_2/O_2. The major findings are:

- **ORP, residual manganese and manganese removal:** Although it was possible to maintain the ORP at 715mV after 12 hours of operation during the 715/715/NR test, it was not possible to prevent the ORP from decreasing to 707 mV and 705 mV in the 715/715/R and 665/715/R tests respectively. Consequently, the residual manganese increased from 49 ppm to 210 ppm and 250 ppm of manganese while the manganese removal decreased from 99% to 95% and 94% respectively. Short-circuiting along with shorter retention time are the suspected causes of the lower manganese removal and ORP drop.
- **Reagent over-stoichiometry:** There were no significant differences in reagent over-stoichiometry among the tests. The average reagent over-stoichiometry factors were 3.3, 5.2 and 26 times for $Mg(OH)_2$, SO_2 and O_2 respectively. As a possible measure of reducing these high over-stoichiometry factors is the implementation of SO_2/O_2 in two steps where in stage 1 the bulk of manganese is removed at high SO_2/O_2 flowrates and ratio while the residual manganese is removed in stage 2 at lower SO_2/O_2 flowrates and ratio.
- **Precipitate's composition and zinc losses:** Due to the high zinc sulphate level of the feed solution, e.g. 150 g/L Zn, the manganese precipitates were heavily contaminated with zinc and sulphur especially. The typical w/w precipitate's composition was 26.7 % Mn, 18.4 % Zn, 5.7% S, 2.2% Cu, 1.6% Mg, 1.1% Na, 0.14% Ca and 0.07% Fe. The average zinc losses were around 2.7%.
- **Particle size distribution:** In every test, particles size increased with the operation time as the system switched from batch to continuous-mode. The largest and the smallest particles present in significant amount were averaging 32 μm and 5μm respectively. The largest average particles size were obtained in the 715/715/R test with particles averaging 16.7 μm compared to 13.2 μm and 12.6 μm in the 665/715/R and 715/715/NR tests respectively.

- **X-Ray diffraction:** The precipitates were poorly crystalline and consisted mainly of a birnessite-like phase having a composition close to $(Na_{0.7}Ca_{0.3})Mn_7O_{14}\bullet 2.8H_2O$. Regarding the extensive precipitate's impurity content and that the birnessite-series compounds are prone to extensive cation substitution, the existence of more complex phases like (Ca, Cu, Mg, Na, Zn)$(SO_4)Mg_xO_y\bullet_zH_2O$ cannot be ruled out. The formation of MnO_2-MnO-H_2O having manganese in a lower oxidation state, i.e. around 3, also appears at least in part possible. This is particularly true when manganese was precipitated at lower ORP like at the very beginning of a test when the system switched from batch-mode to continuous-mode and/or when ORP was set to 665 mV in the first reactor of the 665/715/R test.
- **SEM, Cross-section Imaging and Mapping:** Precipitates appeared to be composed of fairly rounded particles averaging 14.2 μm and having a rough surface. Precipitates synthesized in the 715/715/NR test turned out to be very porous with large solution entrapment while those synthesized in the 715/715/R test were compact without evidence of trapped solution. On the other hand, precipitates synthesized in the 665/715/R test exhibited a layered structure most likely made of superimposed layers of MnO_2-MnO-H_2O and birnessite-like phases. These precipitates were fairly compact without solution entrapment. Mapping conducted on the precipitate's cross-section showed an even distribution of the elements in the particles. No significant difference of composition was found among the different layers of the 665/715/R test precipitates.
- **Settling:** Although the settling rate of the 715/715/NR precipitates was faster than those of the 715/715/R and 665/715/R, it appeared to be mostly related to a lower percentage of solids. Actually, the solids flux was relatively stable around 14.8 $kg/m^2/h$.
- **Scaling:** Scaling was significant in absence of recycling. However, it almost disappeared completely when the step-wise oxidative precipitation technique was employed.

Chapter 5 Conclusion

The main goal of the present work was to determine the optimum conditions for the removal of manganese from a zinc-rich solution at 80°C by oxidative precipitation using an oxidizing gas mixture of sulphur dioxide and oxygen. In an attempt to improve the precipitate's characteristics, a new technique called S.W.O.P for Step-Wise Oxidative Precipitation was also investigated using a continuous-mode set-up. Numerous semi-batch tests were conducted before hand to determine the optimum operating conditions for the continuous-mode tests.

Results of the semi-batch tests suggested conducting the manganese oxidative precipitation at pH 4 with a SO_2/O_2 flowrate equal to 100/500 sccm in a 2 litres "closed reactor" mixed at 2000 RPM by an upward pitched blade impeller on the bottom and a flat blade impeller on the top. Using these experimental conditions, it was possible in semi-batch mode to reach 730mV (vs. Ag/AgCl) at pH 4 and consequently lower the manganese concentration from 4 g/L down to about 22 ppm in 40 minutes. Although manganese could be removed with a SO_2/O_2 ratio of 1, it was shown that using a lower SO_2/O_2 ratio (0.2) yields higher ORP, better manganese removal and lower reagent over-stoichiometry factors. The reagent over-stoichiometry factors were shown to increase as manganese concentration was decreasing and/or SO_2/O_2 flowrate was increasing, due to increased competing sulfuric acid production. Use of seed only slightly improved the manganese removal rate.

Using the results of the semi-batch mode tests, three continuous-mode tests (using a two-reactor cascade) were performed in order to investigate the effect of step-wise oxidative precipitation (and recycling) on manganese removal using SO_2/O_2. The main variables were the SO_2/O_2 flowrate (and consequently the ORP) in the two reactors and the utilization or not of a recycle from the thickener underflow to the first reactor for seeding purposes. Due to difficulties in controlling accurately the continuous-mode set-up and that 12 hours of operation was not sufficient to reach steady-state, the obtained results are considered only semi-quantitative.

In general the precipitates produced in these continuous-mode tests were quite similar in composition and physical characteristics and consisted of fairly rounded particles of 14.2 μm in diameter composed of 26.7 % Mn, 18.4 % Zn, 5.7% S, 2.2% Cu, 1.6% Mg, 1.1% Na, 0.14% Ca and 0.07% Fe. The average zinc losses were around 2.7%. XRD analysis revealed that the precipitates were made-up mainly of a birnessite-like phase, i.e. $(Na_{0.7}Ca_{0.3})Mn_7O_{14}\bullet 2.8H_2O$, contaminated with zinc either in the form of substitution or as intimately co-precipitated zinc sulphate hydrate. The formation of a Mn(III) phase like MnO_2-MnO-H_2O at lower ORP is also likely.

Overall, the oxidative precipitation of manganese using SO_2/O_2 was improved only modestly by the S.W.O.P technique in terms of particle composition/morphology. However, the S.W.O.P technique proved highly effective in completely eliminating scaling which was a serious otherwise problem especially in terms of rendering the probes non functional because of the accumulated scale.

Further test work employing longer operating times so steady-state is attained and greater optimization of operating conditions is expected to further improve the selectivity of the process and the utilization efficiency of the reagents.

References

1. MacKinnon, D.J., Brannen, J.M., Effect of Manganese, Magnesium, Sodium and Potassium Sulphates on Zinc Electrowinning from Synthetic Acid Sulphate Electrolytes, Hydrometallurgy, 27, 1991, pp. 99-111

2. Demopoulos, G. P., Rosato, L., Wang, Q., Method for Removing Manganese from Acidic Sulfate Solutions, US Patent No. 6,391,270, May 21, 2002.

3. CEZinc Information Booklet, Public Edition 2003, Valleyfield, QC, Canada.

4. Vaaramaa, K., Lehto, J., Removal of Metals and Anions from Drinking Water by Ion Exchange, Desalination, 155, 2003, pp. 157-170.

5. Blanchard, C., Manuanyl, M., Martin, G., Removal of Heavy Metals from Waters by Means of Natural Zeolites, Wat. Res., 18, 1984, pp. 1501-1507.

6. Dijkman, H., Buisman, C. J. N., Bayer, H. G., Biotechnology in the Mining and Metallurgical Industries: Cost Savings Through Selective Precipitation of Metal Sulphides, Copper 99, Volume IV, C. Young , D. Dreisinger, R. Hackl, D. Dixon, Eds. TMS Warrendale, PA, 1999, pp. 113-126.

7. Bryson, A. W., Bijsterveld, C. H., Kinetics of the Precipitation of Manganese and Cobalt Sulphides in the Purification of a Manganese Sulphate Electrolyte, Hydrometallurgy, 27, 1991, pp. 75-84.

8. Gupta, C. K., Mukerjee, T. K., Hydrometallurgy in Extraction Processes, CRC Press, Vol II, 1990, pp. 167-169.

9. Barent, M., Johnson, S.W., The Production of Manganese Hydroxide, The Patent Office, No. 814688, London, UK, June 10, 1959.

10. Christensen, A. N., Hydrothermal Preparation and Low Temperature Magnetic Properties of $Mn(OH)_2$, Solid State Communications, 10, 1972, pp. 609-614

11. Patnaik, P., Handbook of Inorganic Chemicals, McGraw-Hill, 2003, pp.538-557.

12. Raghavan, R., Upadhyay, R. N., Innovative Hydrometallurgical Processing Technique for Industrial Zinc and Manganese Process Residues, Hydrometallurgy 51, 1999, pp. 207-226.

13. Kholmogorov, A. G., Zhyzhaev, A. M., Kononov, U. S., Moiseeva, G. A., Pashkov, G. L., The Production of Manganese Dioxide from Manganese Ores of Some Deposits of the Siberian Region of Russia, Hydrometallurgy, 56, 2000, pp. 1-11.

14. Prabhakar Rethinaraj, J., Visvanathan, S., Preparation and Properties of Electrolytic Manganese Dioxide, Journal of Power Sources, 42, 1993, pp. 335-343.

15. Verbaan, B., Mullinder, B., The Simultaneous Electrowinning of Manganese Dioxide and Zinc from Purified Neutral Zinc Sulfate at High Current Efficiencies, Hydrometallurgy, 7, 1981, pp. 339-352.

16. Ilea, P., Popescu, I. C., Urda, M., Oniciu, L., The Electrodeposition of Manganese from Aqueous Solutions of $MnSO_4$.IV:Electrowinning by Galvanostatic Electrolysis, Hydrometallurgy, 46, 1997, pp. 149-156.

17. Tsakiridis, P. E., Agatzini-Leonardou, S., Simultaneous Solvent Extraction of Cobalt and Nickel in the Presence of Manganese and Magnesium from Sulphate Solutions by Cyanex 301, Hydrometallurgy, 72, 2004, pp. 269-278.

18. Devi, N. B., Nathsarma, K. C., Chakravortty, B., Separation of Divalent Manganese and Cobalt Ions from Sulphate solutions Using Sodium Salts of D2EHPA, PC 88A and Cyanex 272, Hydrometallurgy 54, 2000, pp. 117-131.

19. Devi N. B., Nathsarma, K. C., Chakravortty, V., Extraction and Separation of Mn(II) and Zn(II) from Sulphate Solutions by Sodium Salt of Cyanex 272, Hydrometallurgy, 45, 1997, pp. 169-179.

20. Fernandes, J. B., Desai, B. D., Kamat Dalal, V. N., Manganese Dioxide: A Review of a Battery Chemical-Part I: Chemical Syntheses and X-Ray Diffraction Studies of Manganese Dioxides, Journal of Power Sources, 1985, pp. 209-237.

21. Nathsarma, K. C., Bhaskara Sarma, P. V. R., Separation of Iron and Manganese from Sulphate Solutions Obtained from Indian Ocean Nodules, Hydrometallurgy, 17, 1987, pp. 239-249.

22. Nishimura, T., Umetsu, Y., Oxidative Precipitation of Arsenic(III) with Manganese(II) and Iron(II) in Dilute Acidic Solution by Ozone, Hydrometallurgy, 62, 2001, pp. 83-92.

23. Nishimura, T., Umetsu, Y., Characteristics of Manganese Dioxide Produced by Ozone Oxidation in Acidified Sulfate Solutions, Processing Materials for Properties, H. Henein and T. Oki, Eds. TMS, Warrendale, PA, 1993.

24. Letterman, R. D., Water Quality and Treatment (Fifth Edition), McGraw-Hill, Chapter 12, 1990.

25. Nishimura, T., Umetsu, Y., Oxidation-Precipitation Reaction with Ozone in Strongly Acidified $MnSO_4$ Solutions with/without Addition of Other Sulfate, J. Min. Mater. Process. Inst. Jpn., 111, 1995, pp. 329-334.

26. Burkin, A. R., Chouzadjian, K. A., Precipitation of Manganese Dioxide from Zinc Electrolyte Solution using Peroxymonosulphuric Acid, Hydrometallurgy: Research Development and Plant Practice, K. Osseo-Asare, J., Eds. TMS, Warrendale, PA, 1983, pp. 603-615.

27. Ferron, C. J., The Control of Manganese in Acidic Leach Liquors with Special Emphasis to Laterite Leach Liquors, ALTA 2002 Nickel/Cobalt-8 Proceedings, Perth, Australia, 2002.

28. Krause, E., The Oxidation of Ferrous Sulfate Solutions by Sulfur Dioxide and Oxygen, Ph.D. Thesis, Waterloo University, Waterloo, Ontario, 1988.

29. Tiwari, B.L., Kolbe, J., Hayden, H. W. Jr., Oxidation of Ferrous Sulfate in Acid Solution by a Mixture of Sulfur Dioxide and Oxygen, Metallurgical Transactions, 10B, 1979, pp. 607-612.

30. Wallis, A. E., West, D. H., Process of Removing Ferrous Sulfate from Sulfate Solutions Containing Nickel and/or Cobalt, US Patent No. 2,816,819, 1957.

31. Devuyst, E. A., Mosoiu, A., Krause, E., Oxidizing Properties and Applications of the SO_2-O_2 System, Hydrometallurgy: Research, Development and Plant Practice, K. Osseo-Asare, J., Miller, Eds. TMS, Warrendale, PA, 1983, pp. 391-403.

32. Wang, Q., Demopoulos, G.P., Harris, G. B., A Novel Process for Arsenic Oxidation and Fixation, Waste Processing and Recycling III, S.R. Rao et al., Eds., CIM, Montreal, QC, 1998, pp. 375-387.

33. Wang, Q., Removal of Arsenic (III) in Aqueous Solutions by Controlling Oxidation Potential, Ph.D. thesis, Tohoku University, Sendai, Japan, 1997.

34. Wang, Q., Demopoulos, G.P., Harris, G. B., Arsenic Fixation in Metallurgical Plant Effluents in the Form of Crystalline Scorodite via a Non-Autoclave Oxidation-Precipitation Process, Minor Elements 2000-Environmental and Processing Issues for As, Sb, Se, Te, and Bi, C. Young, Eds. SME, Littleton, CO, 2000, pp. 225-237.

35. Zhang, W., Singh, P., Muir, D., Iron(II) Oxidation by SO_2/O_2 in Acidic Media: Part I. Kinetics and Mechanism, Hydrometallurgy, 55 (2000), pp. 229-245.

36. Spiro, M., The Standard Potential of the Peroxysulphate/Sulphate Couple, Electrochimica Acta, 24, 1979, pp. 313-314.

37. Huie, R. E., Neta, P., Chemical Behaviour of $SO_3\bullet^-$ and $SO_5\bullet^-$ Radicals in Aqueous Solution, J. Phys. Chem., 88, 1984, pp. 5665-5669.

38. Kniprath, E., Redox Precipitation of Nonferrous Heavy Metals from Aqueous Solution, US Patent No. 3,685,965, Aug. 22, 1972.

39. Ferron, C. J., Turner, D., Purification of Cobalt Solution Containing Iron and Manganese with Oxidation Mixture of SO_2 and Oxygen, International Patent, WO 00/56943, Sept 28, 2000.

40. Khoe, G. H., Zaw, M., Iron-Catalyzed Oxidation of Manganese and Other Inorganic Species in Aqueous Solutions, US Patent No. 6,558,556, May 6, 2003.

41. Lunt, D., et al, A Method for the Recovery of Cobalt, International Patent, WO 03/054238, July 3, 2003.

42. Zhang, W., Singh, P., Muir, D., Oxidative Precipitation of Manganese with SO_2/O_2 and Separation from Cobalt and Nickel, Hydrometallurgy, 63, 2002, pp. 127-135.

43. Franke, J., Mersmann, A., The Influence of the Operational Conditions on the Precipitation Process, Chem. Eng. Sci., 50, 1995, pp. 1737-1753.

44. Faust, S. D., Aly, O. S., Chemistry of Water Treatment, 2nd Edition, CRC Press, Boca Raton, FL, 1999, pp. 373-380, p. 418.

45. Schwartz, A. M., Myerson, A. S., Handbook of Industrial Crystallization, Butterworth-Heinemann, New York, NY, 2002.

46. Sohnel, O., Garside, J., Precipitation: Basic Principles and Industrial Applications, Butterworth Heinemann, Oxford, U.K., 1992, pp. 1-193.

47. Mersmann, A., Crystallization Technology Handbook, Marcel Dekker, New York, NY, 1995, p. 20.

48. Mullin, J. W., Crystallization, 3rd Edition, Butterworth Heinemann, Oxford, U.K., 1993, pp. 172-263.

49. Elwell, D., Sceel, H.J., Crystal Growth from High Temperature Solutions, Academic Press, London, U.K., 1975, pp. 138-201,.

50. Dirksen, J. A., Ring, T. A., Fundamentals of Crystallization: Kinetics Effects on Particle Size Distributions and Morphology, Chem. Eng. Sci., 46, 1991, pp. 2227-2389.

51. Demopoulos, G. P., Aqueous Precipitation and Crystallization for the Production of Particulate Solids with Desired Properties, Hydrometallurgy, 2005 (in press).

52. Kostenbader, P., Method for Treating Acid Water Containing Metallic Values, US Patent No. 3,738,932, 1973.

53. Mishra, S. K., Wentzler, T. H., Kust, R. N., Savage, E. S., Waste Water Treatment Process Using Improved Recycle of High Density Sludge, US Patent No. 5,039,428, 1991.

54. Herman, S. T., Pfeiffer, J. B., Sewald, R. T., Sterner, C. J., Treatment of Industrial Wastewaters, US Patent No. 4,465,597, 1984.

55. Demopoulos, G. P., Precipitation in Aqueous Processing of Inorganic Materials: A Unified Colloid-Crystallization Approach to the Production of Powders with Controlled Properties, H. Henein and T. Oki, Processing Materials for Properties, Eds. TMS, Warrendale, PA, 1993, pp. 537-540.

56. Demopoulos, G. P., Kondos, P. D., Zinck, J. M., Multiple Stage Precipitation of Heavy Metals from Acidic Aqueous Solution, US Patent No. 5,672,280, 1997.

57. Menard, V., GORO Partial Neutralization Circuit, Internal Report, Submitted to Inco Technical Servicea Limited, Mississauga, Ontario, 2002.

58. Menard, V., Voisey's Bay Iron Removal Circuit Tests, Internal Report, Submitted to Inco Technical Services Limited, Mississauga, Ontario, 2003.

59. Wang, Q., Demopoulos, G. P., Use of SO_2/O_2 (Air) to Control Manganese in Zinc Leach Solution, Final Project Report (submitted to CEZinc), Department of Mining and Metallurgical Engineering, McGill University, 1999.

60. Renuka, R., Ramamurthy, S., An Investigation on Layered Birnessite Type Manganese Dioxides for Battery Applications, Journal of Power Sources, 87, 2000, pp. 144–152.

61. Post, J. E., Manganese Oxide Minerals: Crystal Structures and Economic and Environmental Significance, Proc. Natl. Acad. Sci., 96, 1999, pp. 3447–3454.

62. Appelo, C. A. J., Postma, D., A Consistent Model for Surface Complexation on Birnessite (δ-MnO2) and its Application to a Column Experiment, Geochimica et Cosmochimica Acta, 63, 1999, pp. 3039–3048.

63. http://www.mindat.org/min-680.html

64. http://www.webmineral.com/data/Birnessite.shtml

65. http://www.nexusag.com/products/msds_**zinc**maxi.pdf

66. http://bizbb.com/ChakrasMicroNutrientFertilisers/offer/2/

67. Dick, R. I., Gravity Thickening of Sewage Sludge, Effluent and Water Treatment Journal, 1972, pp. 597-605.